Aminoglycoside tolerance in *Vibrio cholerae* engages translational reprogramming associated with queuosine tRNA modification

Louna Fruchard [1,2,#], Anamaria Babosan [1,#], Andre Carvalho [1], Manon Lang [1], Blaise Li [3], Magalie Duchateau [4], Quentin Giai-Gianetto [4,5], Mariette Matondo [4], Frédéric Bonhomme [6], Isabelle Hatin [7], Hugo Arbes [7], Céline Fabret [7], Enora Corler [7], Guillaume Sanchez [8], Virginie Marchand [8], Yuri Motorin [8], Olivier Namy [7], Valérie de Crécy-Lagard [9,10], Didier Mazel [1,*], Zeynep Baharoglu [1,*].

# equal contribution
*Corresponding authors: baharogl@pasteur.fr, mazel@pasteur.fr

1. Institut Pasteur, Université de Paris Cité, Unité Plasticité du Génome Bactérien, UMR3525, CNRS, 75015, Paris, France
2. Sorbonne Université, Collège Doctoral, F-75005, Paris, France
3. Institut Pasteur, Université Paris Cité, Bioinformatics and Biostatistics Hub, F-75015 Paris, France
4. Institut Pasteur, Université de Paris, Proteomics Platform, Mass Spectrometry for Biology Unit, UAR2024, CNRS 2000, Paris, France.
5. Institut Pasteur, Université de Paris, Department of Computation Biology, Bioinformatics and Biostatistics Hub, Paris, France.
6. Institut Pasteur, Université Paris cité, Epigenetic Chemical Biology Unit, UMR 3523, CNRS, 75015, Paris, France
7. Université Paris-Saclay, CEA, CNRS, Institute for Integrative Biology of the Cell (I2BC), F-91198, Gif-sur-Yvette, France
8. Université de Lorraine, CNRS, Inserm, UAR2008/US40 IBSLor, Epitranscriptomics and RNA Sequencing Core Facility and UMR7365 IMoPA, F-54000, Nancy, France
9. Department of Microbiology and Cell Science, University of Florida, Gainesville, Florida 32611, United States.
10. University of Florida Genetics Institute, Florida 32611, United States

Abstract

Tgt is the enzyme modifying the guanine (G) in tRNAs with GUN anticodon to queuosine (Q). *tgt* is required for optimal growth of *Vibrio cholerae* in the presence of sub-lethal aminoglycoside concentrations. We further explored here the role of the Q34 in the efficiency of codon decoding upon tobramycin exposure. We characterized its impact on the overall bacterial proteome, and elucidated the molecular mechanisms underlying the effects of Q34 modification in antibiotic translational stress response. Using molecular reporters, we showed that Q34 impacts the efficiency of decoding at tyrosine TAT and TAC codons. Proteomics analyses revealed that the anti-SoxR factor RsxA is better translated in the absence of *tgt*. RsxA displays a codon bias towards tyrosine TAT and overabundance of RsxA leads to decreased expression of genes belonging to SoxR oxidative stress regulon. We also identified conditions that regulate *tgt* expression. We propose that regulation of Q34 modification in response to environmental cues leads to translational reprogramming of transcripts bearing a biased tyrosine codon usage. *In silico* analysis further identified candidate genes which could be subject to such translational regulation, among which DNA repair factors. Such transcripts, fitting the definition of modification tunable transcripts, are central in the bacterial response to antibiotics.

Introduction

Antimicrobial resistance is an increasingly serious threat to global public health. Our recent finding that many tRNA modification genes are involved in the response to antibiotics from different families (Babosan et al., 2022) led to further investigate the links between environmental factors (e.g. traces of antibiotics), tRNA modifications and bacterial survival to antibiotics.

The regulatory roles of RNA modifications was first proposed for eukaryotes (Pollo-Oliveira & de Crecy-Lagard, 2019) and their importance in human diseases has recently emerged (Chujo & Tomizawa, 2021; Suzuki, 2021). In bacteria, while some tRNA modifications are essential (Zhong et al., 2019), the absence of many RNA modification shows no growth phenotype in unstressed cells (de Crecy-Lagard & Jaroch, 2021). At the molecular level, the roles of tRNA modifications in differential codon decoding have been described in various species (Bruni, Colantuoni, Sbordone, Cortese, & Blasi, 1977; Parker, 1982; Taylor, Trieber, Trescher, & Bekkering, 1998; Urbonavicius, Qian, Durand, Hagervall, & Bjork, 2001). In most cases, no growth phenotype was associated with these variations in decoding in bacteria. Recent studies, however, do highlight the links between tRNA modifications and stress responses in several bacterial species (Aubee, Olu, & Thompson, 2016; Chionh et al., 2016; de Crecy-Lagard & Jaroch, 2021; Fleming et al., 2022; Hou, Matsubara, Takase, Masuda, & Sulkowska, 2017; Thompson & Gottesman, 2014; Thongdee et al., 2019; Vecerek, Moll, & Blasi, 2007), and new modifications are still being discovered (Kimura, Dedon, & Waldor, 2020). Until recently, few tRNA modification factors have been clearly linked with resistance and persistence to antibiotics, via differential codon decoding in cell membrane and efflux proteins (TrmD (Masuda et al., 2019), MiaA (Taylor et al., 1998)). A link between stress and adaptation was described to occur via the existence of modification tunable transcripts, or MoTTs.

MoTTs were first (and mostly) defined in eukaryotes as transcripts that will be translated more or less efficiently depending on the presence or absence of tRNA modifications (Endres, Dedon, & Begley, 2015), namely upon stress (Advani & Ivanov, 2019). In bacteria, links between tRNA modifications and the response to several stresses are highlighted by studies focusing on the following MoTT/codon and tRNA modification couples (reviewed in (de Crecy-Lagard & Jaroch, 2021)): differential translation of RpoS/leucine codons via MiaA (*E. coli*) (Aubee et al., 2016); Fur/serine codons via MiaB, in response to low iron (*E. coli*) (Vecerek et al., 2007); MgtA/proline codons via TrmD, in response to low magnesium (Hou et al., 2017); catalases/phenylalanine and aspartate codons via TrmB, during oxidative stress (*P. aeruginosa*) (Thongdee et al., 2019). Mycobacterial response to hypoxic stress (Chionh et al., 2016) also features MoTTs. In this latter study, specific stress response genes were identified *in silico,* through their codon usage bias, and then experimentally confirmed for their differential translation. tRNA modification-dependent translational reprogramming in response to antibiotic stress has not been the focus of a study so far in bacteria.

During studies in *V. cholerae*, we recently discovered that t/rRNA modifications play a central role in response to stress caused by antibiotics with very different modes of action (Babosan et al., 2022), not through resistance development, but by modulating tolerance. The identified RNA modification genes had not previously been associated with any antibiotic resistance phenotype. The fact that different tRNA modifications have opposite effects on tolerance to different antibiotics highlights the complexity of such a network, and shows that the observed phenotypes are not merely due to a general mistranslation effect. Since tRNA modifications affect codon decoding and accuracy, it is important to address how differential translation can generate proteome diversity, and eventually adaptation to antibiotics.

In particular, deletion of the *tgt* gene encoding tRNA-guanine transglycosylase (Tgt) in *V. cholerae* confers a strong growth defect in the presence of aminoglycosides at doses below the minimal inhibitory concentration (sub-MIC) (Babosan et al., 2022). Tgt incorporates queuosine (Q) in the place of guanosine (G) in the wobble position of four tRNAs with GUN anticodon ($tRNA^{Asp}_{GUC}$, $tRNA^{Asn}_{GUU}$, $tRNA^{Tyr}_{GUA}$, $tRNA^{His}_{GUG}$) (Ehrenhofer-Murray, 2017). The tRNAs with "AUN" anticodons are not present in the genome, and thus each one of the four GUN tRNAs decodes two synonymous codons (aspartate GAC/GAT, asparagine AAC/AAT, tyrosine TAC/TAT, histidine CAC/CAT which differ in the third

position). Q34 is known to increase or decrease translation error rates in eukaryotes in a codon and organism specific manner (Ehrenhofer-Murray, 2017; Meier, Suter, Grosjean, Keith, & Kubli, 1985). Q34 was shown to induce mild oxidative stress resistance in the eukaryotic parasite *Entamoeba histolytica*, the causative agent of amebic dysentery, and to attenuate its virulence (Nagaraja et al., 2021). In *E. coli*, the absence of Q34 modification was found to decrease mistranslation rates by $tRNA^{Tyr}$, while increasing it for $tRNA^{Asp}$ (Manickam, Joshi, Bhatt, & Farabaugh, 2016; Manickam, Nag, Abbasi, Patel, & Farabaugh, 2014). No significant biological difference was found in *E. coli Δtgt* mutant, except for a slight defect in stationary phase viability (Noguchi, Nishimura, Hirota, & Nishimura, 1982), and more recently an involvement in biofilm formation (Diaz-Rullo & Gonzalez-Pastor, 2023). Recent studies show that the *E. coli tgt* mutant is more sensitive to aminoglycosides but not to ampicillin nor spectinomycin and is more sensitive to oxidative stress but the molecular mechanisms were not elucidated (Pollo-Oliveira et al., 2022).

We asked here how queuosine (Q) modification by Tgt modulates the response to low doses of aminoglycosides. We find that *V. cholerae* Δ*tgt* displays differential decoding of tyrosine TAC versus TAT codons. Molecular reporters, coupled to proteomics and *in silico* analysis, reveal that several proteins with codon usage biased towards TAT (versus TAC) are more efficiently translated in Δ*tgt*. One of these proteins is RsxA, which prevents activation of SoxR oxidative stress response regulon (Koo et al., 2003). We propose that tobramycin treatment leads to increased expression of *tgt* and Q34 modification, which in turn allows for more efficient Sox regulon related oxidative stress response, and better response to tobramycin. Lastly, bioinformatic analysis identified DNA repair gene transcripts with TAT codon bias as transcripts modulated by Q34 modification, which was confirmed by decreased UV susceptibility of *V. cholerae* Δ*tgt.*

Materials and methods

Media and Growth Conditions

Platings were done at 37°C, in Mueller-Hinton (MH) agar media. Liquid cultures were grown at 37°C in MH in aerobic conditions, with 180 rotations per minute.

Competition experiments were performed as described (Babosan et al., 2022): overnight cultures from single colonies of mutant *lacZ*+ and WT *lacZ*- strains were washed in PBS (Phosphate Buffer Saline) and mixed 1:1 (500 µl + 500 µl). At this point 100 µl of the mix were serial diluted and plated on MH agar supplemented with X-gal (5-bromo-4-chloro-3-indolyl-β-D- galactopyranoside) at 40 µg/mL to assess T0 initial 1:1 ratio. At the same time, 10 µl from the mix were added to 2 mL of MH or MH supplemented with sub-MIC antibiotics (concentrations, unless indicated otherwise: TOB: tobramycin 0.6 µg/ml; GEN: 0.5 µg/ml; CIP: ciprofloxacin 0.01 µg/ml, CRB: carbenicillin 2.5 µg/ml), PQ: paraquat 10 µM, or H_2O_2: 0.5 mM. Cultures were incubated with agitation at 37°C for 20 hours, and then diluted and plated on MH agar plates supplemented with X-gal. Plates were incubated overnight at 37°C and the number of blue and white CFUs was assessed. Competitive index was calculated by dividing the number of blue CFUs (*lacZ*+ strain) by the number of white CFUs (*lacZ*- strain) and normalizing this ratio to the T0 initial ratio. When a plasmid was present, antibiotic was added to maintain selection: kanamycin 50 µg/ml for pSEVA.

Construction of complementation and overexpression plasmids in pSEVA238

Genes were amplified on *V. cholerae* genomic DNA using primers listed in Table S4 and cloned into pSEVA238 (Silva-Rocha et al., 2013) under the dependence of the *Pm* promoter (Kessler, Timmis, & de Lorenzo, 1994), by restriction digestion with XbaI+EcoRI and ligation using T4 DNA ligase. Promoter *Pm* is originally derived from the *P. putida* toluate catabolic operon and is positively regulated by the benzoate inducible XylS transcriptional regulator. Sodium benzoate 1 mM was added in the medium as inducer.

Survival/tolerance tests were performed on early exponential phase cultures. The overnight stationary phase cultures were diluted 1000x and grown until OD 600 nm = 0.35 to 0.4, at 37°C with shaking, in Erlenmeyers containing 25 mL fresh MH medium. Appropriate dilutions were plated on MH plates to determine the total number of CFUs in time zero untreated cultures. 5 mL of cultures were collected into 50 mL Falcon tubes and treated with lethal doses of desired antibiotics (5 or 10 times the MIC: tobramycin 5 or 10 µg/mL, carbenicillin 50 µg/mL, ciprofloxacin 0.025 µg/mL) for 30 min, 1 hour, 2 hours and 4 hours if needed, at 37°C with shaking in order to guarantee oxygenation. Appropriate dilutions were then plated on MH agar without antibiotics and proportion of growing CFUs were calculated by doing a ratio with total CFUs at time zero. Experiments were performed 3 to 8 times.

MIC determination

Stationary phase cultures grown in MH were diluted 20 times in PBS, and 300 µL were plated on MH plates and dried for 10 minutes. Etest straps (Biomérieux) were placed on the plates and incubated overnight at 37°C.

Quantification of fluorescent neomycin uptake was performed as described (Lang et al., 2021). Neo-Cy5 is the neomycin aminoglycoside coupled to the fluorophore Cy5, and has been shown to be active against Gram- bacteria (Okuda, 2015; Sabeti Azad et al., 2020). Briefly, overnight cultures were diluted 100-fold in rich MOPS (Teknova EZ rich defined medium). When the bacterial strains reached an OD 600 nm of ~0.25, they were incubated with 0.4 µM of Cy5 labeled neomycin for 15 minutes at 37°C. 10 µl of the incubated culture were then used for flow cytometry, diluting them in 250 µl of PBS before reading fluorescence. WT *V. cholerae*, was incubated simultaneously without neo-Cy5 as a negative control. Flow cytometry experiments were performed as described (Baharoglu, Bikard, & Mazel, 2010) and repeated at least 3 times. For each experiment, 100,000 events were counted on the Miltenyi MACSquant device.

PMF measurements

Quantification of PMF was performed using the Mitotracker Red CMXRos dye (Invitrogen) as described (El Mortaji et al., 2020), in parallel with the neo-Cy5 uptake assay, using the same bacterial cultures. 50 µL of each culture were mixed with 60 µL of PBS. Tetrachlorosalicylanilide TCS (Thermofischer), a protonophore, was used as a negative control with a 500 µM treatment applied for 10 minutes at room temperature. Then, 25 nM of Mitotracker Red were added to each sample and let at room temperature for 15 minutes under aluminium foil. 20 µL of the treated culture were then used for flow cytometry, diluted in 200 µL of PBS before reading fluorescence.

tRNA overexpressions

Synthetic fragments carrying the P*trc* promoter, the desired tRNA sequence and the natural transcriptional terminator sequence of VCt002 were ordered from IDT as double stranded DNA gBlocks, and cloned into pTOPO plasmid. Sequences are indicated in Table S4.

mRNA purification

For RNA extraction, overnight cultures were diluted 1:1000 in MH medium and grown with agitation at 37°C until an OD600 of 0.3-0.4 (exponential phase). 0.5 mL of these cultures were centrifuged and supernatant removed. Pellets were homogenized by resuspension with 1.5 mL of room temperature TRIzol Reagent. Next, 300 µL chloroform were added to the samples following mix by vortexing. Samples were then centrifuged at 4°C for 10 minutes. Upper (aqueous) phase was transferred to a new 2mL tube and mixed with 1 volume of 70% ethanol. From this point, the homogenate was loaded into a RNeasy Mini kit (Qiagen) column and RNA purification proceeded according to the manufacturer's instructions. Samples were then subjected to DNase treatment using TURBO DNA-free Kit (Ambion) according to the manufacturer's instructions.

205 **mRNA quantifications by digital-RT-PCR**
206 qRT-PCR reactions were prepared with 1 µL of diluted RNA samples using the qScript XLT 1-Step RT-
207 qPCR ToughMix (Quanta Biosciences, Gaithersburg, MD, USA) within Sapphire chips. Digital PCR was
208 conducted on a Naica Geode programmed to perform the sample partitioning step into droplets,
209 followed by the thermal cycling program suggested in the user's manual. Primer and probe sequences
210 used in digital qRT-PCR reaction are listed in Table S4. Image acquisition was performed using the Naica
211 Prism3 reader. Images were then analyzed using Crystal Reader software (total droplet enumeration
212 and droplet quality control) and the Crystal Miner software (extracted fluorescence values for each
213 droplet). Values were normalized against expression of the housekeeping gene *gyrA* as previously
214 described (Lo Scrudato & Blokesch, 2012).
215
216 **tRNA level quantification by qRT-PCR**
217 First-strand cDNA synthesis and quantitative real-time PCR were performed with KAPA SYBR® FAST
218 Universal (CliniSciences) on the QuantStudio Real-Time PCR (Thermo Fischer) using the primers
219 indicated in Table S4. Transcript levels of each gene were normalized to *gyrA* as the reference gene
220 control (Lo Scrudato & Blokesch, 2012). Gene expression levels were determined using the $2^{-\Delta\Delta Cq}$
221 method (Bustin et al., 2009; Livak and Schmittgen, 2001) in respect to the MIQE guidelines. Relative
222 fold-difference was expressed either by reference to antibiotic free culture or the WT strain in the
223 same conditions. All experiments were performed as three independent replicates with all samples
224 tested in duplicate. Cq values of technical replicates were averaged for each biological replicate to
225 obtain the ΔCq. After exponential transformation of the ΔCq for the studied and the normalized
226 condition, medians and upper/lower values were determined.
227
228 **Stop codon readthrough quantification assay**
229 *V. cholerae* electrocompetent cells were transformed with reporter dual reporter plasmids that were
230 previously described (Fabret & Namy, 2021). Overnight cultures of transformants were diluted 1:100
231 in MH medium supplemented with 5 µg/mL chloramphenicol to maintain plasmids, 200 µg/mL IPTG
232 (Isopropyl β-D-1-thiogalactopyranoside) and in the presence or not of tobramycine 0,4 µg/mL and
233 grown with shaking at 37°C until an OD600 of 0.3 (exponential phase).
234 Luciferase luminescence was quantified using the luciferase assay system (Promega, WI, USA, Cat.#
235 E1500). Briefly, 90 µL of each culture were aliquoted in 1.5 mL tubes, treated with 10 µL K_2HPO_4 (1 M)
236 and EDTA (20 mM) and quick-frozen in dry ice for 1 min. Tubes were then placed in room-temperature
237 water for 5 min to allow the cultures to thaw. 300 µL of lysis buffer (Cell Culture Lysis Reagent 1X ;
238 lysozyme 1.25mg/ml ; BSA 2.5mg/ml) were added in the tubes that were then placed back in water for
239 10 min. 100 µL of lysate were placed in 5 mL tubes with 100 µL of Luciferase Assay Reagent and
240 luminescence was read for 10 sec using Lumat LB 9507 (EG&G Berthold).
241 For β-galactosidase activity quantification, 2 mL of the cultures were aliquoted and mixed with 50 µL
242 chloroform and 50 µL SDS 0.1%. After vortexing for 45 sec, samples were placed 5 min at RT for cell
243 lysis. 500 µL of the lysates were collected into 5 mL tubes and treated with 1.5 mL Z-Buffer (8.5 mg/mL
244 Na_2HPO_4; 5.5 mg/mL $NaH_2PO_4H_2O$; 0.75 mg/mL KCl; 0.25 mg/mL $MgSO_4,7H_2O$) supplemented with 7
245 µL/ml 2-Mercaptoethanol. After 5 min incubation at 37°C, 500 µL ONPG (4 mg/mL) were added in the
246 samples which were then placed at 37°C for 1h. Reaction has finally been stopped by addition on the
247 tubes of 1mL Na_2CO_3 (1 M). 2 mL suspension were transferred to eppendorf tubes, centrifuged and OD
248 420 nm of the supernatant was read. β-galactosidase activity dosage was used for normalization of
249 luminescence.
250
251 **Construction of gfp reporters where tyrosine 66 chromophore was replaced with another codon**
252 Whole plasmid amplifications were performed on pSC101-gfp using primers introducing the desired
253 point mutation at codon position 66 of GFP. An example is given below for the primers replacing tyr
254 TAT with his CAT.

Forward primer: CACTACTTTCGGT**CAT**GGTGTTCAATGCTTTGCG. Reverse primer: TGAACACC**ATG**ACCGAAAGTAGTGACAAGTGTTGG. PCR: 30 cycles, annealing temperature 55°C, elongation time, 10 minutes.

Construction of *gfp* reporters with codon stretches

The positive control was *gfp*mut3 (stable *gfp*) (Cormack, Valdivia, & Falkow, 1996) under the control of P*trc* promoter, the transcription start site, *rbs* and ATG start codon are indicated in bold and underlined.

TTGACAATTAATCATCCGGCTCGTATAATGTGTGG**A**ATTGTGAGCGGATAACAATTTCACAC**AGGAAAC**AGCG
CCGC**ATG**CGTAAAGGAGAAGAACTTTTCACTGGAGTTGTCCCAATTCTTGTTGAATTAGATGGTGATGTTAATG
GGCACAAATTTTCTGTCAGTGGAGAGGGTGAAGGTGATGCAACATACGGAAAACTTACCCTTAAATTTATTTG
CACTACTGGAAAACTACCTGTTCCATGGCCAACACTTGTCACTACTTTCGGTTATGGTGTTCAATGCTTTGCGAG
ATACCCAGATCATATGAAACAGCATGACTTTTTCAAGAGTGCCATGCCCGAAGGTTATGTACAGGAAAGAACT
ATATTTTTCAAAGATGACGGGAACTACAAGACACGTGCTGAAGTCAAGTTTGAAGGTGATACCCTTGTTAATA
GAATCGAGTTAAAAGGTATTGATTTTAAAGAAGATGGAAACATTCTTGGACACAAATTGGAATACAACTATAA
CTCACACAATGTATACATCATGGCAGACAAACAAAAGAATGGAATCAAAGTTAACTTCAAAATTAGACACAAC
ATTGAAGATGGAAGCGTTCAACTAGCAGACCATTATCAACAAAATACTCCAATTGGCGATGGCCCTGTCCTTTT
ACCAGACAACCATTACCTGTCCACACAATCTGCCCTTTCGAAAGATCCCAACGAAAAGAGAGACCACATGGTCC
TTCTTGAGTTTGTAACAGCTGCTGGGATTACACATGGCATGGATGAACTATACAAATAA

For the tested codon stretches, 6 repeats of the desired codon were added just after the ATG start codon of *gfp*. The DNA fragments were ordered as double stranded *eblocks* from Integrated DNA technologies (IDT), and cloned into pTOPO-Blunt using kanamycin resistance, following the manufacturer's instructions.

For tests of sequence context surrounding tyrosine codons of *rsxA*, DNA was ordered from IDT and cloned into pTOPO as described for codon stretches above, based on the following amino acid sequences (tested sequences in bold):

VC1017RsxA *V. cholerae*

MLLLWQSRIMPGSEANIYITM**TEYLLL**LIGTVLVNNFVLVKFLGLCPFMGVSKKLETAIGMGLATTFVLTLASVCAYL
VESYVLRPLGI**EYLR**TMSFILVIAVVVQFTEMVVHKTSPT**LYRLL**GIFLPLITTNCAVLGVALLNINENHNFIQSIIYGFG
AAVGFSLVLILFASMRERIHVADVPAPFKGASIAMITAGLMSLAFMGFTGLVKL

RsxA *E. coli*

M**TDYLLL**FVGTVLVNNFVLVKFLGLCPFMGVSKKLETAMGMGLATTFVMTLASICAWLIDTWILIPLNLIYLRTLAFIL
VIAVVVQFTEMVVRKTSPV**LYRLL**GIFLPLITTNCAVLGVALLNINLGHNFLQSALYGFSAAVGFSLVMVLFAAIRERL
AVADVPAPFRGNAIALITAGLMSLAFMGFSGLVKL

Quantification of *gfp* fusion expression by fluorescent flow cytometry

Flow cytometry experiments were performed as described (Baharoglu et al., 2010) on overnight cultures and repeated at least 3 times. For each experiment, 50,000 to 100,000 events were counted on the Miltenyi MACSquant device. The mean fluorescence per cell was measured at the FITC channel for each reporter in both WT and *Δtgt* strains, and the relative fluorescence was calculated as the ratio of the mean fluorescence of a given reporter in *Δtgt* over the mean fluorescence of the same reporter in the WT. Native *gfp* (*gfpmut3*) was used as control.

Transcriptional fusion: *rsxA* promoter sequence was amplified using primers ZIP796/ZIP812. gfp was amplified from pZE1-*gfp* (Elowitz & Leibler, 2000) using primers ZIP813/ZIP200. The two fragments were PCR assembled into *PrsxA-gfp* using ZIP796/ZIP200 and cloned into pTOPO-TA cloning vector. The *PrsxA-gfp* fragment was then extracted using *EcoRI* and cloned into the low copy plasmid pSC101 (1 to 5 copies per cell). The plasmid was introduced into desired strains, and fluorescence was measured on indicated conditions, by counting 100,000 cells on the Miltenyi MACSquant device. Likewise, the control plasmid *Pc-gfp* (constitutive) was constructed using primers ZIP513/ZIP200 and similarly cloned in pSC101.

305 For translational fusions, the constitutive P*trc* promoter, the *rsxA* gene (without stop codon) with
306 desired codon usage fused to *gfp* (without ATG start codon) was ordered from IDT in the pUC-IDT
307 vector (carbenicillin resistant).
308 Native sequence of *V. cholerae rsxA* gene, called *rsxA*^{TAT}*gfp* in this manuscript is shown below. For
309 *rsxA*^{TAC}*gfp,* all tyrosine TAT codons were replaced with TAC.
310 ATGACCGAA**TAT**CTTTTGTTGTTAATCGGCACCGTGCTGGTCAATAACTTTGTACTGGTGAAGTTTTTGGGCTT
311 ATGTCCTTTTATGGGCGTATCAAAAAAACTAGAGACCGCCATTGGCATGGGGTTGGCGACGACATTCGTCCTC
312 ACCTTAGCTTCGGTGTGCGCT**TAT**CTGGTGGAAAGT**TAC**GTGTTACGTCCGCTCGGCATTGAG**TAT**CTGCGCA
313 CCATGAGCTTTATTTTGGTGATCGCTGTCGTAGTACAGTTCACCGAAATGGTGGTGCACAAAACCAGTCCGACA
314 CTC**TAT**CGCCTGCTGGGCATTTTCCTGCCACTCATCACCACCAACTGTGCGGTATTAGGGGTTGCGCTGCTCAA
315 CATCAACGAAAATCACAACTTTATTCAATCGATCATT**TAT**GGTTTTGGCGCTGCTGTTGGCTTCTCGCTGGTGCT
316 CATCTTGTTCGCTTCAATGCGTGAGCGAATCCATGTAGCCGATGTCCCCGCTCCCTTTAAGGGCGCATCCATTG
317 CGATGATCACCGCAGGTTTAATGTCTTTGGCCTTTATGGGCTTTACCGGATTGGTGAAACTGGCTAGC
318 *gfp*^{TAC} and *gfp*^{TAT} (tyrosine 11 TAT instead of 11 TAC) were ordered from IDT as synthetic genes under
319 the control of P*trc* promoter in the pUC-IDT plasmid (carbenicillin resistant). The complete sequence
320 of ordered fragments is indicated in Table S4, tyrosine codons are underlined.
321
322 **Construction of *bla* reporters**
323 Point mutations for codon replacements were performed using primer pairs where the desired
324 mutations were introduced and by whole plasmid PCR amplification on circular pTOPO-TA plasmid.
325 Primers are listed Table S4.
326
327 **Tolerance tests with *bla* reporters.**
328 A single colony from fresh transformation plates was inoculated in 24 well plates, each well containing
329 2 mL of MH. Cells were grown to early exponential phase without carbenicillin, and with or without
330 tobramycin 20% of MIC (TOB 0.2 µg/mL). After 2 hours of incubation at 37°C with shaking (early
331 exponential phase), dilutions were spotted in parallel on plates with or without carbenicillin (time T0).
332 Cultures were then treated with carbenicillin at 10xMIC (50 µg/mL) for 20 hours, at 37°C with shaking.
333 Dilutions were spotted on plates with or without carbenicillin. Surviving cells shown here are sensitive
334 to carbenicillin (no growth on carbenicillin containing plates), suggesting that increased or decreased
335 survival was due to increased (erroneous translation) or decreased (faithful translation) β-lactamase
336 activity at the time of treatment.
337
338 **Growth on microtiter plate reader for *bla* reporter assays**
339 Overnight cultures were diluted 1:500 in fresh MH medium, on 96 well plates. Each well contained 200
340 µL. Plates were incubated with shaking on TECAN plate reader device at 37°C, OD 600 nm was
341 measured every 15 min. Tobramycin was used at sub-MIC: TOB 0.2 µg/mL. Kanamycin and carbenicillin
342 were used at selective concentration: CRB 100 µg/mL, KAN 50 µg/mL.
343
344 **Protein extraction**
345 Overnight cultures of *V. cholerae* were diluted 1:100 in MH medium and grown with agitation at 37°C
346 until an OD 600 nm of 0.3 (exponential phase). 50 mL of these cultures were centrifuged for 10 min at
347 4°C and supernatant removed. Lysis was achieved by incubating cells in the presence of lysis buffer (10
348 mM Tris-HCl pH 8, 150 mM Nacl, 1% triton 100X) supplemented with 0.1 mg/mL lysozyme and
349 complete EDTA-free Protease Inhibitor Cocktail (Roche) for 1 hour on ice. Resuspensions were
350 sonicated 3x50 sec (power: 6, pulser: 90%), centrifuged for 1 h at 4°C at 5000 rpm and supernatants
351 were quantified using Pierce™ BCA Protein Assay Kit (Cat. No 23225) following the manufacturer's
352 instructions. Proteins were then stored at -80°C.
353
354 **Proteomics MS and analysis**
355 *Sample preparation for MS*

356 Tryptic digestion was performed using eFASP (enhanced Filter-Aided Sample Preparation) protocol
357 (Erde, Loo, & Loo, 2014). All steps were done in 30 kDa Amicon Ultra 0.5 mL filters (Millipore). Briefly,
358 the sample was diluted with a 8M Urea, 100 mM ammonium bicarbonate buffer to obtain a final urea
359 concentration of 6 M. Samples were reduced for 30 min at room temperature (RT) with 5 mM TCEP.
360 Subsequently, proteins were alkylated in 5 mM iodoacetamide for 1 hour in the darkness at RT and
361 digested overnight at 37°C with 1 µg trypsin (Trypsin Gold Mass Spectrometry Grade, Promega).
362 Peptides were recovered by centrifugation, concentrated to dryness and resuspended in 2%
363 acetonitrile (ACN)/0.1% FA just prior to LC-MS injection.
364 *LC-MS/MS analysis*
365 Samples were analyzed on a high-resolution mass spectrometer, Q Exactive™ Plus Hybrid Quadrupole-
366 Orbitrap™ Mass Spectrometer (Thermo Scientific), coupled with an EASY 1200 nLC system (Thermo
367 Fisher Scientific, Bremen). One µg of peptides was injected onto a home-made 50 cm C18 column (1.9
368 µm particles, 100 Å pore size, ReproSil-Pur Basic C18, Dr. Maisch GmbH, Ammerbuch-Entringen,
369 Germany). Column equilibration and peptide loading were done at 900 bars in buffer A (0.1% FA).
370 Peptides were separated with a multi-step gradient from 3 to 22 % buffer B (80% ACN, 0.1% FA) in 160
371 min, 22 to 50 % buffer B in 70 min, 50 to 90 % buffer B in 5 min at a flow rate of 250 nL/min. Column
372 temperature was set to 60°C. The Q Exactive™ Plus Hybrid Quadrupole-Orbitrap™ Mass Spectrometer
373 (Thermo Scientific) was operated in data-dependent mode using a Full MS/ddMS2 Top 10 experiment.
374 MS scans were acquired at a resolution of 70,000 and MS/MS scans (fixed first mass 100 m/z) at a
375 resolution of 17,500. The AGC target and maximum injection time for the survey scans and the MS/MS
376 scans were set to 3E6, 20ms and 1E6, 60ms, respectively. An automatic selection of the 10 most intense
377 precursor ions was activated (Top 10) with a 35 s dynamic exclusion. The isolation window was set to
378 1.6 m/z and normalized collision energy fixed to 27 for HCD fragmentation. We used an underfill ratio
379 of 1.0 % corresponding to an intensity threshold of 1.7E5. Unassigned precursor ion charge states as
380 well as 1, 7, 8 and >8 charged states were rejected and peptide match was disable.
381 *Data analysis*
382 Acquired Raw data were analyzed using MaxQuant 1.5.3.8 version (Cox et al., 2011) using the
383 Andromeda search engine (Tyanova, Temu, & Cox, 2016) against *Vibrio cholerae* Uniprot reference
384 proteome database (3,782 entries, download date 2020-02-21) concatenated with usual known mass
385 spectrometry contaminants and reversed sequences of all entries. All searches were performed with
386 oxidation of methionine and protein N-terminal acetylation as variable modifications and cysteine
387 carbamidomethylation as fixed modification. Trypsin was selected as protease allowing for up to two
388 missed cleavages. The minimum peptide length was set to 5 amino acids. The false discovery rate (FDR)
389 for peptide and protein identification was set to 0.01. The main search peptide tolerance was set to
390 4.5 ppm and to 20 ppm for the MS/MS match tolerance. One unique peptide to the protein group was
391 required for the protein identification. A false discovery rate cut-off of 1 % was applied at the peptide
392 and protein levels.
393 The statistical analysis of the proteomics data was performed as follows: three biological replicates
394 were acquired per condition. To highlight significantly differentially abundant proteins between two
395 conditions, differential analyses were conducted through the following data analysis pipeline: (1)
396 deleting the reverse and potential contaminant proteins; (2) keeping only proteins with at least two
397 quantified values in one of the three compared conditions to limit misidentifications and ensure a
398 minimum of replicability; (3) log2-transformation of the remaining intensities of proteins; (4)
399 normalizing the intensities by median centering within conditions thanks to the normalizeD function
400 of the R package DAPAR (Wieczorek et al., 2017), (5) putting aside proteins without any value in one
401 of both compared conditions: as they are quantitatively present in a condition and absent in another,
402 they are considered as differentially abundant proteins and (6) performing statistical differential
403 analysis on them by requiring a minimum fold-change of 2.5 between conditions and by using a LIMMA
404 t test (Ritchie et al., 2015) combined with an adaptive Benjamini-Hochberg correction of the *p*-values
405 thanks to the adjust.p function of the R package cp4p (Giai Gianetto et al., 2016). The robust method
406 of Pounds and Cheng was used to estimate the proportion of true null hypotheses among the set of
407 statistical tests (Pounds & Cheng, 2006). The proteins associated with an adjusted *p*- value inferior to

408 an FDR level of 1% have been considered as significantly differentially abundant proteins. Finally, the
409 proteins of interest are therefore the proteins that emerge from this statistical analysis supplemented
410 by those being quantitatively absent from one condition and present in another. The mass
411 spectrometry proteomics data have been deposited to the ProteomeXchange Consortium via the
412 PRIDE partner repository with the dataset identifier PXD035297.
413
414 **RNA purification for RNA-seq**
415 Cultures were diluted 1000X and grown in triplicate in MH supplemented or not with 0.6 µg/ml of
416 tobramycin, corresponding to 50% of the MIC in liquid cultures, to an OD 600nm of 0.4. RNA was
417 purified with the RNAeasy mini kit (Qiagen) according to manufacturer's instructions. Briefly, 4 ml of
418 RNA-protect (Qiagen) reagent were added on 2 ml of bacterial cultures during 5 minutes. After
419 centrifugation, the pellets were conserved at -80°C until extraction. Protocol 2 of the RNA protect
420 Bacteria Reagent Handbook was performed, with the addition of a proteinase K digestion step, such
421 as described in the protocol 4. Quality of RNA was controlled using the Bioanalyzer. Sample collection,
422 total RNA extraction, library preparation, sequencing and analysis were performed as previously
423 described (Krin et al., 2018). The data for this RNA-seq study has been submitted in the GenBank
424 repository under the project number GSE214520.

425 **Gene Ontology (GO) enrichment analysis**
426 GO enrichment analyses were performed on http://geneontology.org/ as follows: Binomial test was
427 used to determine whether a group of genes in the tested list was more or less enriched than expected
428 in a reference group. The annotation dataset used for the analysis was GO biological process complete.
429 The analyzed lists were for each condition (MH/TOB), genes (**Table S3**) with at least 2-fold change in
430 RNA-seq data of WT strain compared to *Δtgt*, and with an adjusted p-value <0,05. The total number of
431 uploaded gene list to be analyzed were 53 genes for MH and 60 genes for TOB. The reference gene list
432 was *Vibrio cholerae* (all genes in database), 3782 genes. Annotation Version: PANTHER
433 Overrepresentation Test (Released 20220712). GO Ontology database DOI: 10.5281/zenodo.6399963
434 Released 2022-03-22
435
436 **Stringent response measurement**
437 *P1rrnB-gfp* fusion was constructed using *gfp* ASV (Andersen et al., 1998), and cloned into plasmid
438 pSC101. *P1rrnB-GFPasv* transcriptional fusion was amplified from strain R438 (E. coli MG1655
439 *attB::P1rrnB gfp-ASV::kan* provided by Ivan Matic) using primers AFC060 and AFC055, thus including
440 42 bp upstream of *rrnB* transcription initiation site. PCR product was then cloned in pTOPOblunt vector
441 and subcloned to pSC101 by *EcoRI* digestion and ligation. The final construct was confirmed by Sanger
442 sequencing. The plasmid was then introduced by electroporation into the tested strains. Overnight
443 cultures were performed in MH + carbenicillin 100 µg/mL and diluted 500x in 10 mL fresh MH or MH+
444 TOB 0.4 µg/mL, in an Erlenmeyer. At time points 0 min, and every 30 during 3 hours, the OD 600 nm
445 was measured and fluorescence was quantified in flow cytometry. For each experiment, 50,000 to
446 100,000 events were counted on the Miltenyi MACSquant device.
447
448 **tRNA enriched RNA extraction**
449 Overnight cultures of *V. cholerae* were diluted 1:1000 in MH medium and grown in aerobic conditions,
450 with 180 rotations per minute at 37°C until an OD 600 nm of 0.5. tRNA enriched RNA extracts were
451 prepared using room temperature TRIzol™ reagent as described (Galvanin, Ayadi, Helm, Motorin, &
452 Marchand, 2019) and contaminating DNA were eliminated using TURBO DNA-free Kit (Ambion). RNA
453 concentration was controlled by UV absorbance using NanoDrop 2000c (Thermo Fisher Scientific). The
454 profile of isolated tRNA fractions was assessed by capillary electrophoresis using an RNA 6000 Pico
455 chip on Bioanalyzer 2100 (Agilent Technologies).
456
457 **tRNA-enriched sample digestion for quantitative analysis of queuosine by mass spectrometry**

458 Purified tRNA enriched RNA fractions were digested to single nucleosides using the New England
459 BioLabs Nucleoside digestion mix (Cat No. M0649S). 10µl of the RNA samples diluted in ultrapure water
460 to 100 ng/µL were mixed with 1µL of enzyme, 2µl of Nucleoside Digestion Mix Reaction Buffer (10X) in
461 a final volume of 20 µL in nuclease-free 1.5 mL tubes. Tubes were wrapped with parafilm to prevent
462 evaporation and incubated at 37°C overnight.
463
464 **Queuosine quantification by LC-MS/MS**
465 Analysis of global levels of queuosine (Q) was performed on a Q exactive mass spectrometer (Thermo
466 Fisher Scientific). It was equipped with an electrospray ionization source (H-ESI II Probe) coupled with
467 an Ultimate 3000 RS HPLC (Thermo Fisher Scientific). The Q standard was purchased from Epitoire
468 (Singapore).
469 Digested RNA was injected onto a ThermoFisher Hypersil Gold aQ chromatography column (100 mm *
470 2.1 mm, 1.9 µm particle size) heated at 30°C. The flow rate was set at 0.3 mL/min and run with an
471 isocratic eluent of 1% acetonitrile in water with 0.1% formic acid for 10 minutes.
472 Parent ions were fragmented in positive ion mode with 10% normalized collision energy in parallel-
473 reaction monitoring (PRM) mode. MS2 resolution was 17,500 with an AGC target of 2e5, a maximum
474 injection time of 50 ms, and an isolation window of 1.0 m/z.
475 The inclusion list contained the following masses: G (284.1) and Q (410.2). Extracted ion
476 chromatograms of base fragments (±5ppm) were used for detection and quantification (152.0565 Da
477 for G; 295.1028 Da for Q). The secondary base fragment 163.0608 was also used to confirm Q detection
478 but not for quantification.
479 Calibration curves were previously generated using synthetic standards in the ranges of 0.2 to 40 pmol
480 injected for G and 0.01 to 1 pmol for Q. Results are expressed as a percentage of total G.
481
482 **Queuosine detection by sequencing**
483 The detection of queuosine was performed as described in (Katanski et al., 2022). Briefly, 200 ng of
484 total RNA were subjected to oxidation by 45 mM of $NaIO_4$ in 50 mM AcONa pH 5.2 buffer for 1h at
485 37°C. The reaction was quenched by addition of 36 mM glucose and incubation for 30 min at 37°C and
486 RNA was precipitated with absolute ethanol. After precipitation and two washes by 80% ethanol, the
487 RNA pellet was resuspended in 3' ligation reaction buffer 1x and subjected to library preparation using
488 the NEBNext® Small RNA Library Prep Set for Illumina® (NEB, #E7330S). Specific primers for *V. cholerae*
489 tRNAAsn_GUU1, tRNAAsn_GUU2, tRNAAsp_GUC, tRNATyr_GUA and tRNAHis_GUG were hybridized
490 instead of RT primer used in NEBNext® Small RNA Library Prep kit, under the same hybridization
491 conditions. The 5'-SR adaptor was ligated, and reverse transcription was performed for 1h at 50°C
492 followed by 10 min at 80°C using Superscript IV RT (instead of Protoscript II used in the kit). PCR
493 amplification was performed as described in the manufacturer's protocol. Libraries were qualified
494 using Tapestation 4150 and quantified using Qubit fluorometer. Libraries were multiplexed and
495 sequenced in a 50 bp single read mode using NextSeq2000 (Illumina, San Diego).

496 Bioinformatic analysis was performed by trimming of raw reads using trimmomatic v0.39 to remove
497 adapter sequences as well as very short and low-quality sequencing reads. Alignment was done by
498 bowtie2 (v2.4.4) in End-to-End mode with *--mp 2 --rdg 0,2* options to favor retention of reads with
499 deletions, only non-ambiguously mapped reads were taken for further analysis. Coverage file was
500 created with *samtools mpileup* and deletion signature extracted for every position using custom R
501 script. Deletion score was calculated as number of deletions divided by number of matching
502 nucleotides at a given position. Analysis of Q tRNA modification in *V. cholerae* strains was performed
503 in triplicate for biological replicates with technical duplicate for each sample.

504 **Analysis of Queuosine tRNA Modification Using APB Northern Blot Assay**
505 Quantification of queuosine in tRNA-Tyr from purified tRNA-enriched RNA fractions was performed
506 using a non-radioactive Northern blot method: the procedure for pouring and running N-acryloyl-3-
507 aminophenylboronic acid (APB) gels was based on the method detailed in (Cirzi & Tuorto, 2021). tRNA-

508 Tyr were detected using the following 3'-end digoxigenin (DIG)-labeled probe: 5' -
509 CTTTGGCCACTCGGGAACCCCTCC - 3'DIG.
510 For 1 gel, ABP gel buffer was prepared by mixing 4.2g urea, 50mg 3-(Acrylamido) phenylboronic acid
511 (Sigma Aldrich Cat No. 771465), 1ml 10X RNase-free TAE, 3.2ml 30% acrylamide and bis-acrylamide
512 solution 37.5:1 and adding water to adjust the final volume to 10ml. After stirring to facilitate
513 dissolution and right before pouring, 10µl TEMED and 60 µL 10% APS were added to the 10ml ABP
514 buffer to catalyze and initiate polymerization respectively. Gels were casted using the Mini-PROTEAN®
515 Bio-Rad handcast system, short plates (70x100 mm), 0.75 mm spacers and 10-well gel combs. Gels
516 were left to polymerize at room temperature for 50 minutes.
517 Alkaline hydrolysis in 100mM of Tris-HCl pH 9 of our tRNA-enriched RNA extracts was carried out at
518 37°C for 30 min to break the ester bonds between tRNAs and their cognate amino acids. 10µl of the
519 deacylated tRNA-enriched RNA samples were mixed with 8 µl of 2X RNA loading dye (Thermo
520 Scientific™ Cat No. R0641), denatured for 3 min at 72°C and the whole volume was loaded onto the
521 gel. Electrophoresis of the gels were carried out in the Mini-PROTEAN® Tetra Vertical Electrophoresis
522 Cell for 30 min at 85V at room temperature followed by 1h30 at 140 V at 4°C. Gels were incubated at
523 room temperature for 15 min with shaking in 50 ml 1X RNAse-free TAE mixed with 10 µl of 10000X
524 SYBR Gold nucleic acid staining solution (Invitrogen™ S11494) and nucleic acids were visualized using
525 a transilluminator. Transfers of the nucleic acids to positively charged nylon membranes were
526 performed at 5 V/gel for 40 min at room temperature using a semi dry blotting system. RNAs were
527 crosslinked to the membrane surface through exposure to 254 nm UV light at a dose of 1.2 Joules.
528 Membranes were transferred into glass bottles containing 5ml of pre-warmed hybridization buffer and
529 incubated for 1 hour at 42°C at a constant rotation in a hybridization oven. Hybridization buffer was
530 obtained by mixing 12.3 ml of 20X SSX, 1ml of 1M Na2HPO4 pH7.2, 17.5ml of 20% SDS, 2ml of 50X
531 Denhardt's solution and 17ml RNase-free H2O. 3µl of the DIG-labeled probe solution at 100 pmol/µl
532 were then added into the 5ml hybridization buffer and the bottles were rotated in the hybridization
533 oven at 42°C overnight. Membranes were washed 2 time with 2X SSC/5% SDS for 15 min at 42°C and
534 1 time with 1X SSC/1% SDS for 15min at 42°C.
535 Nucleic acids wash and immunological detection of the DIG-labeled probes were performed using the
536 DIG Wash and Block Buffer Set (Roche, Cat No. 11585762001) according to the manufacturer's
537 protocols. Membranes were placed in a plastic container filled with 15ml of the blocking solution for
538 nonspecific binding sites blocking. After 30min incubation at room temperature with rotation, 3µl of
539 the alkaline phosphatase-coupled anti-DIG antibody (Fab fragments, Roche, Cat No. 11093274910)
540 were added to the buffer and incubation at room temperature on a belly-dancer was allowed for 30
541 more min. Next, membranes were washed 3 times 15 min with DIG-wash buffer and once with DIG-
542 detection buffer for 5min. For chemiluminescence visualization of the probe, 1ml of CDP-Star®
543 Chemiluminescent Substrate (Disodium 2-chloro-5-(4-methoxyspiro[1,2-dioxetane-3,2'-(5-
544 chlorotricyclo[3.3.1.13.7]decan])-4-yl]-1-phenyl phosphate) (Roche, Cat No. 11685627001) was added
545 to 9ml of DIG-detection buffer and membranes were then incubated with the substrate for 5 min. The
546 chemiluminescent signal was detected with the iBright Imaging Systems.
547 **Ribosome profiling (Ribo-seq)**
548 Pellet from 200 ml of *Vibrio cholerae* at 0.25 OD_{600nm} WT or mutant *Δtgt* in triplicates, with or without
549 tobramycin were flash frozen in liquid nitrogen and stored at -80°C. The polysomes were extracted
550 with 200 µl of extraction buffer (20 mM Tris pH8-150 mM $Mg(CH_3COO)_2$-100 mM NH_4Cl, 5 mM $CaCl_2$-
551 0,4% Triton X100-1% Nonidet P40) added of 2x cocktail anti proteases Roche and 60U RNase Inhibitor
552 Murine to the buffer, DNase I and glass beads (diameter <106 micrometers), vortexed during 30 min
553 at 4°C. The supernatant of this crude extract was centrifugated 10 min at 21 krcf at +4°C. The
554 absorbance was measured at 260nm on 1 µl from 1/10 extract. After 1 hour of digestion at 25°C with
555 0.75 U MNase/0.025 UA_{260nm} of crude extract, the reaction was stopped by the addition of 3 µl 0.5 M
556 EGTA pH8. The monosomes generated by digestion were purified through a 24% sucrose cushion
557 centrifuged 90 min at 110 krpm on a TLA110 rotor at +4°C. The monosomes pellet was rinsed with 200
558 µl of resuspension buffer (20 mM Tris-HCl pH 7,4 - 100 mM NH_4Cl - 15 mM $Mg(CH_3COO)_2$ - 5 mM $CaCl_2$

559) and then recovered with 100 µl. RNA were extracted by acid phenol at 65°C, $CHCL_3$ and precipitated
560 by Ethanol with 0.3M CH_3COONa pH 5.2. Resuspended RNA was loaded on 17% polyacrylamide (19 :1);
561 7 M urea in 1x TAE buffer at 100 V during 6 hours and stained with SYBRgold. RNA fragments
562 corresponding to 28-34 nt were retrieved from gel and precipitated in ethanol with 0.3 M CH_3COONa
563 pH 5.2 in presence of 100 µg glycogen. rRNA were depleted using MicrobExpress Bacterial mRNA
564 Enrichment kit from Invitrogen. The supernatant containing the ribosome footprints were recovered
565 and RNA were precipitated in ethanol in presence of glycogen overnight at -20°C. The RNA
566 concentration was measured by Quant-iT microRNA assay kit (Invitrogen). The RNA was
567 dephosphorylated in 3' and then phosphorylated in 5' to generate cDNA libraries using the NebNext
568 Small RNA Sample Prep kit with 3' sRNA Adapter (Illumina) according to the manufacturer's protocol
569 with 12 cycles of PCR amplification in the last step followed by DNA purification with Monarch PCR
570 DNA cleanup kit (NEB). Library molarity was measured with the Qubit DNAds HS assay kit from
571 Invitrogen and the quality was analyzed using Bioanalyzer DNA Analysis kit (Agilent) and an equimolar
572 pool of the 12 libraries was sequenced by the High-throughput sequencing facility of I2BC with NextSeq
573 500/550 High output kit V2 (75 cycles) (Illumina) with 10 % PhiX.
574 Sequencing data is available at GSE231087.
575
576 **Analysis of ribosome profiling data**
577 RiboSeq analysis was performed using the RiboDoc package (Francois, Arbes, Demais, Baudin-Baillieu,
578 & Namy, 2021) for statistical analysis of differential gene expression (DEseq2). Sequencing reads are
579 first trimmed to remove adaptors then aligned to the two *V. cholerae* chromosomes (NC_002505 and
580 NC_002506). Reads aligned uniquely are used to perform the differential gene expression analysis.
581 MNase shows significant sequence specificity at A and T (Dingwall, Lomonossoff, & Laskey, 1981). Due
582 to this specificity and A-T biases in *V. cholerae* genome, ribosome profiling data exhibit a high level of
583 noise that prevents the obtention of a resolution at the nucleotide level. The effect of ribosome stalling
584 at TAT codons on total mRNA ribosome occupancy is likely highly variable, depending on the location
585 of the TAT codon(s) within the CDS and the gene's expression level. We therefore interpreted genes in
586 the "Up" category as ones that mainly correspond to genes that are more translated because the
587 impact of pausing at TAT codons is probably not strong enough.
588
589 **UV sensitivity measurements**
590 Overnight cultures were diluted 1:100 in MH medium and grown with agitation at 37°C until an OD
591 600 nm of 0.5-0.7. Appropriate dilutions were then plated on MH agar. The proportion of growing CFUs
592 after irradiation at 60 Joules over total population before irradiation was calculated, doing a ratio with
593 total CFUs. Experiments were performed 3 to 8 times.
594
595 **Quantification and statistical analysis**
596 For comparisons between 2 groups, first an F-test was performed in order to determine whether
597 variances are equal or different between comparisons. For comparisons with equal variance, Student's
598 t-test was used. For comparisons with significantly different variances, we used Welch's t-test. For
599 multiple comparisons, we used ANOVA to determine the statistical differences (*p*-value) between
600 groups. **** means $p<0.0001$, *** means $p<0.001$, ** means $p<0.01$, * means $p<0.05$. For survival
601 tests, data were first log transformed in order to achieve normal distribution, and statistical tests were
602 performed on these log-transformed data. The number of replicates for each experiment was $3<n<6$.
603 Means and geometric means for logarithmic values were also calculated using GraphPad Prism.
604
605 **Bioinformatic analysis for whole genome codon bias determinations**
606 *Data.* Genomic data (fasta files containing CDS sequences and their translation, and GFF annotations)
607 for *Vibrio cholerae* (assembly ASM674v1) were downloaded from the NCBI FTP site
608 (ftp://ftp.ncbi.nlm.nih.gov).

Codon counting. For each gene, the codons were counted in the CDS sequence, assuming it to be in-frame. This step was performed using Python 3.8.3, with the help of the Mappy 2.20 (Li, 2018) and Pandas 1.2.4 (McKinney, 2010; Reback J, 2021) libraries.

Gene filtering. Genes whose CDS did not start with a valid start codon were excluded from further computations. A valid start codon is one among ATA, ATC, ATG, ATT, CTG, GTG, TTG, according to the genetic code for bacteria, archaea and plastids (translation table 11 provided by the NCBI at ftp://ftp.ncbi.nlm.nih.gov/entrez/misc/data/gc.prt). Further computations were performed on 3590 genes that had a valid start codon.

Codon usage bias computation. The global codon counts were computed for each codon by summing over the above selected genes. For each gene as well as for the global total, the codons were grouped by encoded amino acid. Within each group, the proportion of each codon was computed by dividing its count by the sum of the counts of the codons in the group. The codon usage bias for a given codon and a given gene was then computed by subtracting the corresponding proportion obtained from the global counts from the proportion obtained for this gene. Codon usage biases were then standardized by dividing each of the above difference by the standard deviation of these differences across all genes, resulting in standardized codon usage biases "by amino acid" ("SCUB by aa" in short). All these computations were performed using the already mentioned Pandas 1.2.4 Python library.

Associating genes to their preferred codon. For each codon group, genes were associated to the codon for which they had the highest "SCUB by aa" value. This defined a series of gene clusters denoted using the "aa_codon" pattern. For instance, "*_TAT" contains the genes for which TAT is the codon with the highest standardized usage bias among tyrosine codons.

Extracting most positively biased genes from each cluster. Within each cluster, the distribution of "SCUB by aa" values for each codon was represented using violin plots. Visual inspections of these violin plots revealed that in most cases, the distribution was multi-modal. An automated method was devised to further extract from a given cluster the genes corresponding to the sub-group with the highest "SCUB by aa" for each codon. This was done by estimating a density distribution for "SCUB by aa" values using a Gaussian Kernel Density Estimate and finding a minimum in this distribution. The location of this minimum was used as a threshold above which genes were considered to belong to the most positively biased genes. This was done using the SciPy 1.7.0 (Virtanen et al., 2020) Python library. Violin plots were generated using the Matplotlib 3.4.2 (JD., 2007) and Seaborn 0.11.1 (ML, 2021) Python libraries.

Code availability. All codes to perform these analyses were implemented in the form of Python scripts, Jupyter notebooks (Kluyver T, 2016) and Snakemake (Molder et al., 2021) workflows, and are available in the following git repository: https://gitlab.pasteur.fr/bli/17009_only. Data are available for whole genome codon usage of *V. cholerae* in excel sheet and *V. cholerae* codon usage biased gene lists at zenodo public repository with the following doi: 10.5281/zenodo.6875293.

Results

Tobramycin tolerance is decreased in *Δtgt* without any difference in uptake

We performed competition experiments of *Δtgt* against the WT strain in the absence of stress and with various stresses including antibiotics (tobramycin, ciprofloxacin, carbenicillin) and oxidative agents (paraquat, H_2O_2). We confirmed *V. cholerae Δtgt* strain's growth defect in low-dose tobramycin (sub-MIC TOB) (**Fig. 1A**) and that expression of *tgt* in trans restores growth in these conditions (**Fig. 1B**). We further tested tolerance to lethal antibiotic concentrations by measuring survival after antibiotic treatment during 15 minutes to 4 hours with antibiotics at 5-times or 10-times the minimal inhibitory concentration. As expected, *Δtgt* is less tolerant than WT to tobramycin (**Fig. 1CD**), but had no impact in ciprofloxacin (CIP) or carbenicillin (CRB) (**Fig. 1EF**).

We asked whether the growth defect of *Δtgt* is due to increased aminoglycoside entry and/or a change in proton-motive force (PMF) (Carvalho, Mazel, & Baharoglu, 2021; Lang et al., 2021). We used a *ΔtolA* strain as a positive control for disruption of outer membrane integrity and aminoglycoside uptake (Rivera, Hancock, Sawyer, Haug, & McGroarty, 1988). No changes either in proton-motive force

661 (**Fig. 1G**), nor in uptake of the fluorescent aminoglycoside molecule Neomycin-Cy5 (**Fig. 1H**) (Sabeti
662 Azad et al., 2020) were detected in the *Δtgt* strain, indicating that the increased susceptibility of *Δtgt*
663 to TOB is not due to increased aminoglycoside entry into the *V. cholerae* cell.
664
665 **Overexpression of the canonical $tRNA^{Tyr}_{GUA}$ rescues growth of *Δtgt* in TOB**
666 We next investigated whether all four tRNAs with GUN anticodon modified to QUN by Tgt, are
667 equally important for the TOB sensitivity phenotype of the *Δtgt* mutant: Aspartate (Asp)/Asparagine
668 (Asn)/Tyrosine (Tyr)/Histidine (His). The absence of Q34 could have direct effects at the level of codon
669 decoding but also indirect effects such as influencing tRNAs' degradation (Kimura & Waldor, 2019).
670 qRT-PCR analysis of $tRNA^{Tyr}$ levels showed no major differences between WT and *Δtgt* strains, making
671 it unlikely that the effect of Q34 modification on codon decoding is caused by altered synthesis or
672 degradation of $tRNA^{Tyr}$ (**Sup. Fig. S1A**). The levels of the other three tRNAs modified by Tgt also
673 remained unchanged (**Sup. Fig. S1A**). These results do not however exclude a more subtle or
674 heterogeneous effect of Q34 modification on tRNA levels, which would be below the detection limits
675 of the technique in a bacterial whole population.
676 We next adopted a tRNA overexpression strategy from a high copy plasmid. The following tRNAs-
677 $_{GUN}$ are the canonical tRNAs which are present in the genome: Tyr_{GUA} (codon TAC), His_{GUG} (codon CAC),
678 two isoforms of Asn_{GUU} (codon AAC), Asp_{GUC} (codon GAT). The following tRNAs-$_{AUN}$ are synthetic tRNAs
679 which are not present in the genome: Tyr_{AUA}, His_{AUG}, Asn_{AUU}, Asp_{AUC}. $tRNA^{Phe}_{GAA}$ was also used as non
680 Tgt-modified control. Overexpression of $tRNA^{Tyr}_{GUA}$, but not $tRNA^{Tyr}_{AUA}$ rescues the *Δtgt* mutant's
681 growth defect in sub-MIC TOB (**Fig. 1I**). Overexpression of $tRNA^{His}_{AUG}$ also seemed to confer a benefit
682 compared to empty plasmid (p0), but not as strong as $tRNA^{Tyr}_{GUA}$ (**Sup. Fig. S1B**). We do not observe
683 any major rescue of tobramycin sensitive phenotypes when the other tRNAs are overexpressed,
684 suggesting that changes in Tyr codon decoding is mostly responsible for the *Δtgt* mutant's tobramycin
685 susceptibility phenotype.
686
687 **Q modification influences amino acid incorporation at tyrosine codons**
688 We decided to measure the efficiency of amino acid incorporation at corresponding codons in *Δtgt*,
689 using *gfp* reporters. First, we confirmed that GFP fluorescence from native GFP (encoded by *gfpmut3*)
690 is not affected in *Δtgt* compared to WT (*gfp+* in **Fig. 2**), indicating that there are no major differences
691 on expression or folding of the GFP in *Δtgt*. We next constructed *gfp* fluorescent reporters by
692 introducing within their coding sequence, stretches of repeated identical codons, for Asp/Asn/Tyr/His.
693 This set of reporters revealed that the absence of Q34 leads to an increase of amino acid incorporation
694 at Tyr TAT codons, both without and with tobramycin (**Fig. 2A** NT and TOB). This was not the case for
695 Asp (**Fig. 2B**), nor for Asn (**Fig. 2D**), and we observed a slighter and more variable change for His (**Fig.
696 2C**). No significant effect of *tgt* was observed for 2nd near-cognate codons obtained by changing 1 base
697 of the triplet for TAC and TAT codons **(Fig. 2E**): Phe TTC/TTT, Cys TGT/TGC, Ser TCT/TCC (the 3rd near-
698 cognate stop codons TAA and TAG were not tested in this setup). Thus, Q34 modification strongly
699 impacts the decoding of Tyr codons, and to a lesser extent His codons in this reporter system.
700 We also tested decoding reporters for TAT/TAC in WT and *Δtgt* overexpressing $tRNA^{Tyr}$ in trans (**Fig.
701 S1C**). The presence of the plasmid (empty p0) amplified differences between the two strains with
702 decreased decoding of TAC (and increased TAT, as expected) in *Δtgt* compared to WT. Overexpression
703 of $tRNA^{Tyr}_{GUA}$ did not significantly impact decoding of TAT and increased decoding of TAC, as expected.
704 Since overexpression of $tRNA^{Tyr}_{GUA}$ rescues *Δtgt* in tobramycin (Fig. 1I) and facilitates TAC decoding,
705 this suggests that issues with TAC codon decoding contribute to the fitness defect observed in *Δtgt*
706 upon growth with tobramycin. Overexpression of $tRNA^{Tyr}_{AUA}$ increased decoding of TAT in WT but did
707 not change it in *Δtgt* where it is already high. Unexpectedly, overexpression of $tRNA^{Tyr}_{AUA}$ also increased
708 decoding of TAC in WT. Thus, overexpression of $tRNA^{Tyr}_{AUA}$ possibly changes the equilibrium between
709 the decoding of TAC vs TAT and may restore translation of TAC enriched transcripts.
710 GFP reporters tested above with codon stretches were pivotal for the identification of codons for
711 which decoding efficiency differs between WT and *Δtgt*, even though it's not a natural setup. We next
712 developed a biologically relevant β-lactamase reporter tool to assess differences in the decoding of

713 the tyrosine codons in WT and *Δtg*t strains. The amino acids Tyr103 and Asp129 of the β-lactamase,
714 were previously shown to be important for its function in resistance to β-lactam antibiotics, such as
715 carbenicillin (Doucet, De Wals, & Pelletier, 2004; Escobar, Miller, & Fink, 1994; Jacob, Joris, Lepage,
716 Dusart, & Frere, 1990).
717 We replaced the native Tyr103 TAC with the synonymous codon Tyr103 TAT (**Fig. 3A**). While in the
718 WT, both versions of β-lactamase conferred similar growth in carbenicillin with or without sub-MIC
719 TOB, in the *Δtgt* strain the Tyr-TAT version grows better than the Tyr TAC version upon exposure to
720 TOB stress. This suggests a more efficient translation of the Tyr103 TAT β-lactamase mRNA, compared
721 to the native Tyr103 TAC version, in stressed *Δtgt* strain.
722 Like Tyr103, Asp129 was shown to be important for resistance to β-lactams (Doucet et al., 2004;
723 Escobar et al., 1994; Jacob et al., 1990). When we replaced the native Asp129 GAT with the
724 synonymous codon Asp129 GAC, the GAC version did not appear to produce functional β-lactamase in
725 *Δtgt* (**Fig. 3B**), suggesting increased mistranslation or inefficient decoding of the GAC codon by $tRNA^{Asp}$
726 in the absence of Q. Decoding of GAT codon was also affected in *Δtgt* in the presence of tobramycin.

727 **Q modification impacts decoding fidelity in *V. cholerae*.**

728 To test whether a defect in Q34 modification influences the fidelity of translation in the presence
729 and absence of tobramycin, previously developed reporter tools were used (Fabret & Namy, 2021), to
730 measure stop codons readthrough in *V. cholerae Δtgt* and wild-type strains. The system consists of
731 vectors containing readthrough promoting signals inserted between the *lacZ* and *luc* sequences,
732 encoding β-galactosidase and luciferase, respectively. Luciferase activity reflects the readthrough
733 efficiency, while β-galactosidase activity serves as an internal control of expression level, integrating a
734 number of possible sources of variability (plasmid copy number, transcriptional activity, mRNA
735 stability, and translation rate). We found increased readthrough at stop codons UAA and to a lesser
736 extent at UAG for *Δtgt*, and this increase was amplified for UAG in presence of tobramycin (**Fig. S2,**
737 **stop readthrough**). In the case of UAA, tobramycin appears to decrease readthrough, this may be
738 artefactual, due to the toxic effect of tobramycin on *Δtgt*.

739 Mistranslation at specific codons can also impact protein synthesis. To further investigate
740 mistranslation levels by $tRNA^{Tyr}$ in WT and *Δtgt*, we designed a set of *gfp* mutants where the codon for
741 the catalytic tyrosine required for fluorescence (TAT at position 66) was substituted by near-cognate
742 codons (**Fig. S2**). Results suggest that in this sequence context, particularly in the presence of
743 tobramycin, non-modified $tRNA^{Tyr}$ mistakenly decodes Asp GAC, His CAC and also Ser UCC, Ala GCU,
744 Gly GGU, Leu CUU and Val GUC codons, suggesting that Q34 increases the fidelity of $tRNA^{Tyr}$.
745 In parallel, we replaced Tyr103 of the β-lactamase described above, with Asp codons GAT or GAC.
746 The expression of the resulting mutant β-lactamase is expected to yield a carbenicillin sensitive
747 phenotype. In this system, increased tyrosine misincorporation (more mistakes) by $tRNA^{Tyr}$ at the
748 mutated Asp codon, will lead to increased synthesis of active β-lactamase, which can be evaluated by
749 carbenicillin tolerance tests. As such, amino-acid misincorporation leads here to phenotypic (transient)
750 tolerance, while genetic reversion mutations result in resistance (growth on carbenicillin). The
751 rationale is summarized in **Fig. 3C**. When the Tyr103 codon was replaced with either Asp codons, we
752 observe increased β-lactamase tolerance (**Fig. 3D, left**), suggesting increased misincorporation of
753 tyrosine by $tRNA^{Tyr}$ at Asp codons in the absence of Q, again suggesting that Q34 prevents misdecoding
754 of Asp codons by $tRNA^{Tyr}$.
755 In order to test any effect on an additional tRNA modified by Tgt, namely $tRNA^{Asp}$, we mutated the
756 Asp129 (GAT) codon of the β-lactamase. When Asp129 was mutated to Tyr TAT (**Fig. 3D, right)**, we
757 observe reduced tolerance in *Δtgt,* but not when it was mutated to Tyr TAC, suggesting less
758 misincorporation of aspartate by $tRNA^{Asp}$ at the Tyr UAU codon in the absence of Q. In summary,
759 absence of Q34 increases misdecoding by $tRNA^{Tyr}$ at Asp codons, but decreases misdecoding by $tRNA^{Asp}$
760 at Tyr UAU.
761 This supports the fact that tRNA Q34 modification is involved in translation fidelity during antibiotic
762 stress, and that the effects can be different on different tRNAs, e.g. $tRNA^{Tyr}$ and $tRNA^{Asp}$ tested here.

763
764 **Proteomics study identifies RsxA among factors for which translation is most impacted in *Δtgt***
765 These observations show a link between Q34 modification of tRNA, differential decoding of
766 Tyr codons (among others) and susceptibility to aminoglycosides. We hypothesized that proteins that
767 are differentially translated according to their Tyr codon usage could be involved in the decreased
768 efficiency of the response to aminoglycoside stress in *Δtgt.* We conducted a proteomics study
769 comparing WT vs *Δtgt,* in the absence and presence of tobramycin (proteomics T**able S1 and Fig. 4**).
770 Loss of Q34 results in generally decreased detection of many proteins in tobramycin (shift towards the
771 left in the volcano plot **Fig. 4AB**), and in increases in the levels of 96 proteins. Among those, RsxA
772 (encoded by VC1017) is 13-fold more abundant in the *Δtgt* strain compared to WT in tobramycin. RsxA
773 is part of an anti-SoxR complex. SoxR is an oxidative stress response regulator (Koo et al., 2003) that
774 controls *sodA* (VC2694, superoxide dismutase) and *acrA* (VC0913, efflux), among other genes of the
775 regulon. The Rsx complex reduces and inactivates SoxR, preventing the induction of the regulon.
776 Consistently, we find that the levels of SodA and AcrA proteins are decreased in *Δtgt* compared to WT
777 in TOB (indicated in **Fig. 4B**).
778 With 83% of Tyr TAT codons, instead of the expected 53% average, RsxA has a clear codon usage bias.
779 To test whether some of the differentially abundant protein groups in the Q34 deficient mutant show
780 similar biases, the Tyr codon usage was calculated for the 96 more abundant and 195 less abundant
781 proteins expressed in TOB. More abundant proteins in *Δtgt* TOB with a codon usage bias towards TAT
782 vs TAC are represented as light blue dots in **Fig. 4AB**. No statistically significant difference was detected
783 for TAT codon usage in neither sets of proteins. Thus, one cannot draw conclusions or infer predictions
784 about codon decoding efficiencies in a tRNA modification mutant such as *Δtgt* from the proteomics
785 data alone.
786 We thus performed Ribo-seq (ribosome profiling) analysis on extracts from WT and *Δtgt* strains
787 grown in presence of sub-MIC TOB. Unlike for eukaryotes, technical limitations (e.g. the RNase which
788 is used displays significant sequence specificity), do not necessarily allow to obtain codon resolution in
789 bacteria (Mohammad, Green, & Buskirk, 2019). However, we determined 159 transcripts with
790 increased and 197 with decreased translation in *Δtgt* and we plotted their standardized codon usage
791 bias for codons of interest (Fig. 4DEFG). The calculation of this value is explained in details in the
792 materials and methods section, and shown for *rsxA* as example in **Fig 4C**. Briefly, we took as reference
793 the mean proportion of the codons of interest in the genome (e.g. for tyrosine: TAT= 0.53 and TAC=
794 0.47, meaning that for a random *V. cholerae* gene, 53% of tyrosine codons are TAT). For each gene, we
795 calculated the proportion of each codon (e.g. for *rsxA*: TAT=0.83 and TAC=0.17). We next calculated
796 the codon usage bias as the difference between a given gene's codon usage and the mean codon usage
797 (e.g. for *rsxA*, the codon usage bias for TAT is 0.83-0.53=+0.30). Finally, in order to consider the codon
798 distribution on the genome and obtain statistically significant values, we calculated standardized bias
799 by dividing the codon usage bias by standard deviation for each codon (e.g. for *rsxA*, 0.30/0.25 = +1.20).
800 This is done to adjust standard deviation to 1, and thus to get comparable (standardized) values, for
801 each codon.
802 Ribo-seq data **(Table S2**) shows that TAT codon usage was decreased in the list of transcripts
803 with decreased translation efficiency in *Δtgt*, while it was increased in the list of transcripts with
804 increased translation efficiency (**Fig. 4DE**). No difference was detected for AAT and CAT (**Fig. 4FG**).
805 In addition to mistranslation and codon decoding efficiency, other factors also influence
806 detected protein levels, such as transcription, degradation, etc. Moreover, the localization and
807 sequence context of the codons for which the efficiency of translation is impacted, may be important.
808 Nevertheless, as translation of proteins with a codon usage bias towards TAC or TAT may be impacted
809 in *Δtgt*, and as the most abundant protein RsxA in *Δtgt* in TOB shows a strong TAT bias, we decided to
810 evaluate whether RsxA is post-transcriptionally regulated by the Q34 modification and whether it may
811 affect fitness in the presence of tobramycin.
812
813 **RsxA is post-transcriptionally upregulated in *Δtgt* due to more efficient decoding of tyrosine TAT**
814 **codons in the absence of Q34 modification**

815 Transcriptomic analysis comparing at least 2-fold differentially expressed genes between *V.*
816 *cholerae Δtgt* and WT strains (**Table S3**) showed that, respectively, 53 and 26 genes were significantly
817 downregulated in MH and tobramycin, and 34 were up in tobramycin. Gene ontology (GO) enrichment
818 analysis showed that the most impacted gene ontlogoly categories were bacteriocin transport and iron
819 import into the cell (45- and 40-fold enriched) in MH, and proteolysis and response to heat (38- and
820 15-fold enriched) in TOB. In both conditions, the levels of *rsxA* transcript remained unchanged.
821 RsxA carries 6 tyrosine codons among which the first 5 are TAT and the last one is TAC. RsxA is
822 13-fold more abundant in *Δtgt* than WT, but transcript levels measured by digital RT-PCR are
823 comparable in both strains **(Fig. 5A**), consistent with RNA-seq data. We constructed transcriptional and
824 translational *gfp* fusions in order to evaluate the expression of *rsxA* in WT and *Δtgt* strains. As expected
825 from digital RT-PCR results, no significant differences in fluorescence were observed for the
826 transcriptional fusion of the *rsxA* promoter with *gfp* (**Fig. 5B**), excluding transcriptional regulation of
827 *rsxA* in this context. For translational fusions, we used either the native *rsxA* sequence bearing 5 TAT +
828 1 TAC codons, or a mutant *rsxA* allele carrying all 6 TAC codons (hereafter called respectively $RsxA^{TAT}$
829 and $RsxA^{TAC}$). Confirming the proteomics results, the $RsxA^{TAT}$-GFP fusion was more fluorescent in the
830 *Δtgt* mutant, but not the $RsxA^{TAC}$-GFP one (**Fig. 5C** and detailed flow cytometry data in **Sup. Fig. S3ABC**).
831 Since increased *rsxA* expression appeared to be somewhat toxic for growth, and in order to test
832 translation on a reporter which confers no growth defect, we chose to test directly the translation of
833 *gfp*, which originally carries 4 TAT (36%) and 7 TAC (64%) codons in its native sequence. We constructed
834 two synonymous versions of the GFP protein, with all 11 tyrosine codons either changed to TAT or to
835 TAC. Similar to what we observed with *rsxA*, the GFP^{TAT} version, but not the GFP^{TAC} one, generated
836 more fluorescence in the *Δtgt* background, (**Fig. 5C** and detailed flow cytometry data in **Sup. Fig.**
837 **S3DEF**).
838 Since not all TAT biased proteins are found to be enriched in *Δtgt* proteomics data, the sequence
839 context surrounding TAT codons could affect their decoding. To illustrate this, we inserted after the
840 *gfp* start codon, various tyrosine containing sequences displayed by *rsxA* (**Fig. S3G**). The native
841 tyrosines were all TAT codons, our synthetic constructs were either TAT or TAC, while keeping the
842 remaining sequence unchanged. We observe that the production of GFP carrying the $TEY^{TAT}LLL$
843 sequence from RsxA is increased in *Δtgt* compared to WT, while it is unchanged with $TEY^{TAC}LLL$.
844 However, production of the GFP with the sequences $LY^{TAT}RLL/LY^{TAC}RLL$ and $EY^{TAT}LR/ EY^{TAC}LR$ was not
845 unaffected (or even decreased for the latter) by the absence of *tgt*. Overall, our results demonstrate
846 that RsxA is upregulated in the *Δtgt* strain at the translational level, and that proteins with a codon
847 usage bias towards tyrosine TAT are prone to be more efficiently translated in the absence of Q
848 modification, but this is also dependent on the sequence context.
849
850 **Increased expression of RsxA hampers growth in sub-MIC TOB**
851 We asked whether high levels of RsxA could be responsible of *Δtgt* strain's increased sensitivity
852 to tobramycin. *rsxA* cannot be deleted since it is essential in *V. cholerae* (see our TN-seq data (Babosan
853 et al., 2022; Negro et al., 2019)). We overexpressed *rsxA* from an inducible plasmid in WT strain. In the
854 presence of tobramycin, overexpression of *rsxA* in the WT strain strongly reduces growth (**Fig. 5D with**
855 **inducer, black curve compared to blue**), while overexpression of *tgt* restores growth of the *Δtgt* strain
856 (**Fig. 5D with inducer, green curve**)**.** This shows that increased *rsxA* levels can be toxic during growth
857 in sub-MIC TOB and is consistent with decreased growth of the *Δtgt* strain.
858 Unlike for *V. cholerae*, *rsxA* is not an essential gene in *E. coli*, and does not bear a TAT bias. It
859 has however the same function. Note that this is not the first instance where we observe differences
860 between *E. coli* and *V. cholerae* regarding oxidative stress (Baharoglu, Krin, & Mazel, 2013; Baharoglu
861 & Mazel, 2011; Baharoglu & Mazel, 2014) and respiration processes (Krin, Carvalho, Lang, Mazel, &
862 Baharoglu, 2023): the dispensability of *rsxA* in *E. coli* could either be due to the presence of an
863 additional redundant pathway in this species, or alternatively to general differences in how the two
864 species respond to stress.
865 In order to confirm that the presence of RsxA can be toxic during growth in tobramycin, we
866 additionally performed competition experiments in *E. coli* with simple and double mutants of *tgt* and

867 *rsxA*. Since *Δtgt* strain's growth is more affected than WT at TOB 0.5 µg/ml (indicated with an arrow in
868 **Sup. Fig. S4A)**, we chose this concentration for competition and growth experiments. The results
869 confirm that inactivation of *rsxA* in *Δtgt* restores fitness in tobramycin (**Sup. Fig. S4B**), and that
870 overproduction of RsxA decreases growth in TOB.
871
872 ***tgt* transcription is repressed by CRP and slightly induced by tobramycin in *V. cholerae***
873 *tgt* was previously observed to be upregulated in *E. coli* isolates from urinary tract infection
874 (Bielecki et al., 2014) and in *V. cholerae* after mitomycin C treatment (through indirect SOS induction
875 (Krin et al., 2018)). We measured *tgt* transcript levels using digital RT-PCR in various transcriptional
876 regulator deficient mutants (iron uptake repressor Fur, general stress response and stationary phase
877 sigma factor RpoS and carbon catabolite control regulator CRP), as well as upon exposure to antibiotics,
878 particularly because *tgt* is required for growth in sub-MIC TOB. We also tested the iron chelator
879 dipyridyl (DP), the oxidant agent paraquat (PQ) and serine hydroxamate (SHX) which induces the
880 stringent response.
881 Among all tested conditions, we found that sub-MIC tobramycin and the stringent response mildly
882 increase *tgt* transcript levels, while the carbon catabolite regulator CRP appears to repress it (**Fig. 6A**).
883 We found a sequence between ATG -129 to -114: TTC**G**C^{AGGGAA}A**C**GCG which shows some similarity (in
884 blue) to the *V. cholerae* CRP binding consensus
885 $(^{T}/_{A})_1(^{G}/_{T})_2(^{T}/_{C})_3\mathbf{G}_4(^{A}/_{C})_5{}^{NNNNNN}(^{T}/_{G})_{12}\mathbf{C_{13}}(^{A}/_{G})_{14}(^{C}/_{A})_{15}(^{T}/_{A})_{16}$. However, CRP binding was not previously
886 detected by ChIP-seq in the promoter region of *tgt* in *V. cholerae* (Manneh-Roussel et al., 2018). CRP
887 binding could be transitory or the repression of *tgt* expression by CRP could be an indirect effect.
888 Regarding induction by tobramycin, the mechanism remains to be determined. We previously
889 showed that sub-MIC TOB induces the stringent response (Babosan et al., 2022; Carvalho, Krin,
890 Korlowski, Mazel, & Baharoglu, 2021). Since induction of *tgt* expression by SHX and by tobramycin
891 seems to be in the same order of magnitude, we hypothesized that tobramycin could induce *tgt*
892 through the activation of the stringent response. Using a *P1rrnB-gfp* fusion (Babosan et al., 2022),
893 which is down-regulated upon stringent response induction (Kolmsee, Delic, Agyenim, Calles, &
894 Wagner, 2011) (**Fig. 6B**), we found that the stringent response is significantly induced by tobramycin,
895 both in WT and *Δtgt*. Tobramycin may induce *tgt* expression through stringent response activation or
896 through an independent pathway.
897
898 **Q modification levels can be dynamic and are directly influenced by *tgt* transcription levels**
899 We have identified conditions regulating *tgt* expression. We next addressed whether up/down-
900 regulation of *tgt* affects the actual Q34 modification levels of tRNA. We measured Q34 levels by mass
901 spectrometry in WT and the *Δcrp* strain, where the strongest impact on *tgt* expression was observed
902 (**Fig. 6C**). We find a significant 1.6-fold increase in Q34 levels in *Δcrp*. We also tested the effect of sub-
903 MIC TOB, but smaller differences are probably not detected using our approach of mass spectrometry
904 in bulk cultures.
905 In order to get deeper insight into modification level of *V. cholerae* tRNAs potentially having Q34
906 modification, we decided to adapt a recently published protocol for the detection and quantification
907 of queuosine by deep sequencing (Katanski et al., 2022). This allowed us to validate the presence of
908 Q34 modification in the *V. cholerae* tRNAs Asp, His and Asn GTT2 and precisely measure its level and
909 modulation under different growth conditions (**Fig. S5**). We also showed that Q34 detection is robust
910 and reproducible, and reveals increased Q34 content for tRNA^{His} and tRNA^{Asn} in *Δcrp* strain where *tgt*
911 expression was induced, while for tRNA^{Asp} Q34 level remains relatively constant. *V. cholerae*
912 tRNA^{Asn}GTT1 is very low expressed and likely contains only sub-stoichiometric amounts of Q34, while
913 analysis of tRNA^{Tyr} is impeded by the presence of other modifications in the anticodon loop (namely
914 i^{6}A37 or its derivatives), which prevents the correct mapping and quantification of Q34 modifications
915 using deletion signature.
916 In order to evaluate Q34 levels in tRNA^{Tyr} more specifically, we performed APB northern blots allowing
917 visualization and quantification of Q-modified and unmodified tRNAs (Cirzi & Tuorto, 2021). As

anticipated from increased *tgt* expression, Q-modified tRNA levels were strongly increased in *Δcrp* strain. Sub-MIC TOB also increases the proportion of Q34 containing $tRNA^{Tyr}$ compared to the non-treated condition (**Fig. 6D**). However, this result was variable suggesting a subtle fine-tuning of the Q34 levels depending on growth state (optical density) and TOB concentration. These results show that tRNA Q34 modification levels are dynamic and correlate with variations in *tgt* expression, depending on the tRNA.

DNA repair genes are TAT-biased

We further analyzed *in silico* the codon usage of *V. cholerae* genome, and for each gene, we assigned a codon usage value to each codon (**Fig. 4C and doi:10.5281/zenodo.6875293**). This allowed the generation of lists of genes with divergent codon usage, for each codon.

For genes with a tyrosine codon usage bias towards TAT in *V. cholerae,* gene ontology enrichment analysis (**Sup. Fig. S6)** highlights the DNA repair category with a *p-value* of 2.28×10^{-2} **(Sup. Fig. S6C.)**. **Fig. 7A** shows Tyr codon usage of *V. cholerae* DNA repair genes. We hypothesized that translation of DNA repair transcripts could be more efficient in *Δtgt*, and that such basal pre-induction would be beneficial during genotoxic treatments as UV irradiation (single stranded DNA breaks). UV associated DNA damage is repaired through RecA, RecFOR and RuvAB dependent homologous recombination. Five of these genes, *recO, recR, recA* and *ruvA-ruvB*, are biased towards TAT in *V. cholerae* (Fig. 7A, red arrows), while their repressor LexA bears a strong bias towards TAC. DNA repair genes (e.g. *ruvA* with 80% TAT, *ruvB* with 83% TAT, *dinB* with 75% TAT) were also found to be up for Δ*tgt* in the Ribo-seq data, with unchanged transcription levels. *V. cholerae Δtgt* appears to be 4 to 9 times more resistant to UV irradiation than the WT strain (**Fig. 7B**). Better response to UV in the *V. cholerae Δtgt* strain is consistent with the possibility of increased DNA repair efficiency, although the results do not exclude another mechanism underlying the UV phenotype, such as oxidative stress response.

In *E. coli*, it was previously proposed that overexpression of *tgt* could be linked with UV resistance (Morgante, Mirete, de Figueras, Postigo Cacho, & Gonzalez-Pastor, 2015). We also analyzed tyrosine codon usage for the DNA repair genes in *E. coli*, and did not observe the same bias (**Fig. 7C**), with 51% TAT bias, i.e. the expected level for a random group of genes of the *E coli* genome, and with a TAC bias for *recOR* and *recA* (red arrows) and strong TAT bias for *lexA* (blue arrow) (**Sup. Fig. S6B**, whole genome *E. coli*). These genes thus show the exact opposite bias in *E. coli* (**Fig. 7C**). Unlike for *V. cholerae*, *E. coli Δtgt* mutant did not show increased UV resistance (**Fig. 7D**). This is consistent with the hypothesis that modification-tuned translation of codon biased transcripts can be an additional means of regulation building upon already described and well characterized transcriptional regulation pathways.

Discussion

We show here that Q34 modification levels can be dynamic in bacteria and respond to external conditions; and that Q34 levels on *V. cholerae* $tRNA^{Tyr}$ correlate with *tgt* expression. This is clearer in conditions where *tgt* transcription is highly induced (*Δcrp*), and more variable in conditions where this induction is low (tobramycin). As summarized in **Fig. 8**, we propose that exposure to aminoglycosides increases *tgt* expression in *V. cholerae*, and impacts the decoding of tyrosine codons. As a consequence, transcripts with biased tyrosine codon usage are differentially translated. One such transcript codes for RsxA, an anti-SoxR factor. SoxR controls a regulon involved in oxidative stress response and sub-MIC aminoglycosides trigger oxidative stress in *V. cholerae* (Baharoglu et al., 2013), pointing to an involvement of oxidative stress response in the response to sub-MIC tobramycin stress. A link between Q34 and oxidative stress has previously been found in eukaryotic organisms (Nagaraja et al., 2021). Note that our results do not exclude the involvement of additional Q-regulated translation of other transcripts in the response to tobramycin. Q34 modification leads to reprogramming of the whole proteome, not only for other transcripts with codon usage bias, but also through an impact on the levels of stop codon readthrough and mistranslation at specific codons, as supported by our data.

969 In the tested conditions, we observe more efficient decoding of TAT versus TAC codons in the absence
970 of Q, in *V. cholerae.* This is consistent with findings in human tRNAs, where the presence of Q34
971 increases translation of transcripts biased in C-ending codons (Huber et al., 2022). However, the
972 opposite was shown in *E. coli* regarding tyrosine codon decoding efficiency (Diaz-Rullo & Gonzalez-
973 Pastor, 2023). Recent studies in eukaryotes also indicate slower translation of U-ending codons in the
974 absence of Q34 (Cirzi et al., 2023; Kulkarni et al., 2021; Tuorto et al., 2018). It's important to note here,
975 that in *V. cholerae Δtgt*, better decoding of U-ending codons is observed only with tyrosine, and not
976 with the other three NAC/U codons (Histidine, Aspartate, Asparagine). This is interesting because it
977 suggests that what we observe with tyrosine here, may not adhere to a general rule about the decoding
978 efficiency of U- or C-ending codons, but instead seems to be specific to $tRNA^{Tyr}$, at least in the context
979 of *V. cholerae*. Such exceptions may also exist in other organisms. For example, in human cells, Q34
980 increases efficiency of decoding for U- ending codons and slows decoding of C- ending codons except
981 for AAC, i.e. $tRNA^{Asn}$ (X. Zhao et al., 2023). In mammalian cells (Tuorto et al., 2018), ribosome pausing
982 at U-ending codons is strongly seen for Asp, His and Asn, but less with Tyr. In *Trypanosoma brucei*
983 (Kulkarni et al., 2021), reporters with a combination of the 4 NAC/NAU codons for Asp, Asn, Tyr, His
984 have been tested, showing slow translation at U- ending version of the reporter in the absence of Q,
985 but the effect on individual codons (e.g. Tyr only) was not tested. In mice (Cirzi et al., 2023), ribosome
986 slowdown is seen for the Asn, Asp, His U-ending codons but not for the Tyr U-ending codon. In
987 summary, Q34 generally increases decoding efficiency of U- ending codons in multiple organisms, but
988 there appears to be additional parameters which affect tyrosine UAU decoding, at least in *V. cholerae*.
989 Additional factors such as mRNA secondary structures or mistranslation may also contribute to the
990 better translation of UAU versions of tested genes. Mistranslation could be an important factor. If
991 codon decoding fidelity impacts decoding speed, then mistranslation could also contribute to decoding
992 efficiency of Tyr UAU/UAC codons and proteome composition.

993 Overall, our findings are in accordance with the concept of the so-called modification tunable
994 transcripts (MoTTs) (Endres et al., 2015). We show that in *V. cholerae*, a proteins' codon content can
995 influence its translation in a Q34 modification dependent way, and that this can also impact the
996 translation of antibiotic resistance genes (here β-lactamase). Finally, we show that we can predict *in*
997 *silico*, candidates for which translation can be modulated by the presence or absence of Q34
998 modification (e.g. DNA repair genes), which was confirmed using phenotypic tests (UV resistance).
999 Essential/housekeeping genes are generally TAC biased (**Sup. Fig. S6AB**), as well as ribosomal
1000 proteins, which carry mostly tyrosine TAC codons both in *V. cholerae* and *E. coli*. It has been proposed
1001 that codon bias corresponding to abundant tRNAs at such highly expressed genes, guarantees their
1002 proper expression and avoids titration of tRNAs, allowing for efficient expression of the rest of the
1003 proteome (Frumkin et al., 2018). Induction of *tgt* by stress could also possibly be a signal for the cell to
1004 favor the synthesis of essential factors. Our results are also consistent with the fact that synonymous
1005 mutations can influence the expression of genes (Kudla, Murray, Tollervey, & Plotkin, 2009).
1006 Studies, mostly in eukaryotes, reveal that tRNA modifications are dynamic and not static as
1007 initially thought (Chan et al., 2010; Chan et al., 2012; Torrent, Chalancon, de Groot, Wuster, & Madan
1008 Babu, 2018). Modification levels depend on growth (Keith, Rogg, Dirheimer, Menichi, & Heyham, 1976;
1009 Moukadiri, Garzon, Bjork, & Armengod, 2014), environmental changes (Frey, McCloskey, Kersten, &
1010 Kersten, 1988) and stress (reviewed in (Barraud & Tisne, 2019)). Stress regulated tRNA modification
1011 levels have an impact on the translation of regulators, which in turn trigger translational
1012 reprogramming and optimized responses to stress (Galvanin et al., 2020; Persson, 1993; Pollo-Oliveira
1013 & de Crecy-Lagard, 2019). We show here that *tgt* expression is regulated by tobramycin, the stringent
1014 response and the carbohydrate utilization regulator CRP, and that $tRNA^{Tyr}$ Q34 modification levels
1015 increase with *tgt* expression. The fact that such correlation between *tgt* expression and Q34 levels
1016 does not occur for all tRNAs (e.g. $tRNA^{Asp}$), indicates that other parameters also influence Q34
1017 modification levels. One possibility is that other modifications, such as those on the anticodon loop of
1018 $tRNA^{Tyr}$, may influence the way Tgt modifies these tRNAs, as documented for other modification

circuits (Ehrenhofer-Murray, 2017; Han & Phizicky, 2018). Tgt may also bind these tRNAs differently (for a review on modification specificity (Barraud & Tisne, 2019)).

Our results also demonstrate that we can identify other Q-dependent MoTT candidates using *in silico* codon usage analysis. In fact, since we now have extensively calculated the codon usage biases at all codons for *V. cholerae* and *E. coli* genes, this approach is readily adaptable to any tRNA modification for which we know the differentially translated codons. Such regulation may be a possible way to tune the expression of essential or newly acquired genes, differing in GC-content. It may also, in some cases, explain antibiotic resistance profiles in bacterial collections with established genome sequences, and for which observed phenotypic resistance does not always correlate with known resistance factors (Oprea et al., 2020). Further studies are needed to characterize the determinants of tRNA modification-dependent translational reprogramming.

Ideas and Speculation

Q34 modification is dynamically regulated. How tobramycin increases *tgt* expression remains an open question. Since there is a correlation between tobramycin and stringent response dependent induction of *tgt*, one hypothesis could be that tobramycin induces *tgt* through stringent response activation. The stringent response is usually triggered upon starvation, for example when amino acids are scarce. *tgt* expression was recently shown to be regulated by tyrosine levels and to affect $tRNA^{Tyr}$ codon choice in *Trypanosoma brucei* (Dixit et al., 2021). Tyrosine import into cells occurs through the TyrP transporter (Whipp & Pittard, 1977). Note that in *V. cholerae*, sub-MIC TOB strongly decreases *tyrP* (VCA0772) expression (Carvalho, Krin, et al., 2021), and thus likely decreases tyrosine intake. We could not detect the TyrP protein in our proteomics data, we can thus not compare TyrP levels in *Δtgt* vs WT. We wondered whether supplementation with tyrosine or TyrP overexpression would reverse the *Δtgt* TOB sensitive fitness phenotype, but we observed no notable difference (not shown). Nevertheless, TyrP downregulation could be a signal mimicking tyrosine shortage and inducing *tgt,* leading to more efficient translation of TAC biased proteins, such as TyrP itself.

Regarding CRP, the carbon catabolite regulator, it represses transcription of *tgt*. Interestingly, *V. cholerae crp* carries only TAC codons for tyrosine, and is strongly down-regulated in *Δtgt* in our Ribo-seq data, while its transcription levels remain unchanged. The downregulation of CRP translation when Q34 modifications are low (as in the *Δtgt* strain), could be a way to de-repress *tgt* and increase Q34 modification levels. Note that CRP is involved in natural competence of *V. cholerae*, during growth on crustacean shells where horizontal gene transfer occurs. One can thus speculate that during exogenous DNA uptake, *tgt* repression by CRP could lead to better decoding of AT rich (i.e. TAT biased) mRNAs. Thus, modulation of *tgt* levels during natural transformation may modulate the expression of horizontally transferred genes, which by definition may bear different GC content and codon usage. Moreover, if *tgt* expression is repressed by CRP during competence state, this would favor the translation of TAT-biased DNA repair genes and possibly recombination of incoming DNA into the chromosome. Translational reprogramming in response to DNA damage can thus be an advantageous property selected during evolution.

V. cholerae is the model organism for different species of *Vibrio*. We have previously shown that *V. cholerae's* response to sub-MIC antibiotic stress can be applied to other Gram-negative pathogens (Baharoglu et al., 2013; Gutierrez et al., 2013), while there are differences between *E. coli* and *V. cholerae*, in the response to sub-MIC antibiotics and oxidative stress phenotypes (Baharoglu et al., 2013; Baharoglu & Mazel, 2011; Gutierrez et al., 2013). Here, we have also addressed some of the effects of TOB in *E. coli Δtgt* mutant. In *E. coli,* the deletion of *tgt* has a less dramatic effect on the susceptibility to TOB ((Babosan et al., 2022) and **Sup. Fig S4**). *V. cholerae* and *E. coli* globally show similar tyrosine codon usage in their genomes (**Sup. Fig. S6AB**). However, *E. coli rsxA* does not display a codon bias towards TAT, and neither do DNA repair genes. One can think that in regard to MoTTs, different organisms have evolved according to the environments where they grow, selecting the integration of specific stress response pathways under specific post-transcriptional regulations.

It was recently shown that *E. coli Δtgt* strain is more resistant than the WT to nickel toxicity, most certainly because the nickel importer genes *nikABCDE* are less expressed, but the underlying molecular mechanism had not been elucidated (Pollo-Oliveira et al., 2022). As NikR, the repressor of the *nik* operon is enriched in TAT codons (100%), a more efficient translation of the *nikR* gene in the absence of Q34 would lead to the observed repression phenotype. In addition, the nickel exporter gene *rcnA* is also enriched is TAT (100%), while one of the genes for subunits of the nickel importer *nikD* is enriched in TAC codons (100%). In combination this could explain the clear resistance of the *tgt* strain to high levels of nickel.

However, protein levels are not always in line with the codon bias predictions. The positions of the codons of interest and their sequence context may also be important for differential translation. There could be an interplay or synergies between different codons decoded by Q-modified tRNAs. The presence of the codons of interest in the 5'-end vs 3'-end of a transcript could have a bigger impact on the efficiency of translation (Boel et al., 2016; Osterman et al., 2020). A recent study testing TAC/TAT codons placed between two genes in a translational fusion yielded different results compared to our constructs with the tested codons at the 5' of the transcript (Kimura et al., 2022). Similarly, the distance between two codons of interest, or the identity of the nearby codons may be important. The translation of highly transcribed genes and genes with low levels of mRNAs could be dissimilar. Codon usage may also directly impact gene expression at mRNA levels with an effect on transcription termination (F. Zhao et al., 2021), especially for constitutive genes. Thus, the search for MoTTs could be facilitated by comparing transcriptomics to proteomics data, and additional experiments need to be performed to elucidate post-transcriptional regulation-related phenotypes, but the differential expression of specific TAT/TAC biased proteins finally allows to propose a model for the pleiotropic phenotype caused by Q34 deficiency in *E. coli.*

Finally, the presence or absence of a modification could also affect aminoacylation of the tRNA. Both TAT and TAC codons are decoded by the same and only one tRNA, $tRNA^{TYR}_{GUA}$. In this case, a defect in aminoacylation of this tRNA would impact the decoding of both codons. Our results do not support such an aminoacylation problem, because the efficiency of decoding decreases for one codon (TAC) and not for the other (TAT) in *Δtgt*, and the difference is clearer in TOB. These results are also consistent with rescue of TOB-sensitive phenotype by $tRNA^{Tyr}_{GUA}$ but not $tRNA^{Tyr}_{AUA}$ overexpression in *Δtgt*.

This study, and others mentioned in the introduction, indicate that stress regulated tRNA modifications can facilitate homeostasis by reprogramming the translation of stress response genes. The diversity of tRNA modifications, their specific effects on various proteins and stress responses thus them a promising field of study.

Acknowledgements

We thank Dr. Francesca Tuorto for sharing the protocol for boronated northern blots. Many thanks to Dr. Paola Arimondo for discussions about setting up the queuosine mass spectrometry experiments. We also thank, for RNA-seq experiments, E. Turc, L. Lemée, T. Cokelaer, Biomics Platform, C2RT, Institut Pasteur, Paris, France, supported by France Génomique (ANR-10-INBS-09) and IBISA. We would like to acknowledge Valérie Bourguignon (IMoPA, UMR7365 CNRS-UL) for her help in validation of queuosine modification protocol.

This research was funded by the Institut Pasteur, the Centre National de la Recherche Scientifique (CNRS-UMR 3525), ANR ModRNAntibio (ANR-21-CE35-0012), ANR-LabEx [ANR-10-LABX-62-IBEID], the Fondation pour la Recherche Médicale (FRM EQU202103012569), the Institut Pasteur grant PTR 245-19 and by the National Institute of General Medical Sciences (NIGMS) grant GM70641 to V dC-L. AB was funded by Institut Pasteur Roux-Cantarini fellowship. The authors acknowledge a DIM1Health 2019 grant from the Région Ile de France to the project EpiK for the LCMS equipment.

Author contributions

Conceived and designed the analysis: ZB, DM; Collected the data: ZB, LF, AB, AC, ML, MD, BL, QG-G, FB, CF, GS, IH; Contributed data or analysis tools: BL, ON, CF, MM, MD, QG-G, FB, HA, VdC-L, VM, YM; Performed the analysis: ZB, LF, AB, AC, ML, BL; Wrote the paper: ZB, VdC-L.

1122 **References**

1123

1124 Advani, V. M., & Ivanov, P. (2019). Translational Control under Stress: Reshaping the Translatome.
1125 *Bioessays, 41*(5), e1900009. doi:10.1002/bies.201900009

1126 Andersen, J. B., Sternberg, C., Poulsen, L. K., Bjorn, S. P., Givskov, M., & Molin, S. (1998). New unstable
1127 variants of green fluorescent protein for studies of transient gene expression in bacteria. *Appl*
1128 *Environ Microbiol, 64*(6), 2240-2246. doi:10.1128/AEM.64.6.2240-2246.1998

1129 Aubee, J. I., Olu, M., & Thompson, K. M. (2016). The i6A37 tRNA modification is essential for proper
1130 decoding of UUX-Leucine codons during rpoS and iraP translation. *RNA, 22*(5), 729-742.
1131 doi:10.1261/rna.053165.115

1132 Babosan, A., Fruchard, L., Krin, E., Carvalho, A., Mazel, D., & Baharoglu, Z. (2022). Non-essential tRNA
1133 and rRNA modifications impact the bacterial response to sub-MIC antibiotic stress. *microLife*.
1134 doi:10.1093/femsml/uqac019

1135 Baharoglu, Z., Bikard, D., & Mazel, D. (2010). Conjugative DNA transfer induces the bacterial SOS
1136 response and promotes antibiotic resistance development through integron activation. *PLoS*
1137 *Genet, 6*(10), e1001165. doi:10.1371/journal.pgen.1001165

1138 Baharoglu, Z., Krin, E., & Mazel, D. (2013). RpoS Plays a Central Role in the SOS Induction by Sub-Lethal
1139 Aminoglycoside Concentrations in Vibrio cholerae. *PLoS Genetics, 9*(4).
1140 doi:10.1371/journal.pgen.1003421

1141 Baharoglu, Z., & Mazel, D. (2011). Vibrio cholerae Triggers SOS and Mutagenesis in Response to a Wide
1142 Range of Antibiotics: a Route towards Multiresistance. *Antimicrobial Agents and*
1143 *Chemotherapy, 55*(5), 2438-2441. doi:10.1128/AAC.01549-10

1144 Baharoglu, Z., & Mazel, D. (2014). Influence of very short patch mismatch repair on SOS inducing
1145 lesions after aminoglycoside treatment in Escherichia coli. *Res Microbiol*.
1146 doi:10.1016/j.resmic.2014.05.039

1147 Barraud, P., & Tisne, C. (2019). To be or not to be modified: Miscellaneous aspects influencing
1148 nucleotide modifications in tRNAs. *IUBMB Life, 71*(8), 1126-1140. doi:10.1002/iub.2041

1149 Bielecki, P., Muthukumarasamy, U., Eckweiler, D., Bielecka, A., Pohl, S., Schanz, A., . . . Haussler, S.
1150 (2014). In vivo mRNA profiling of uropathogenic Escherichia coli from diverse phylogroups
1151 reveals common and group-specific gene expression profiles. *MBio, 5*(4), e01075-01014.
1152 doi:10.1128/mBio.01075-14

1153 Boel, G., Letso, R., Neely, H., Price, W. N., Wong, K. H., Su, M., . . . Hunt, J. F. (2016). Codon influence
1154 on protein expression in E. coli correlates with mRNA levels. *Nature, 529*(7586), 358-363.
1155 doi:10.1038/nature16509

1156 Bruni, C. B., Colantuoni, V., Sbordone, L., Cortese, R., & Blasi, F. (1977). Biochemical and regulatory
1157 properties of Escherichia coli K-12 hisT mutants. *J Bacteriol, 130*(1), 4-10.
1158 doi:10.1128/JB.130.1.4-10.1977

1159 Carvalho, A., Krin, E., Korlowski, C., Mazel, D., & Baharoglu, Z. (2021). Interplay between Sublethal
1160 Aminoglycosides and Quorum Sensing: Consequences on Survival in V. cholerae. *Cells, 10*(11).
1161 doi:ARTN 3227

1162 10.3390/cells10113227

1163 Carvalho, A., Mazel, D., & Baharoglu, Z. (2021). Deficiency in cytosine DNA methylation leads to high
1164 chaperonin expression and tolerance to aminoglycosides in Vibrio cholerae. *PLoS Genetics,*
1165 *17*(10). doi:ARTN e1009748

1166 10.1371/journal.pgen.1009748

Chan, C. T., Dyavaiah, M., DeMott, M. S., Taghizadeh, K., Dedon, P. C., & Begley, T. J. (2010). A quantitative systems approach reveals dynamic control of tRNA modifications during cellular stress. *PLoS Genet, 6*(12), e1001247. doi:10.1371/journal.pgen.1001247

Chan, C. T., Pang, Y. L., Deng, W., Babu, I. R., Dyavaiah, M., Begley, T. J., & Dedon, P. C. (2012). Reprogramming of tRNA modifications controls the oxidative stress response by codon-biased translation of proteins. *Nat Commun, 3*, 937. doi:10.1038/ncomms1938

Chionh, Y. H., McBee, M., Babu, I. R., Hia, F., Lin, W., Zhao, W., . . . Dedon, P. C. (2016). tRNA-mediated codon-biased translation in mycobacterial hypoxic persistence. *Nat Commun, 7*, 13302. doi:10.1038/ncomms13302

Chujo, T., & Tomizawa, K. (2021). Human transfer RNA modopathies: diseases caused by aberrations in transfer RNA modifications. *FEBS J, 288*(24), 7096-7122. doi:10.1111/febs.15736

Cirzi, C., Dyckow, J., Legrand, C., Schott, J., Guo, W., Perez Hernandez, D., . . . Tuorto, F. (2023). Queuosine-tRNA promotes sex-dependent learning and memory formation by maintaining codon-biased translation elongation speed. *EMBO J, 42*(19), e112507. doi:10.15252/embj.2022112507

Cirzi, C., & Tuorto, F. (2021). Analysis of Queuosine tRNA Modification Using APB Northern Blot Assay. *Methods Mol Biol, 2298*, 217-230. doi:10.1007/978-1-0716-1374-0_14

Cormack, B. P., Valdivia, R. H., & Falkow, S. (1996). FACS-optimized mutants of the green fluorescent protein (GFP). *Gene, 173*(1 Spec No), 33-38. doi:10.1016/0378-1119(95)00685-0

Cox, J., Neuhauser, N., Michalski, A., Scheltema, R. A., Olsen, J. V., & Mann, M. (2011). Andromeda: a peptide search engine integrated into the MaxQuant environment. *J Proteome Res, 10*(4), 1794-1805. doi:10.1021/pr101065j

de Crecy-Lagard, V., & Jaroch, M. (2021). Functions of Bacterial tRNA Modifications: From Ubiquity to Diversity. *Trends Microbiol, 29*(1), 41-53. doi:10.1016/j.tim.2020.06.010

Diaz-Rullo, J., & Gonzalez-Pastor, J. E. (2023). tRNA queuosine modification is involved in biofilm formation and virulence in bacteria. *Nucleic Acids Res, 51*(18), 9821-9837. doi:10.1093/nar/gkad667

Dingwall, C., Lomonossoff, G. P., & Laskey, R. A. (1981). High sequence specificity of micrococcal nuclease. *Nucleic Acids Res, 9*(12), 2659-2673. doi:10.1093/nar/9.12.2659

Dixit, S., Kessler, A. C., Henderson, J., Pan, X., Zhao, R., D'Almeida, G. S., . . . Alfonzo, J. D. (2021). Dynamic queuosine changes in tRNA couple nutrient levels to codon choice in Trypanosoma brucei. *Nucleic Acids Res, 49*(22), 12986-12999. doi:10.1093/nar/gkab1204

Doucet, N., De Wals, P. Y., & Pelletier, J. N. (2004). Site-saturation mutagenesis of Tyr-105 reveals its importance in substrate stabilization and discrimination in TEM-1 beta-lactamase. *J Biol Chem, 279*(44), 46295-46303. doi:10.1074/jbc.M407606200

Ehrenhofer-Murray, A. E. (2017). Cross-Talk between Dnmt2-Dependent tRNA Methylation and Queuosine Modification. *Biomolecules, 7*(1). doi:10.3390/biom7010014

El Mortaji, L., Tejada-Arranz, A., Rifflet, A., Boneca, I. G., Pehau-Arnaudet, G., Radicella, J. P., . . . De Reuse, H. (2020). A peptide of a type I toxin-antitoxin system induces Helicobacter pylori morphological transformation from spiral shape to coccoids. *Proc Natl Acad Sci U S A, 117*(49), 31398-31409. doi:10.1073/pnas.2016195117

Elowitz, M. B., & Leibler, S. (2000). A synthetic oscillatory network of transcriptional regulators. *Nature, 403*(6767), 335-338. doi:10.1038/35002125

Endres, L., Dedon, P. C., & Begley, T. J. (2015). Codon-biased translation can be regulated by wobble-base tRNA modification systems during cellular stress responses. *RNA Biol, 12*(6), 603-614. doi:10.1080/15476286.2015.1031947

Erde, J., Loo, R. R., & Loo, J. A. (2014). Enhanced FASP (eFASP) to increase proteome coverage and sample recovery for quantitative proteomic experiments. *J Proteome Res, 13*(4), 1885-1895. doi:10.1021/pr4010019

Escobar, W. A., Miller, J., & Fink, A. L. (1994). Effects of site-specific mutagenesis of tyrosine 105 in a class A beta-lactamase. *Biochem J, 303 (Pt 2)*, 555-558. doi:10.1042/bj3030555

Fabret, C., & Namy, O. (2021). Translational accuracy of a tethered ribosome. *Nucleic Acids Res, 49*(9), 5308-5318. doi:10.1093/nar/gkab259

Fleming, B. A., Blango, M. G., Rousek, A. A., Kincannon, W. M., Tran, A., Lewis, A. J., . . . Mulvey, M. A. (2022). A tRNA modifying enzyme as a tunable regulatory nexus for bacterial stress responses and virulence. *Nucleic Acids Res*. doi:10.1093/nar/gkac116

Francois, P., Arbes, H., Demais, S., Baudin-Baillieu, A., & Namy, O. (2021). RiboDoc: A Docker-based package for ribosome profiling analysis. *Comput Struct Biotechnol J, 19*, 2851-2860. doi:10.1016/j.csbj.2021.05.014

Frey, B., McCloskey, J., Kersten, W., & Kersten, H. (1988). New function of vitamin B12: cobamide-dependent reduction of epoxyqueuosine to queuosine in tRNAs of Escherichia coli and Salmonella typhimurium. *J Bacteriol, 170*(5), 2078-2082. doi:10.1128/jb.170.5.2078-2082.1988

Frumkin, I., Lajoie, M. J., Gregg, C. J., Hornung, G., Church, G. M., & Pilpel, Y. (2018). Codon usage of highly expressed genes affects proteome-wide translation efficiency. *Proc Natl Acad Sci U S A, 115*(21), E4940-E4949. doi:10.1073/pnas.1719375115

Galvanin, A., Ayadi, L., Helm, M., Motorin, Y., & Marchand, V. (2019). Mapping and Quantification of tRNA 2'-O-Methylation by RiboMethSeq. *Methods Mol Biol, 1870*, 273-295. doi:10.1007/978-1-4939-8808-2_21

Galvanin, A., Vogt, L. M., Grober, A., Freund, I., Ayadi, L., Bourguignon-Igel, V., . . . Motorin, Y. (2020). Bacterial tRNA 2'-O-methylation is dynamically regulated under stress conditions and modulates innate immune response. *Nucleic Acids Res, 48*(22), 12833-12844. doi:10.1093/nar/gkaa1123

Giai Gianetto, Q., Combes, F., Ramus, C., Bruley, C., Coute, Y., & Burger, T. (2016). Calibration plot for proteomics: A graphical tool to visually check the assumptions underlying FDR control in quantitative experiments. *Proteomics, 16*(1), 29-32. doi:10.1002/pmic.201500189

Gutierrez, A., Laureti, L., Crussard, S., Abida, H., Rodriguez-Rojas, A., Blazquez, J., . . . Matic, I. (2013). beta-lactam antibiotics promote bacterial mutagenesis via an RpoS-mediated reduction in replication fidelity. *Nat Commun, 4*, 1610. doi:ncomms2607 [pii]

10.1038/ncomms2607

Han, L., & Phizicky, E. M. (2018). A rationale for tRNA modification circuits in the anticodon loop. *RNA, 24*(10), 1277-1284. doi:10.1261/rna.067736.118

Hou, Y. M., Matsubara, R., Takase, R., Masuda, I., & Sulkowska, J. I. (2017). TrmD: A Methyl Transferase for tRNA Methylation With m(1)G37. *Enzymes, 41*, 89-115. doi:10.1016/bs.enz.2017.03.003

Huber, S. M., Begley, U., Sarkar, A., Gasperi, W., Davis, E. T., Surampudi, V., . . . Begley, T. J. (2022). Arsenite toxicity is regulated by queuine availability and oxidation-induced reprogramming of the human tRNA epitranscriptome. *Proc Natl Acad Sci U S A, 119*(38), e2123529119. doi:10.1073/pnas.2123529119

Jacob, F., Joris, B., Lepage, S., Dusart, J., & Frere, J. M. (1990). Role of the conserved amino acids of the 'SDN' loop (Ser130, Asp131 and Asn132) in a class A beta-lactamase studied by site-directed mutagenesis. *Biochem J, 271*(2), 399-406. doi:10.1042/bj2710399

JD., H. (2007). Matplotlib: A 2D Graphics Environment. . *Computing in Science & Engineering, 9*, 90--95. doi:10.1109/MCSE.2007.55

Katanski, C. D., Watkins, C. P., Zhang, W., Reyer, M., Miller, S., & Pan, T. (2022). Analysis of queuosine and 2-thio tRNA modifications by high throughput sequencing. *Nucleic Acids Res, 50*(17), e99. doi:10.1093/nar/gkac517

Keith, G., Rogg, H., Dirheimer, G., Menichi, B., & Heyham, T. (1976). Post-transcriptional modification of tyrosine tRNA as a function of growth in Bacillus subtilis. *FEBS Lett, 61*(2), 120-123. doi:10.1016/0014-5793(76)81017-4

Kessler, B., Timmis, K. N., & de Lorenzo, V. (1994). The organization of the Pm promoter of the TOL plasmid reflects the structure of its cognate activator protein XylS. *Mol Gen Genet, 244*(6), 596-605. doi:10.1007/BF00282749

Kimura, S., Dedon, P. C., & Waldor, M. K. (2020). Comparative tRNA sequencing and RNA mass spectrometry for surveying tRNA modifications. *Nat Chem Biol, 16*(9), 964-972. doi:10.1038/s41589-020-0558-1

Kimura, S., Srisuknimit, V., McCarty, K. L., Dedon, P. C., Kranzusch, P. J., & Waldor, M. K. (2022). Sequential action of a tRNA base editor in conversion of cytidine to pseudouridine. *Nat Commun, 13*(1), 5994. doi:10.1038/s41467-022-33714-x

Kimura, S., & Waldor, M. K. (2019). The RNA degradosome promotes tRNA quality control through clearance of hypomodified tRNA. *Proc Natl Acad Sci U S A, 116*(4), 1394-1403. doi:10.1073/pnas.1814130116

Kluyver T, R.-K. B., Pérez F, Granger B, Bussonnier M, Frederic J, et al. (2016). Jupyter Notebooks -- a publishing format for reproducible computational workflows*., Loizides Fernando, Scmidt Birgit, editors*(Positioning and Power in Academic Publishing: Players, Agents and Agendas), 87--90.

Kolmsee, T., Delic, D., Agyenim, T., Calles, C., & Wagner, R. (2011). Differential stringent control of Escherichia coli rRNA promoters: effects of ppGpp, DksA and the initiating nucleotides. *Microbiology (Reading), 157*(Pt 10), 2871-2879. doi:10.1099/mic.0.052357-0

Koo, M. S., Lee, J. H., Rah, S. Y., Yeo, W. S., Lee, J. W., Lee, K. L., . . . Roe, J. H. (2003). A reducing system of the superoxide sensor SoxR in Escherichia coli. *EMBO J, 22*(11), 2614-2622. doi:10.1093/emboj/cdg252

Krin, E., Carvalho, A., Lang, M., Mazel, D., & Baharoglu, Z. (2023). RavA-ViaA antibiotic response is linked to Cpx and Zra2 envelope stress systems in Vibrio cholerae. *Microbiology Spectrum, in press*.

Krin, E., Pierle, S. A., Sismeiro, O., Jagla, B., Dillies, M. A., Varet, H., . . . Mazel, D. (2018). Expansion of the SOS regulon of Vibrio cholerae through extensive transcriptome analysis and experimental validation. *BMC Genomics, 19*(1), 373. doi:10.1186/s12864-018-4716-8

Kudla, G., Murray, A. W., Tollervey, D., & Plotkin, J. B. (2009). Coding-sequence determinants of gene expression in Escherichia coli. *Science, 324*(5924), 255-258. doi:10.1126/science.1170160

Kulkarni, S., Rubio, M. A. T., Hegedusova, E., Ross, R. L., Limbach, P. A., Alfonzo, J. D., & Paris, Z. (2021). Preferential import of queuosine-modified tRNAs into Trypanosoma brucei mitochondrion is critical for organellar protein synthesis. *Nucleic Acids Res, 49*(14), 8247-8260. doi:10.1093/nar/gkab567

Lang, M. N., Krin, E., Korlowski, C., Sismeiro, O., Varet, H., Coppee, J. Y., . . . Baharoglu, Z. (2021). Sleeping ribosomes: Bacterial signaling triggers RaiA mediated persistence to aminoglycosides. *iScience, 24*(10). doi:ARTN 103128

10.1016/j.isci.2021.103128

Li, H. (2018). Minimap2: pairwise alignment for nucleotide sequences. *Bioinformatics, 34*(18), 3094-3100. doi:10.1093/bioinformatics/bty191

Lo Scrudato, M., & Blokesch, M. (2012). The regulatory network of natural competence and transformation of Vibrio cholerae. *PLoS Genet, 8*(6), e1002778. doi:10.1371/journal.pgen.1002778

PGENETICS-D-12-00108 [pii]

Manickam, N., Joshi, K., Bhatt, M. J., & Farabaugh, P. J. (2016). Effects of tRNA modification on translational accuracy depend on intrinsic codon-anticodon strength. *Nucleic Acids Res, 44*(4), 1871-1881. doi:10.1093/nar/gkv1506

Manickam, N., Nag, N., Abbasi, A., Patel, K., & Farabaugh, P. J. (2014). Studies of translational misreading in vivo show that the ribosome very efficiently discriminates against most potential errors. *RNA, 20*(1), 9-15. doi:10.1261/rna.039792.113

Manneh-Roussel, J., Haycocks, J. R. J., Magan, A., Perez-Soto, N., Voelz, K., Camilli, A., . . . Grainger, D. C. (2018). cAMP Receptor Protein Controls Vibrio cholerae Gene Expression in Response to Host Colonization. *MBio, 9*(4). doi:10.1128/mBio.00966-18

Masuda, I., Matsubara, R., Christian, T., Rojas, E. R., Yadavalli, S. S., Zhang, L., . . . Hou, Y. M. (2019). tRNA Methylation Is a Global Determinant of Bacterial Multi-drug Resistance. *Cell Syst, 8*(4), 302-314 e308. doi:10.1016/j.cels.2019.03.008

McKinney, W. (2010). Data Structures for Statistical Computing in Python. *Stéfan van der Walt, Jarrod Millman, editors. , Proceedings of the 9th Python in Science Conference*, 56--61. doi:10.25080/Majora-92bf1922-00a

Meier, F., Suter, B., Grosjean, H., Keith, G., & Kubli, E. (1985). Queuosine modification of the wobble base in tRNAHis influences 'in vivo' decoding properties. *EMBO J, 4*(3), 823-827. Retrieved from https://www.ncbi.nlm.nih.gov/pubmed/2988936

https://www.ncbi.nlm.nih.gov/pmc/articles/PMC554263/pdf/emboj00268-0241.pdf

ML, W. (2021). Seaborn: Statistical Data Visualization. *Journal of Open Source Software, 6*, :3021. doi:10.21105/joss.03021

Mohammad, F., Green, R., & Buskirk, A. R. (2019). A systematically-revised ribosome profiling method for bacteria reveals pauses at single-codon resolution. *Elife, 8*. doi:10.7554/eLife.42591

Molder, F., Jablonski, K. P., Letcher, B., Hall, M. B., Tomkins-Tinch, C. H., Sochat, V., . . . Koster, J. (2021). Sustainable data analysis with Snakemake. *F1000Res, 10*, 33. doi:10.12688/f1000research.29032.2

Morgante, V., Mirete, S., de Figueras, C. G., Postigo Cacho, M., & Gonzalez-Pastor, J. E. (2015). Exploring the diversity of arsenic resistance genes from acid mine drainage microorganisms. *Environ Microbiol, 17*(6), 1910-1925. doi:10.1111/1462-2920.12505

Moukadiri, I., Garzon, M. J., Bjork, G. R., & Armengod, M. E. (2014). The output of the tRNA modification pathways controlled by the Escherichia coli MnmEG and MnmC enzymes depends on the growth conditions and the tRNA species. *Nucleic Acids Res, 42*(4), 2602-2623. doi:10.1093/nar/gkt1228

Nagaraja, S., Cai, M. W., Sun, J., Varet, H., Sarid, L., Trebicz-Geffen, M., . . . Ankri, S. (2021). Queuine Is a Nutritional Regulator of Entamoeba histolytica Response to Oxidative Stress and a Virulence Attenuator. *MBio, 12*(2). doi:10.1128/mBio.03549-20

Negro, V., Krin, E., Aguilar Pierle, S., Chaze, T., Giai Gianetto, Q., Kennedy, S. P., . . . Baharoglu, Z. (2019). RadD Contributes to R-Loop Avoidance in Sub-MIC Tobramycin. *MBio, 10*(4). doi:10.1128/mBio.01173-19

Noguchi, S., Nishimura, Y., Hirota, Y., & Nishimura, S. (1982). Isolation and characterization of an Escherichia coli mutant lacking tRNA-guanine transglycosylase. Function and biosynthesis of queuosine in tRNA. *J Biol Chem, 257*(11), 6544-6550. Retrieved from https://www.ncbi.nlm.nih.gov/pubmed/6804468

http://www.jbc.org/content/257/11/6544.full.pdf

Okuda, M. (2015). *Mechanism of action of a class of antibiotics from their entry to their target in bacteria : a real time visualization.* Université Paris Sud - Paris XI, Retrieved from https://tel.archives-ouvertes.fr/tel-01599239 Star

Cnrs

Cea

Cea-upsay-saclay

I2bc

Dsv

Univ-paris-saclay

Cea-drf

Cea-upsay

Joliot database. (2015PA112239)

Oprea, M., Njamkepo, E., Cristea, D., Zhukova, A., Clark, C. G., Kravetz, A. N., . . . Weill, F. X. (2020). The seventh pandemic of cholera in Europe revisited by microbial genomics. *Nat Commun, 11*(1), 5347. doi:10.1038/s41467-020-19185-y

Osterman, I. A., Chervontseva, Z. S., Evfratov, S. A., Sorokina, A. V., Rodin, V. A., Rubtsova, M. P., . . . Sergiev, P. V. (2020). Translation at first sight: the influence of leading codons. *Nucleic Acids Res, 48*(12), 6931-6942. doi:10.1093/nar/gkaa430

Parker, J. (1982). Specific mistranslation in hisT mutants of Escherichia coli. *Mol Gen Genet, 187*(3), 405-409. doi:10.1007/BF00332619

Persson, B. C. (1993). Modification of tRNA as a regulatory device. *Mol Microbiol, 8*(6), 1011-1016. doi:10.1111/j.1365-2958.1993.tb01645.x

Pollo-Oliveira, L., Davis, N., Hossain, I., Ho, P., Yuan, Y., Garcia, P. S., . . . de Crecy-Lagard, V. (2022). The absence of the Queuosine tRNA modification leads to pleiotropic phenotypes revealing perturbations of metal and oxidative stress homeostasis in Escherichia coli K12. *Metallomics*. doi:10.1093/mtomcs/mfac065

Pollo-Oliveira, L., & de Crecy-Lagard, V. (2019). Can Protein Expression Be Regulated by Modulation of tRNA Modification Profiles? *Biochemistry, 58*(5), 355-362. doi:10.1021/acs.biochem.8b01035

Pounds, S., & Cheng, C. (2006). Robust estimation of the false discovery rate. *Bioinformatics, 22*(16), 1979-1987. doi:10.1093/bioinformatics/btl328

Reback J, M. W., jbrockmendel, den Bossche JV, Augspurger T, Cloud P, et al. (2021). pandas-dev/pandas: Pandas 1.2.4. doi:10.5281/zenodo.4681666

Ritchie, M. E., Phipson, B., Wu, D., Hu, Y., Law, C. W., Shi, W., & Smyth, G. K. (2015). limma powers differential expression analyses for RNA-sequencing and microarray studies. *Nucleic Acids Res, 43*(7), e47. doi:10.1093/nar/gkv007

Rivera, M., Hancock, R. E., Sawyer, J. G., Haug, A., & McGroarty, E. J. (1988). Enhanced binding of polycationic antibiotics to lipopolysaccharide from an aminoglycoside-supersusceptible, tolA mutant strain of Pseudomonas aeruginosa. *Antimicrob Agents Chemother, 32*(5), 649-655. doi:10.1128/AAC.32.5.649

Sabeti Azad, M., Okuda, M., Cyrenne, M., Bourge, M., Heck, M. P., Yoshizawa, S., & Fourmy, D. (2020). Fluorescent aminoglycoside antibiotics and methods for accurately monitoring uptake by bacteria. *ACS Infect Dis*. doi:10.1021/acsinfecdis.9b00421

Silva-Rocha, R., Martinez-Garcia, E., Calles, B., Chavarria, M., Arce-Rodriguez, A., de Las Heras, A., . . . de Lorenzo, V. (2013). The Standard European Vector Architecture (SEVA): a coherent platform for the analysis and deployment of complex prokaryotic phenotypes. *Nucleic Acids Res, 41*(Database issue), D666-675. doi:10.1093/nar/gks1119

Suzuki, T. (2021). The expanding world of tRNA modifications and their disease relevance. *Nat Rev Mol Cell Biol*. doi:10.1038/s41580-021-00342-0

Taylor, D. E., Trieber, C. A., Trescher, G., & Bekkering, M. (1998). Host mutations (miaA and rpsL) reduce tetracycline resistance mediated by Tet(O) and Tet(M). *Antimicrob Agents Chemother, 42*(1), 59-64. doi:10.1128/AAC.42.1.59

Thompson, K. M., & Gottesman, S. (2014). The MiaA tRNA modification enzyme is necessary for robust RpoS expression in Escherichia coli. *J Bacteriol, 196*(4), 754-761. doi:10.1128/JB.01013-13

Thongdee, N., Jaroensuk, J., Atichartpongkul, S., Chittrakanwong, J., Chooyoung, K., Srimahaeak, T., . . . Fuangthong, M. (2019). TrmB, a tRNA m7G46 methyltransferase, plays a role in hydrogen peroxide resistance and positively modulates the translation of katA and katB mRNAs in Pseudomonas aeruginosa. *Nucleic Acids Res, 47*(17), 9271-9281. doi:10.1093/nar/gkz702

Torrent, M., Chalancon, G., de Groot, N. S., Wuster, A., & Madan Babu, M. (2018). Cells alter their tRNA abundance to selectively regulate protein synthesis during stress conditions. *Sci Signal, 11*(546). doi:10.1126/scisignal.aat6409

Tuorto, F., Legrand, C., Cirzi, C., Federico, G., Liebers, R., Muller, M., . . . Lyko, F. (2018). Queuosine-modified tRNAs confer nutritional control of protein translation. *EMBO J, 37*(18). doi:10.15252/embj.201899777

Tyanova, S., Temu, T., & Cox, J. (2016). The MaxQuant computational platform for mass spectrometry-based shotgun proteomics. *Nat Protoc, 11*(12), 2301-2319. doi:10.1038/nprot.2016.136

Urbonavicius, J., Qian, Q., Durand, J. M., Hagervall, T. G., & Bjork, G. R. (2001). Improvement of reading frame maintenance is a common function for several tRNA modifications. *EMBO J, 20*(17), 4863-4873. doi:10.1093/emboj/20.17.4863

Vecerek, B., Moll, I., & Blasi, U. (2007). Control of Fur synthesis by the non-coding RNA RyhB and iron-responsive decoding. *EMBO J, 26*(4), 965-975. doi:10.1038/sj.emboj.7601553

Virtanen, P., Gommers, R., Oliphant, T. E., Haberland, M., Reddy, T., Cournapeau, D., . . . SciPy, C. (2020). SciPy 1.0: fundamental algorithms for scientific computing in Python. *Nat Methods, 17*(3), 261-272. doi:10.1038/s41592-019-0686-2

Whipp, M. J., & Pittard, A. J. (1977). Regulation of aromatic amino acid transport systems in Escherichia coli K-12. *J Bacteriol, 132*(2), 453-461. doi:10.1128/jb.132.2.453-461.1977

Wieczorek, S., Combes, F., Lazar, C., Giai Gianetto, Q., Gatto, L., Dorffer, A., . . . Burger, T. (2017). DAPAR & ProStaR: software to perform statistical analyses in quantitative discovery proteomics. *Bioinformatics, 33*(1), 135-136. doi:10.1093/bioinformatics/btw580

Zhao, F., Zhou, Z., Dang, Y., Na, H., Adam, C., Lipzen, A., . . . Liu, Y. (2021). Genome-wide role of codon usage on transcription and identification of potential regulators. *Proc Natl Acad Sci U S A, 118*(6). doi:10.1073/pnas.2022590118

Zhao, X., Ma, D., Ishiguro, K., Saito, H., Akichika, S., Matsuzawa, I., . . . Suzuki, T. (2023). Glycosylated queuosines in tRNAs optimize translational rate and post-embryonic growth. *Cell, 186*(25), 5517-5535 e5524. doi:10.1016/j.cell.2023.10.026

Zhong, W., Koay, A., Ngo, A., Li, Y., Nah, Q., Wong, Y. H., . . . Dedon, P. (2019). Targeting the Bacterial Epitranscriptome for Antibiotic Development: Discovery of Novel tRNA-(N(1)G37) Methyltransferase (TrmD) Inhibitors. *ACS Infect Dis, 5*(3), 326-335. doi:10.1021/acsinfecdis.8b00275

1444 **Figure legends**

1445 **Figure 1. *V. cholerae Δtgt* shows decreased aminoglycoside tolerance. A.** Competition experiments between
1446 WT and *Δtgt* with the indicated antibiotic or oxidant at sub-MIC concentration*. NT: non-treated.* TOB: tobramycin
1447 0.6 µg/ml; CIP: ciprofloxacin 0.01 µg/ml; CRB: carbenicillin 2.5 µg/ml; PQ: paraquat 10 µM; H_2O_2: 2mM. **B.**
1448 Competition experiments between WT and *Δtgt* carrying the indicated plasmids. pSEVA-*tgt*: plasmid expressing
1449 *tgt* using the XylS regulated Pm promoter, which is activated using sodium benzoate. MH: *non-treated*. **CDEF**.
1450 Survival of exponential phase cultures after various times of incubation (indicated in minutes on the X-axis) with
1451 the indicated antibiotic at lethal concentration: 5MIC: 5 times the MIC; 10MIC: 10 times the MIC. **G.** PMF
1452 measurement of exponential phase cultures using fluorescent Mitotracker dye, measured using flow cytometry.
1453 **H**. Neomycin uptake measurement by flow cytometry using fluorescent Cy5 coupled neomycin. **I.** Competition
1454 experiments between WT and *Δtgt* carrying either empty plasmid (p0), or a plasmid overexpressing $tRNA^{Tyr}$ with
1455 the native GUA anti-codon, or with the synthetic AUA anticodon. The anticodon sequence is indicated (e.g.
1456 $tRNA^{Tyr}_{AUA}$ decodes the UAU codon). *NT: non-treated.* TOB: tobramycin 0.6 µg/ml. For multiple comparisons, we
1457 used one-way ANOVA. **** means p<0.0001, *** means p<0.001, ** means p<0.01, * means p<0.05. ns: non-
1458 significant. Number of replicates for each experiment: 3<n<8.

1459 **Figure 2. Codon decoding differences for *V. cholerae* WT and *Δtgt*. A. to E. Codon specific translation efficiency**
1460 **in WT and *Δtgt* using 6xcodon stretches inserted in GFP.** Y axis represents the relative fluorescence of a given
1461 GFP in Δtgt over the same construct in WT. NT: non-treated; TOB: tobramycin at 0.4 µg/ml. Each specified codon
1462 is repeated 6x within the coding sequence of the GFP (e.g. TACTACTACTACTACTAC). For multiple comparisons,
1463 we used one-way ANOVA. **** means p<0.0001, *** means p<0.001, ** means p<0.01, * means p<0.05. ns:
1464 non-significant. Number of replicates for each experiment: 3<n, each dot represents one replicate.

1465 **Figure 3. Differential translation at tyrosine and aspartate codons evaluated by growth on carbenicillin of**
1466 **mutated β-lactamase reporters**. **A.** The catalytic tyrosine at position 103 was tested in its native sequence (TAC),
1467 or with the synonymous TAT mutation. **B**. The catalytic aspartate at position 129 was tested in its native sequence
1468 (GAT), or with the synonymous GAC mutation. **A and B.** Growth on microtiter plates. Growth was followed by
1469 measuring the OD 620 nm every 15 minutes during 600 minutes. CARB was used at 100 µg/ml. When present,
1470 TOB was used 0.2 µg/ml (20% of MIC). Curves represent mean and standard errors from biological duplicates. **C:**
1471 rationale. **D.** Cells were grown to early exponential phase without carbenicillin, and with (down) or without (top)
1472 tobramycin 20% of MIC, and treated with carbenicillin at 10xMIC for 20h. Dilutions were spotted on plate without
1473 carbenicillin. Surviving cells shown here are sensitive to carbenicillin (no growth on carbenicillin containing
1474 plates), suggesting that increased or decreased survival was due to increased (erroneous translation) or
1475 decreased (faithful translation) β-lactamase activity at the time of treatment. Number of replicates for each
1476 experiment: 3. One representative experiment is shown.
1477

1478 **Figure 4. Post-transcriptional regulation in *Δtgt* and Tyr codon usage bias. A. and B.** Volcano plots showing less
1479 and more abundant proteins in proteomics analysis (performed in triplicates) in *Δtgt* compared to WT during
1480 growth without antibiotics (A. where MH is the growth medium), or in sub-MIC TOB at 0.4 µg/ml (B.). **C.** Codon
1481 usage bias calculation example with VC1017 *rsxA* tyrosine TAC and TAT codons. **D. to G.** Plots showing codon
1482 usage bias for genes lists that are up or down in ribosome profiling analysis (performed in triplicates), normalized
1483 to RNA-seq values for each gene, for codons decoded by tRNAs with Q modification. Each dot represents one
1484 gene of the lists.

1485

1486 **Figure 5. Post-transcriptional upregulation of RsxA in *Δtgt* due to a Tyr codon bias towards TAT and toxicity in**
1487 **sub-MIC TOB. A.** *rsxA* mRNA levels measured by digital RT-PCR. 4 biological replicates. **B.** Transcriptional
1488 expression levels from the *rsxA* promoter measured by flow cytometry. 6 biological replicates **C.** Translational
1489 fusion of *rsxA* to *gfp* and *gfp* alone, with differences in codon usage. 3 biological replicates. One-way ANOVA was
1490 used to determine the statistical differences (p-value) between groups. *** means p<0.001, ** means p<0.01,
1491 ns: non-significant. **D.** Growth curves in microtiter plate reader, in *V. cholerae* in indicated conditions. P-*tgt*+:
1492 pSEVA expressing *tgt*. P-*rsx*+: pSEVA expressing rsxA. P-control: empty pSEVA. Inducer: DAPG (see methods). 2
1493 biological replicates and standard errors are shown for each curve.

1494 **Figure 6. Regulation of *tgt* expression and tRNA Q levels. A:** *tgt* transcript levels measured by digital-RT-PCR. Y-
1495 axis represents relative abundance compared to the non-treated (NT) condition in WT. **B.** Stringent response

1496 induction measured with *P1rrn-gfp* reporter shown as fluorescence (Y-axis) as a function of growth (X-axis: OD
1497 600 nm). **C.** Q levels in tRNA enriched RNA extracts, measured by mass spectrometry**. D.** Northern blot and
1498 quantification of Q levels in $tRNA^{Tyr}$. The lower band in the gel corresponds to unmodified $tRNA^{Tyr}$. The upper
1499 band corresponds to Q-modified tRNA-Tyr. *Δtgt* is the negative control without modification of $tRNA^{Tyr}$. A
1500 representative gel is shown. Histograms show the quantification of Q-modified $tRNA^{Tyr}$ over total $tRNA^{Tyr}$**,** as
1501 follows: Q-modified $tRNA^{Tyr}$/(Q-modified $tRNA^{Tyr}$ + $tRNA^{Tyr}$ without Q)= upper band/(upper band + lower band).
1502 2.5 µg of in tRNA enriched RNA extracts were deposited in lanes WT NT, WT TOB and *Δcrp*. 0.9 µg was deposited
1503 in lanes *Δtgt.* Number of replicates for each experiment: 3. For multiple comparisons, we used one-way ANOVA
1504 (for A. C. E.). **** means $p<0.0001$, *** means $p<0.001$, ** means $p<0.01$. Only significant differences are shown.

1505

1506 **Figure 7. DNA repair after UV irradiation is more efficient in *V. cholerae Δtgt*. A and C**. Tyrosine codon usage of
1507 DNA repair genes A: in *V. cholerae. C: in E. coli.* Red indicates positive codon usage bias, i.e. TAT bias. Blue
1508 indicates negative codon usage bias for TAT, i.e. TAC bias. **B and D.** Survival of *Δtgt* relative to WT after UV
1509 irradiation (linear scale) B: in *V. cholerae. D: in E. coli.* For multiple comparisons, we used one-way ANOVA. ****
1510 means p<0.0001, ns: non-significant.

1511 **Figure 8. Model.** Upon exposure to sub-MIC aminoglycosides, the expression of *tgt* is up-regulated in *V. cholerae*
1512 and influences the decoding of tyrosine TAC vs TAT codons. This leads to differential translation from transcripts
1513 bearing a codon usage bias for tyrosine codons. The *rsxA* transcript bears a tyrosine codon bias and its translation
1514 can be tuned by tRNA Q modification. RsxA is an anti-SoxR factor. SoxR controls a regulon involved in oxidative
1515 stress response. When RsxA levels are high, SoxR is increasingly inactivated and oxidative stress response
1516 efficiency decreases. It has been previously shown that sub-MIC aminoglycosides trigger oxidative stress in *V.*
1517 *cholerae*(Baharoglu et al., 2013). Increasing RsxA levels thus reduces fitness in TOB by hampering efficient
1518 oxidative stress response. As a corollary, decreased RsxA would lead to increased expression of the SoxR regulon,
1519 which would allow for more efficient response to oxidative stress, and increased fitness in the presence of sub-
1520 MIC TOB. We propose that when Tgt/Q levels in tRNA increase, RsxA synthesis is low and active SoxR levels are
1521 high, facilitating the bacterial response to aminoglycoside dependent oxidative stress. Created with
1522 BioRender.com

1523
1524

1525
1526 **Table S1: Proteomics identify differentially abundant proteins**
1527

Uniprot	Gene Name	Fasta headers
		I - More abundant in WT
		I – 1. PresentF606WT_AbsentJ420tgt
Q9KTY9	tgt	Queuine tRNA-ribosyltransferase
Q9KNM6	VC_2706	queuosine precursor transporter
Q9KNH8	VC_2761	Bcr/CflA family efflux transporter
Q9KMV7	VC_A0211	Sensory box sensor histidine kinase
Q9KN55	VC_A0110	Uncharacterized protein
Q9KP41	VC_2538	Thiamine ABC transporter, permease protein,
Q9KTU0	VC_0798	Citrate lyase, beta subunit
Q9KSB8	VC_1340	PrpE protein
Q9KRW0	VC_1524	ABC transporter, permease protein
Q9KMB6	VC_A0457	Uncharacterized protein
Q9KUU0	VC_0425	lacZ
Q9KND5	VC_A0030	Uncharacterized protein
Q9KNP5	zapB	Cell division protein ZapB
Q9KUS6	VC_0439	ThrE_2 domain-containing protein
Q9KLK9	VC_A0734	Uncharacterized protein
Q9KRP8	VC_1588	Transcriptional regulator, LysR family
Q9KRB9	VC_1723	TVP38/TMEM64 family membrane protein
Q9KNT7	argB	Acetylglutamate kinase
Q9KRX3	VC_1510	Uncharacterized protein
Q9KPM7	VC_2340	HD-GYP domain-containing protein
Q9KL36	VC_A0913	Hemin ABC transporter, periplasmic hemin-binding protein HutB
Q9KVY3	VC_0005	Putative membrane protein insertion efficiency factor
Q9KQV1	VC_1897	Hit family protein
Q9KMY2	VC_A0184	cspE Cold shock DNA-binding domain protein
Q9KL45	VC_A0903	Uncharacterized protein glycertae kinase
Q9KRM7	VC_1609	Uncharacterized protein ABC-2 type transport system permease
Q9KSC1	VC_1337	Citrate synthase
Q9KLD9	VC_A0807	ABC transporter, periplasmic substrate-binding protein
Q9KT63	VC_1042	Long-chain fatty acid transport protein
Q9KN12	VC_A0154	Uncharacterized protein Na+:H+ antiporter subunit E
Q9KN05	tnaA	Tryptophanase
Q9KS94	queE	7-carboxy-7-deazaguanine synthase
Q9KQI2	tmk	Thymidylate kinase
Q9KVP6	ubiC	Probable chorismate pyruvate-lyase
Q9KMP2	VC_A0281	Integrase
Q9KUW3	VC_0396	Transcriptional regulator, LuxR family
Q9KUK3	VC_0515	Uncharacterized protein
Q9KSC8	VC_1330	Uncharacterized protein

Q9KUQ7	VC_0458	UPF0235 protein yggU			
		I – 2. MoreF606wt_ThanJ420tgt	**log2FC WT/tgt**	**p value**	**Adjusted p value**
Q9KTJ4	gmhB	D-glycero-beta-D-manno-heptose-1,7-bisphosphate 7-phosphatase	3,51	0,0001	0,0005
Q9KTU3	VC_0795	Citrate/sodium symporter	3,46	0,0085	0,0068
Q9KSB4	VC_1345	Putative dioxygenase	3,35	0,0024	0,0034
Q9KS61	cheR2	Chemotaxis protein methyltransferase	2,93	0,0053	0,0050
Q9KN74	VC_A0091	UPF0251 protein VC_A0091	2,86	0,0013	0,0025
Q9KR81	VC_1762	EH_Signature domain-containing protein	2,54	0,0023	0,0034
Q9KM90	VC_A0491	Uncharacterized protein	2,26	0,0013	0,0025
Q9KQ10	VC_2197	Flagellar hook protein FlgE	2,23	0,0036	0,0042
Q9KVI7	murI	Glutamate racemase	2,11	0,0015	0,0028
Q9KV46	VC_0312	NAD(P)H-flavin reductase	2,10	0,0004	0,0014
Q9KL60	VC_A0888	Transcriptional regulator malT , LuxR family	2,01	0,0038	0,0042
Q9KSV5	VC_1151	Uncharacterized protein lysO	1,85	0,0003	0,0012
Q9KUR5	VC_0450	Membrane-bound lytic murein transglycosylase C	1,81	0,0057	0,0052
Q9KVM8	VC_0113	ubiG? Methyltransferase-related protein	1,76	0,0047	0,0046
Q9KPC7	VC_2445	gspA General secretion pathway protein A	1,75	0,0039	0,0042
Q9KNL2	nfuA	Fe/S biogenesis protein NfuA	1,68	0,0010	0,0022
Q9KVI5	VC_0161	Transcriptional activator IlvY	1,63	0,0128	0,0090
Q9KL10	VC_A0940	Transcriptional regulator, DeoR family	1,62	0,0003	0,0012
Q9KR73	VC_1770	Uncharacterized protein	1,52	0,0112	0,0082
Q9KKR5	VC_A1037	Amino acid ABC transporter, ATP-binding protein	1,43	0,0080	0,0065
H9L4R1	VC_0412	MshO Uncharacterized protein	1,43	0,0094	0,0071
Q9KKN4	VC_A1068	LRP Transcriptional regulator, AsnC family	1,43	0,0061	0,0053
P45784	epsN	Type II secretion system protein N	1,38	0,0022	0,0034
Q9KU51	VC_0673	Probable membrane transporter protein	1,37	0,0076	0,0063
Q9KNR9	VC_2662	Uncharacterized protein	1,24	0,0008	0,0019
Q9KRY1	rsmF	Ribosomal RNA small subunit methyltransferase F	1,18	0,0060	0,0053
Q9KLX1	VC_A0620	Thiosulfate sulfurtransferase SseA, putative	1,10	0,0020	0,0034
Q9KV88	VC_0268	ygaJ Uncharacterized protein	1,09	0,0070	0,0060
Q9KPI7	VC_2380	Cobalamin biosynthesis protein CbiB, putative	1,00	0,0042	0,0042
		I – 3. PresentF606TOB_AbsentJ420TOB			
P0C6D1	irgB	Iron-regulated virulence regulatory protein IrgB			
P0C6D6	tcpN	TCP pilus virulence regulatory protein			
Q56632	vibA	Vibriobactin-specific 2,3-dihydro-2,3-dihydroxybenzoate dehydrogenase			
Q9KKP3	VC_A1059	Putative pseudouridine methyltransferase			
Q9KL40	hutX	Intracellular heme transport protein HutX			
Q9KLG0	fabV2	Enoyl-[acyl-carrier-protein] reductase [NADH] 2			
Q9KLJ6	glpB	Anaerobic glycerol-3-phosphate dehydrogenase subunit B			
Q9KLR1	VC_A0681	33-cGAMP-specific phosphodiesterase 1			
Q9KMY6	pepT	Peptidase T			
Q9KNL4	bioH	Pimeloyl-[acyl-carrier protein] methyl ester esterase			
Q9KPE3	coaE	Dephospho-CoA kinase			

Q9KRQ1	VC_1585	Catalase
Q9KS61	cheR2	Chemotaxis protein methyltransferase 2
Q9KSB4	VC_1345	Putative dioxygenase
Q9KSW7	hisI	Histidine biosynthesis bifunctional protein HisIE
Q9KTY9	tgt	Queuine tRNA-ribosyltransferase
Q9KU27	VC_0702	Inosine/xanthosine triphosphatase
H9L4T3	VC_2212	Uncharacterized protein
Q9K2M8	VC_A0348	Uncharacterized protein
Q9KKK0	VC_A1105	DNA-binding response regulator
Q9KKX8	VC_A0972	MFS domain-containing protein
Q9KL71	VC_A0876	D-serine deaminase activator
Q9KLB3	VC_A0833	Transcriptional regulator, LysR family
Q9KLG6	VC_A0778	AHS2 domain-containing protein
Q9KLK5	VC_A0738	Uncharacterized protein
Q9KLK9	VC_A0734	Uncharacterized protein
Q9KLQ1	VC_A0691	Acetoacetyl-CoA reductase
Q9KM02	VC_A0587	PPC domain-containing protein
Q9KM77	VC_A0511	Anaerobic ribonucleoside-triphosphate reductase
Q9KM86	VC_A0496	Glutathione S-transferase, putative
Q9KM98	VC_A0483	Uncharacterized protein
Q9KMX3	VC_A0193	Na+/H+ antiporter, putative
Q9KN01	VC_A0165	GGDEF family protein
Q9KN09	VC_A0157	NADH dehydrogenase, putative
Q9KN25	VC_A0141	C4-dicarboxylate transport sensor protein, putative
Q9KN46	VC_A0119	ImpA_N domain-containing protein
Q9KN85	VC_A0080	GGDEF family protein
Q9KN89	VC_A0076	Gate domain-containing protein
Q9KN99	VC_A0066	Uncharacterized protein
Q9KNA1	VC_A0064	TonB system receptor, putative
Q9KNA2	VC_A0063	Protease II
Q9KNB4	VC_A0051	Uncharacterized protein
Q9KNE3	VC_A0022	Glutathione S-transfersae-related protein
Q9KNF6	VC_A0008	Methyl-accepting chemotaxis protein
Q9KNM6	VC_2706	Probable queuosine precursor transporter
Q9KNN0	VC_2702	Transcriptional regulator, LuxR family
Q9KPD7	cpdA	3,5-cyclic adenosine monophosphate phosphodiesterase CpdA
Q9KPJ7	VC_2370	Sensory box/GGDEF family protein
Q9KPR2	VC_2304	Uncharacterized protein
Q9KPY8	VC_2224	GGDEF family protein
Q9KQ04	VC_2203	Flagellar protein, putative
Q9KQ78	fliP	Flagellar biosynthetic protein FliP
Q9KQN1	VC_1967	Methyl-accepting chemotaxis protein
Q9KQQ9	VC_1939	Uncharacterized protein
Q9KQW7	VC_1880	DUF2062 domain-containing protein
Q9KR48	VC_1798	Eha protein

Q9KRH6	VC_1666	VIBCH ABC transporter, ATP-binding protein, putative
Q9KRJ6	VC_1644	Uncharacterized protein
Q9KRL9	VC_1617	Transcriptional regulator, LysR family
Q9KRN2	VC_1604	Transcriptional regulatory protein
Q9KRW9	VC_1515	Chaperone, formate dehydrogenase-specific, putative
Q9KSC1	VC_1337	Citrate synthase
Q9KSC6	VC_1332	Uncharacterized protein
Q9KSC9	VC_1329	Opacity protein-related protein
Q9KSE2	VC_1315	Sensor histidine kinase
Q9KSP0	VC_1216	GGDEF family protein
Q9KSV5	VC_1151	Uncharacterized protein
Q9KT20	VC_1085	Sensor histidine kinase
Q9KT74	VC_1031	Inosine monophosphate dehydrogenase-related protein
Q9KTC3	VC_0979	Oxidoreductase, short-chain dehydrogenase/reductase family
Q9KTI4	VC_0918	UDP-N-acetyl-D-mannosaminuronic acid dehydrogenase
Q9KTV0	VC_0787	Transcriptional regulator, LysR family
Q9KU51	VC_0673	Probable membrane transporter protein
Q9KUQ1	VC_0464	Transcriptional regulator, LuxR family
Q9KUW6	VC_0393	Uncharacterized protein
Q9KV54	VC_0303	Sensor histidine kinase
Q9KVM2	VC_0119	Uroporphyrinogen-III synthase
Q9KVM8	VC_0113	Methyltransferase-related protein
Q9KVP4	VC_0097	Flagellar protein FliL
Q9KVS6	VC_0063	ThiF protein

I – 4. MoreF606TOB_ThanJ420TOB			log2 FC WT/tgt	p value	Adjusted p value
Q9KMV8	VC_A0210	33-cGAMP-specific phosphodiesterase 2	5,21	0,00000	0,00005
Q9KSR2	VC_1194	J domain-containing protein	3,68	0,00929	0,00488
Q9KKY6	VC_A0964	Glycine cleavage operon activator, putative	5,30	0,00002	0,00043
Q9KKL6	VC_A1087	Anti-sigma F factor antagonist, putative	3,72	0,00060	0,00202
Q9KSK7	VC_1249	ACT domain-containing protein	2,37	0,00973	0,00488
Q9KS89	VC_1370	GGDEF family protein	3,51	0,00007	0,00062
Q9KNA0	VC_A0065	P/Homo B domain-containing protein	3,48	0,00876	0,00488
Q9KT21	VC_1084	Sensory box sensor histidine kinase	1,77	0,00183	0,00235
Q9KRA1	VC_1741	Transcriptional regulator, TetR family	1,71	0,01423	0,00606
Q9KU00	cutC	Copper homeostasis protein CutC	1,85	0,01810	0,00696
Q9KTH7	VC_0925	Polysaccharide biosynthesis protein, putative	3,09	0,00236	0,00256
Q9KSD3	VC_1325	Galactoside ABC transporter, periplasmic D-galactose/D-glucose-binding protein SV=1"	1,77	0,02018	0,00745
Q9KUU2	arcA	ARCA_VIBCH Arginine deiminase	2,78	0,00191	0,00235
Q9KLB8	phhA	PH4H_VIBCH Phenylalanine-4-hydroxylase	2,16	0,03098	0,00967
Q9KPI7	VC_2380	Cobalamin biosynthesis protein CbiB, putative	1,83	0,00973	0,00488
Q9KSE3	VC_1314	Transporter, putative	2,64	0,02472	0,00834
Q9KQX3	VC_1874	Uncharacterized protein	2,66	0,00403	0,00309
Q9KMJ2	VC_A0356	Uncharacterized protein	2,60	0,00439	0,00321

Q9KRW3	VC_1521	Sensor histidine kinase	2,69	0,00011	0,00085
Q9KN34	rbsK	Ribokinase	2,49	0,00270	0,00269
Q9KQX5	VC_1872	AAA_PrkA domain-containing protein	2,94	0,00216	0,00245
Q9KS12	rtxA	Multifunctional-autoprocessing repeats-in-toxin	3,68	0,01920	0,00716
Q9KQ01	VC_2206	Uncharacterized protein	2,76	0,00003	0,00043
P45774	epsH	Type II secretion system protein H	2,58	0,02202	0,00772
Q9KU02	VC_0728	PPK2 domain-containing protein	3,08	0,01270	0,00574
Q9KKL7	VC_A1086	Response regulator	2,65	0,02350	0,00806
Q9KSG5	VC_1291	Uncharacterized protein	3,38	0,00096	0,00223
Q9KSV0	VC_1156	Sensor histidine kinase	2,48	0,00113	0,00224
Q9KN48	VC_A0117	Sigma-54 dependent transcriptional regulator	1,56	0,00974	0,00488
Q9KRG0	VC_1682	Peptide ABC transporter, permease protein	2,56	0,00020	0,00109
Q9KRG1	VC_1681	Peptide ABC transporter, permease protein	2,86	0,00015	0,00099
Q9KSD1	mglA	Galactose/methyl galactoside import ATP-binding protein MglA	2,08	0,02068	0,00754
Q9KLT8	VC_A0653	PTS system, sucrose-specific IIBC component	2,43	0,00003	0,00043
P0C6Q8	dam	DNA adenine methylase	2,26	0,00448	0,00324
P0C6D3	vibB	Vibriobactin-specific isochorismatase	2,32	0,00194	0,00235
Q9KLF1	VC_A0795	Resolvase, putative	2,33	0,00078	0,00215
Q9KNN7	VC_2694	Superoxide dismutase	1,34	0,00647	0,00419
Q9KNW3	VC_2617	Arginine N-succinyltransferase OS=Vibrio cholerae serotype	1,27	0,02884	0,00915
Q9KUA1	VC_0622	Histidine kinase	1,89	0,00950	0,00488
Q9KQX9	VC_1868	Methyl-accepting chemotaxis protein	2,27	0,01417	0,00606
Q9KS63	VC_1397	Chemotaxis protein CheA	2,42	0,02557	0,00852
Q9KR16	VC_1831	Sensor histidine kinase	2,54	0,00188	0,00235
Q9KKR5	VC_A1037	Amino acid ABC transporter, ATP-binding protein	1,56	0,02096	0,00754
Q9KPK6	grcA	GRCA_VIBCH Autonomous glycyl radical cofactor	2,66	0,00332	0,00269
Q9KQX4	VC_1873	UPF0229 protein VC_1873	2,70	0,02180	0,00770
Q9KTI9	VC_0913	HlyD_D23 domain-containing protein	1,71	0,02570	0,00852
Q9KTC7	VC_0975	NfeD domain-containing protein	2,07	0,00048	0,00177
Q9KU65	VC_0658	C-di-GMP phosphodiesterase A-related protein	2,14	0,00930	0,00488
Q9KNB6	VC_A0049	GGDEF family protein	2,45	0,00175	0,00235
Q9KNY0	VC_2600	Uncharacterized protein	1,81	0,00123	0,00224
Q9KTF2	mrdA	Peptidoglycan D,D-transpeptidase MrdA	1,65	0,01002	0,00488
Q9KQY2	VC_1865	Uncharacterized protein	1,78	0,00316	0,00269
Q9KL39	VC_A0909	Oxygen-independent coproporphyrinogen III oxidase, putative	2,04	0,01389	0,00602
Q9KVF6	VC_0190	DNA helicase uvrD	1,94	0,01686	0,00663
Q9KUM9	VC_0486	Transcriptional regulator, DeoR family	1,92	0,03066	0,00961
Q9KRI2	VC_1659	Uncharacterized protein	2,10	0,01469	0,00612
Q9KNJ0	VC_2748	Nitrogen regulation protein	1,87	0,00126	0,00224
Q9KP22	VC_2557	Uncharacterized protein OS	1,81	0,00291	0,00269
Q9KRV1	VC_1533	DTW domain-containing protein	1,83	0,00205	0,00235
Q9KQC8	VC_2072	Peptidase, insulinase family	1,58	0,00893	0,00488
Q9KUM3	VC_0492	Uncharacterized protein	2,34	0,00243	0,00259
Q9KQI3	VC_2015	DNA polymerase III, delta prime subunit	1,77	0,00063	0,00202

Q9KPT7	crl	Sigma factor-binding protein Crl	1,58	0,00088	0,00219
Q9KS69	VC_1390	Transcriptional regulator, LysR family	1,89	0,00007	0,00062
Q9KSC3	VC_1335	Transcriptional regulator, GntR family	1,55	0,00321	0,00269
Q9KRL1	VC_1629	Uncharacterized protein	1,89	0,00322	0,00269
Q9KLS5	VC_A0666	L-serine dehydratase	1,71	0,00079	0,00215
Q9KM52	VC_A0537	Uncharacterized protein	1,27	0,01088	0,00511
Q9KRI6	VC_1655	Magnesium transporter MgtE	1,72	0,00363	0,00282
Q9KTJ1	VC_0911	Trehalose-6-phosphate hydrolase	1,70	0,00042	0,00166
Q9KPZ9	VC_2208	Uncharacterized protein	1,79	0,01534	0,00629
Q9KM32	VC_A0557	GGDEF family protein	1,37	0,02135	0,00762
Q9KSA6	VC_1353	GGDEF family protein	1,52	0,00156	0,00231
Q9KUC2	VC_0600	AB hydrolase-1 domain-containing protein	1,72	0,00123	0,00224
Q9KM15	VC_A0574	N-acetyltransferase domain-containing protein	1,39	0,01767	0,00683
Q9KS83	VC_1376	GGDEF family protein	1,51	0,00363	0,00282
Q9KPT2	VC_2280	Uncharacterized protein	1,45	0,00471	0,00331
Q9KVN8	VC_0103	Uncharacterized protein	1,55	0,00249	0,00262
Q9KT24	VC_1081	Response regulator	1,65	0,02632	0,00861
Q9KRJ1	VC_1649	Trypsin, putative	1,54	0,00092	0,00220
Q9KLP6	VC_A0697	Sensory box/GGDEF family protein	1,63	0,00022	0,00109
Q9KQ23	ispE	ISPE_VIBCH 4-diphosphocytidyl-2-C-methyl-D-erythritol kinase ispE	1,57	0,00119	0,00224
H9L4T1	VC_A0450	Uncharacterized protein	1,76	0,00290	0,00269
Q9KU16	VC_0714	Uncharacterized protein	1,60	0,02409	0,00820
Q9KRS6	katG	KATG_VIBCH Catalase-peroxidase katG	1,39	0,01256	0,00571
P29485	tcpP	Toxin coregulated pilus biosynthesis protein P tcpP	1,56	0,00124	0,00224
Q9KU53	rppH	RPPH_VIBCH RNA pyrophosphohydrolase rppH	2,03	0,00467	0,00331
Q9KKX3	VC_A0977	ABC transporter, ATP-binding protein	1,84	0,02092	0,00754
Q9KQL5	VC_1983	Peptidase, putative	2,47	0,02205	0,00772
Q9KSG0	VC_1296	Phosphomethylpyrimidine kinase	3,54	0,00005	0,00054
Q9KPJ4	VC_2373	Glutamate synthase, large subunit	1,53	0,00120	0,00224
Q9KS96	VC_1363	Siroheme synthase component enzyme	1,31	0,00930	0,00488
Q9KP89	VC_2484	Long-chain-fatty-acid--CoA ligase, putative	1,53	0,00535	0,00367
Q9KSM2	VC_1234	Exodeoxyribonuclease I	1,59	0,02087	0,00754
Q9KSX5	VC_1131	Na_H_antiporter domain-containing protein	2,07	0,01089	0,00511
Q9KTJ2	VC_0910	PTS system, trehalose-specific IIBC component	1,33	0,00205	0,00235
Q9KKZ7	VC_A0953	Peptidyl-prolyl cis-trans isomerase C	1,30	0,00997	0,00488
Q9KUU7	VC_0418	dTTP/UTP pyrophosphatase	1,24	0,00258	0,00267
Q9KV39	birA	Bifunctional ligase/repressor BirA	1,47	0,00649	0,00419
Q9KS28	VC_1433	Uncharacterized protein	1,23	0,00965	0,00488
Q9KMM4	VC_A0307	HNHc domain-containing protein	1,46	0,00110	0,00224
Q9KUJ8	VC_0522	Beta-ketoadipate enol-lactone hydrolase, putative	1,37	0,00202	0,00235
Q9KVT7	purE	N5-carboxyaminoimidazole ribonucleotide mutase	1,45	0,00886	0,00488
Q9KRU5	VC_1539	Probable ketoamine kinase VC_1539	1,09	0,01619	0,00652
Q9KSU7	serC	Phosphoserine aminotransferase	1,41	0,00147	0,00231
Q9KQU2	VC_1906	Methyltranfer_dom domain-containing protein	2,00	0,00065	0,00202
Q9KRW4	VC_1520	ABC transporter, ATP-binding protein	1,17	0,00887	0,00488
Q9KU52	VC_0672	Phosphoenolpyruvate-protein phosphotransferase	1,41	0,00145	0,00231

Q9KLI6	VC_A0758	Arginine ABC transporter, permease protein	1,24	0,01152	0,00534
Q9KPQ9	panE	2-dehydropantoate 2-reductase	1,32	0,02013	0,00745
Q9KNW7	VC_2613	Phosphoribulokinase	1,22	0,00346	0,00278
Q9KT18	VC_1087	Response regulator	1,12	0,00908	0,00488
Q9KPP6	recB	RecBCD enzyme subunit RecB	1,24	0,00085	0,00218
Q9KQK1	VC_1997	Uncharacterized protein	1,16	0,00200	0,00235
Q9KUN3	argP	ARGP_VIBCH HTH-type transcriptional regulator ArgP	1,53	0,00885	0,00488
Q9KMW8	VC_A0198	Site-specific DNA-methyltransferase, putative	1,15	0,00300	0,00269
Q9KVB8	VC_0228	Uncharacterized protein	1,27	0,00223	0,00248
Q9KVE7	VC_0199	Hemolysin secretion ATP-binding protein, putative	1,29	0,00999	0,00488
Q9KQM5	menB	1,4-dihydroxy-2-naphthoyl-CoA synthase menB	1,40	0,00328	0,00269
Q9KR89	VC_1753	Paraquat-inducible protein A	1,11	0,00739	0,00467
Q9KQJ7	VC_2001	Putative glucose-6-phosphate 1-epimerase	1,57	0,01040	0,00501
P57070	lolB	Outer-membrane lipoprotein LolB	1,04	0,01285	0,00577
Q9KL63	VC_A0884	Uncharacterized protein	1,15	0,02695	0,00863
H9L4P1	VC_0259	Lipopolysaccharide biosynthesis protein RfbV	1,21	0,00560	0,00377
Q9KMU4	VC_A0225	Glutamine amidotransferase type-2 domain-containing protein	1,14	0,00164	0,00235
Q9KKU5	VC_A1005	Transcriptional regulator, MarR family	1,14	0,02484	0,00834
Q9KVK1	VC_0142	DUF4145 domain-containing protein	1,20	0,01451	0,00609
Q9KVB5	VC_0231	Uncharacterized protein	1,09	0,00932	0,00488
Q9KKS4	VC_A1026	Uncharacterized protein	1,31	0,00883	0,00488
Q9KUU0	VC_0425	Uncharacterized protein	1,54	0,01872	0,00702
Q9KTA5	VC_0998	Uncharacterized protein	1,15	0,00530	0,00367
Q9KNC4	gltS	Sodium/glutamate symporter	1,21	0,02667	0,00862
Q9KRS8	VC_1558	6-phospho-beta-glucosidase	1,37	0,00196	0,00235
Q9KMT9	VC_A0230	Iron(III) ABC transporter, ATP-binding protein	1,08	0,01196	0,00547
Q9KPZ0	VC_2222	Smr domain-containing protein	1,04	0,02562	0,00852
Q9KQE2	VC_2058	Uncharacterized protein	1,05	0,00651	0,00419
P57066	lolD	LOLD_VIBCH Lipoprotein-releasing system ATP-binding protein LolD	1,01	0,00981	0,00488
Q9KLE5	VC_A0801	Q9KLE5_VIBCH Inosine-guanosine kinase	1,00	0,02622	0,00861
Q9KS35	VC_1426	Spermidine/putrescine ABC transporter, permease protein	1,11	0,00158	0,00231
Q9KSV4	VC_1152	HDOD domain-containing protein	1,07	0,00926	0,00488
Q9KUM2	VC_0493	Q9KUM2_VIBCH Uncharacterized protein	1,76	0,01375	0,00600
Q9KNA9	VC_A0056	Q9KNA9_VIBCH Transcriptional regulator, MerR family	1,07	0,01454	0,00609
Q9KQ71	VC_2130	Flagellum-specific ATP synthase FliI	1,15	0,00357	0,00282
Q9KLD8	VC_A0808	NodN-related protein	1,27	0,00802	0,00488
Q9KP78	VC_2497	HD-GYP domain-containing protein	1,09	0,00149	0,00231
Q60153	tcpA	TCPA_VIBCH Toxin coregulated pilin	1,01	0,02653	0,00862
Q9KRU1	VC_1543	Uncharacterized protein	1,09	0,00268	0,00269
Q9KQ38	VC_2166	Trp repressor-binding protein	1,46	0,01086	0,00511
Q9KQN3	VC_1965	TetR_C_33 domain-containing protein	1,28	0,00698	0,00445
Q9KN86	VC_A0079	Uncharacterized protein	1,23	0,00556	0,00377
Q9KRD3	VC_1709	Zinc protease, insulinase family	1,25	0,00993	0,00488

Q9KKS7	VC_A1023	Uncharacterized protein	1,16	0,00537	0,00367
Q9KVB7	VC_0229	Uncharacterized protein	1,66	0,01838	0,00696
Q9KNR2	VC_2669	5-carboxymethyl-2-hydroxymuconate delta isomerase, putative	1,22	0,01524	0,00628
Q9KUI6	mutS	MUTS_VIBCH DNA mismatch repair protein MutS	1,07	0,00298	0,00269
Q9KVF0	VC_0196	ATP-dependent DNA helicase RecQ	1,04	0,00303	0,00269
Q9KTJ3	VC_0909	Trehalose operon repressor	1,03	0,00981	0,00488
Q9KVH1	VC_0175	Deoxycytidylate deaminase-related protein	1,28	0,01307	0,00584
Q9KR77	VC_1766	Uncharacterized protein	1,01	0,01408	0,00606
Q9KTL4	truC	tRNA pseudouridine synthase C truC	1,09	0,00416	0,00310
Q9KUM4	VC_0491	Uncharacterized protein	1,10	0,00571	0,00379
P52022	dnaE	DNA polymerase III subunit alpha	1,07	0,00324	0,00269
Q9KP97	VC_2476	UPF0149 protein VC_2476	1,70	0,02715	0,00865
Q9KS92	VC_1367	GGDEF family protein	1,19	0,00957	0,00488
Q9KU08	ppx	Exopolyphosphatase ppx	1,04	0,01694	0,00663
Q9KSI6	VC_1270	Glyoxylase II family protein	1,32	0,01645	0,00653
Q9KRA6	bpt	Aspartate/glutamate leucyltransferase bpt	1,04	0,01838	0,00696
Q9KQF5	topB	DNA topoisomerase 3 topB	1,05	0,02938	0,00928
Q9KNF3	malT	HTH-type transcriptional regulator MalT	1,10	0,00227	0,00249
Q9KPE8	VC_2420	Flavodoxin	1,39	0,00897	0,00488
Q9KNT4	ppc	Phosphoenolpyruvate carboxylase ppc	1,05	0,00302	0,00269
Q9KU29	VC_0700	Soluble lytic murein transglycosylase	1,07	0,00291	0,00269
Q9KQV0	VC_1898	Methyl-accepting chemotaxis protein	1,01	0,00574	0,00379
Q9KPE7	VC_2421	ampD protein	1,04	0,02430	0,00824
Q9KU20	rluD	Ribosomal large subunit pseudouridine synthase D rluD	1,03	0,00290	0,00269
Q9KNQ5	VC_2676	Cell division protein FtsN, putative	1,20	0,01452	0,00609
H9L4T5	VC_0847	Integrase, phage family	1,28	0,02687	0,00863
Q9KQ28	VC_2176	UPF0162 protein VC_2176	1,04	0,00311	0,00269
Q9KUC0	mrcB	PBPB_VIBCH Penicillin-binding protein 1B	1,15	0,01050	0,00502
Q9KPV6	uppS	UPPS_VIBCH Ditrans,polycis-undecaprenyl-diphosphate synthase	1,03	0,00800	0,00488
Q9KVU5	rsmB	RSMB_VIBCH Ribosomal RNA small subunit methyltransferase B	1,02	0,01178	0,00542
Q9KMC3	VC_A0441	Uncharacterized protein	1,17	0,00930	0,00488
Q9KVL9	VC_0122	Adenylate cyclase	1,23	0,02356	0,00806
Q9KUW9	metH	Methionine synthase	1,28	0,02670	0,00862
Q9KL09	VC_A0941	Acyl-CoA thioester hydrolase-related protein	1,03	0,02584	0,00853
Q9KMY4	VC_A0182	Sigma-54 dependent transcriptional regulator	1,00	0,00859	0,00488
Q9KQ13	flgH	Flagellar L-ring protein	1,06	0,01335	0,00593
Q9KT38	VC_1067	GGDEF domain-containing protein	1,04	0,02971	0,00935
Q9KM78	VC_A0510	Uncharacterized protein	1,01	0,01640	0,00653
P0C6R0	irgA	IRGA_VIBCH Iron-regulated outer membrane virulence protein	1,03	0,02028	0,00745
Q9KPD8	VC_2432	Uncharacterized protein	1,23	0,03115	0,00968
Q9KVS4	thiG	THIG_VIBCH Thiazole synthase	1,50	0,03191	0,00983
Q9KMG4	higA-1	Antitoxin HigA-1	1,30	0,01712	0,00665
Q9KUY5	VC_0373	Uncharacterized protein	1,25	0,02357	0,00806

Q9KMG8	VC_A0388	Uncharacterized protein	1,58	0,00081	0,00215

1528

Uniprot	Gene Name	Fasta headers
		II - More abundant in *Δtgt*
		II – 1. PresentJ420tgt_AbsentF606wt
O34419	rstR1	Cryptic phage CTXphi transcriptional repressor RstR
Q9KN37	rbsA	Ribose import ATP-binding protein RbsA
Q9KT77	moaE	Molybdopterin synthase catalytic subunit
Q9KVG9	vspR	Transcriptional regulator VspR
H9L4R3	VC_A0444	RelE protein
Q9KKW7	VC_A0983	L-lactate permease
Q9KL14	VC_A0935	Uncharacterized protein
Q9KLD8	VC_A0808	NodN-related protein
Q9KLF6	VC_A0788	DnaJ-related protein
Q9KLJ2	VC_A0752	Thioredoxin 2
Q9KLV6	VC_A0635	Transcriptional regulator, LysR family
Q9KM02	VC_A0587	PPC domain-containing protein
Q9KM27	VC_A0562	Uncharacterized protein
Q9KMP9	VC_A0271	Uncharacterized protein
Q9KNC6	VC_A0039	Uncharacterized protein
Q9KNE3	VC_A0022	Glutathione S-transfersae-related protein
Q9KNI2	VC_2757	Uncharacterized protein
Q9KNM7	VC_2705	Sodium/solute symporter, putative
Q9KPF0	VC_2418	Thiol:disulfide interchange protein
Q9KQ76	VC_2125	Flagellar motor switch protein FliN
Q9KQG6	VC_2032	Uncharacterized protein
Q9KQS3	VC_1925	C4-dicarboxylate transport sensor protein
Q9KR71	VC_1772	WYL domain-containing protein
Q9KRG4	VC_1678	Phage shock protein A
Q9KRH0	VC_1672	DNA-3-methyladenine glycosidase I
Q9KRM1	VC_1615	Uncharacterized protein
Q9KRR5	VC_1571	Quinol oxidase, subunit I
Q9KSM4	VC_1232	Uncharacterized protein
Q9KSN9	VC_1217	N-acetyltransferase domain-containing protein
Q9KTS9	VC_0809	SWIM-type domain-containing protein
Q9KTV0	VC_0787	Transcriptional regulator, LysR family
Q9KUN2	VC_0483	Uncharacterized protein
Q9KUW6	VC_0393	Uncharacterized protein
Q9KVR9	VC_0070	Uncharacterized protein

		II – 2. MoreJ420tgt_ThanF606wt	**log2 wt/tgt**	**p value**	**Adjusted p value**
Q9KNX3	kefG	Glutathione-regulated potassium-efflux system ancillary protein KefG	-7,30	0,00001	0,00036
Q9KLB8	phhA	Phenylalanine-4-hydroxylase	-4,14	0,00010	0,00068

P09545	hlyA	Hemolysin	-3,90	0,00039	0,00140
Q9KQN1	VC_1967	Methyl-accepting chemotaxis protein	-3,84	0,00567	0,00521
Q9KV16	queG	Epoxyqueuosine reductase	-3,39	0,00416	0,00420
H9L4T3	VC_2212	Uncharacterized protein - putative Fe3+-citrate ABC transporter	-3,32	0,00017	0,00094
Q9KTJ9	syd	Syd	-3,29	0,00057	0,00177
Q9KNW3	VC_2617	Arginine N-succinyltransferase	-2,93	0,00002	0,00050
Q9KU56	mutH	DNA mismatch repair protein MutH	-2,90	0,00004	0,00050
Q9KTZ6	VC_0734	Malate synthase	-2,81	0,00306	0,00389
Q9KKQ7	mtlA	PTS system mannitol-specific EIICBA component	-2,80	0,00214	0,00343
Q9KLB3	VC_A0833	Transcriptional regulator, LysR family	-2,66	0,00379	0,00420
Q9KTM2	VC_0880	Uncharacterized protein	-2,50	0,00364	0,00420
Q9KSQ4	hutH	Histidine ammonia-lyase	-2,42	0,00105	0,00227
Q9KPR5	VC_2301	Transcriptional activator, putative	-2,39	0,00075	0,00195
Q9KNF6	VC_A0008	Methyl-accepting chemotaxis protein	-2,27	0,00264	0,00357
Q9KRF2	VC_1690	Alpha-1,6-galactosidase, putative	-2,25	0,00022	0,00110
Q9KS52	VC_1408	Transcriptional regulator, TetR family	-2,20	0,00047	0,00154
Q9KUN3	argP	HTH-type transcriptional regulator ArgP	-2,20	0,00006	0,00050
Q9KU74	VC_0649	Transcriptional regulator, MarR family	-2,08	0,00232	0,00343
Q9KRA1	VC_1741	Transcriptional regulator, TetR family	-2,03	0,00074	0,00195
Q9KQ71	VC_2130	Flagellum-specific ATP synthase FliI	-1,89	0,00016	0,00094
Q9KUU2	arcA	Arginine deiminase	-1,88	0,00990	0,00732
Q9KM69	VC_A0519	Fructose repressor	-1,80	0,00183	0,00331
Q9KS51	VC_1409	Multidrug resistance protein, putative	-1,77	0,00895	0,00699
Q9KS17	VC_1444	Uncharacterized protein	-1,73	0,01228	0,00882
P0C6Q5	tcpF	Toxin coregulated pilus biosynthesis protein F	-1,72	0,00006	0,00050
Q9KVH8	VC_0168	Cytochrome c5	-1,65	0,00187	0,00331
Q9KP69	VC_2507	PINc domain-containing protein	-1,62	0,00903	0,00699
Q9KM51	VC_A0538	Cytochrome b561, putative	-1,62	0,00417	0,00420
Q9KTY1	VC_0749	Iron-sulfur cluster assembly scaffold protein IscU	-1,59	0,00072	0,00195
Q9KMJ5	VC_A0351	Uncharacterized protein	-1,56	0,00615	0,00534
Q9KS13	VC_1449	Uncharacterized protein	-1,54	0,01266	0,00895
Q9KLM0	VC_A0723	3-hydroxy-3-methylglutaryl CoA reductase	-1,53	0,00266	0,00357
Q9KV51	VC_0306	Thioredoxin	-1,50	0,00255	0,00357
Q9KRR1	VC_1575	Uncharacterized protein	-1,32	0,00274	0,00358
Q9F854	hisD	Histidinol dehydrogenase	-1,28	0,00385	0,00420
Q9KUS1	pdxA	4-hydroxythreonine-4-phosphate dehydrogenase	-1,25	0,00082	0,00195
Q9KSI8	VC_1268	Uncharacterized protein	-1,13	0,00714	0,00600
Q9KPA8	VC_2465	Sigma-E factor regulatory protein RseB	-1,08	0,00400	0,00420
Q9KLG6	VC_A0778	AHS2 domain-containing protein	-1,08	0,00343	0,00420
Q9KVJ1	VC_0153	Uncharacterized protein	-1,05	0,00936	0,00708
	II – 3. PresentJ420tgtTOB_AbsentF606wtTOB				
Q9KNM4	gmk	Guanylate kinase			
Q9KNC1	VC_A0044	Uncharacterized protein put mb protease			

Q9KRS9	VC_1557	Transcriptional regulator, LacI family lipid A biosynthesis acyltransferase			
Q9KQH2	VC_2026	Uncharacterized protein rRNA accumulation protein YceD			
Q9KRR2	VC_1574	Uncharacterized protein put Transmembrane signal peptide protein			
Q9KT04	VC_1101	Uncharacterized protein putative tryptophan/tyrosine transport system substrate-binding protein or T6SS			
Q9KVH8	VC_0168	Cytochrome c5			
Q9KR31	VC_1816	Uncharacterized protein 1 HYP TRANSPORTER			
Q9KQN0	VC_1968	Transcriptional regulator, HTH_3 family sutR regulator utilization of sulfur			
Q9KNT7	argB	Acetylglutamate kinase ornithine and arginine biosynthesis			
Q9KU61	VC_0662	Branched-chain amino acid transport system carrier protein brnQ transport leucine, valine, and isoleucine			
Q9KPR5	VC_2301	Transcriptional activator, putative putative anti-ECFsigma factor, ChrR			
Q9KQ26	prmC	Release factor glutamine methyltransferase			
Q9KM00	VC_A0589	Peptide ABC transporter, permease protein, putative oligopeptide ABC transporter membrane subunit YejE			
Q9KVR7	VC_0072	Sensory box/GGDEF family protein			
II – 4. MoreJ420tgtTOB_ThanF606wtTOB			**log2 wt/tgt**	**p value**	**Adjusted p value**
Q9KSP4	VC_1212	DNA polymerase	-2,38	0,01099	0,00512
Q9KR61	nanK	N-acetylmannosamine kinase	-4,31	0,00003	0,00043
Q9KT86	rnfA/rsxA	Ion-translocating oxidoreductase complex subunit A	-3,56	0,00002	0,00043
Q9KRT1	VC_1555	Uncharacterized protein	-1,48	0,00902	0,00488
Q9KV51	VC_0306	Thioredoxin trxA	-1,69	0,02226	0,00776
Q9KM51	VC_A0538	Cytochrome b561, putative	-2,87	0,00756	0,00474
Q9KNR9	VC_2662	Uncharacterized protein	-1,31	0,03255	0,00995
Q9KR73	VC_1770	Uncharacterized protein	-1,31	0,01849	0,00696
P0C6C8	fur	Ferric uptake regulation protein	-2,39	0,00030	0,00141
Q9KMN5	VC_A0293	Uncharacterized protein	-2,14	0,00017	0,00099
Q9KV88	VC_0268	Uncharacterized protein	-2,11	0,00406	0,00309
Q9KNQ9	rraA	Regulator of ribonuclease activity A	-2,42	0,00310	0,00269
Q9KPZ5	VC_2217	Beta-N-acetylhexosaminidase	-2,91	0,00054	0,00191
Q9KTN7	tadA	tRNA-specific adenosine deaminase	-2,04	0,00110	0,00224
Q9KRP5	VC_1591	Oxidoreductase, short-chain dehydrogenase/reductase family	-2,14	0,00804	0,00488
P0C6C4	flaB	Flagellin B	-1,88	0,00131	0,00228
Q9KTZ8	VC_0732	Transcriptional regulator, LysR family oxyR like	-1,96	0,00070	0,00210
Q9KSV6	VC_1150	Uncharacterized protein	-1,29	0,01007	0,00488
Q9KVM9	VC_0112	Cytochrome c4	-2,60	0,01486	0,00616
Q9KVK6	cdgJ	Cyclic di-GMP phosphodiesterase CdgJ	-3,89	0,00017	0,00099
Q9KR96	VC_1746	Transcriptional regulator, TetR family	-1,85	0,00299	0,00269
P0C6C5	flaC	Flagellin C OS=Vibrio cholerae serotype	-1,82	0,00042	0,00166
Q9KPX7	VC_2235	Methyltransf_11 domain-containing protein	-1,53	0,00144	0,00231

Q9KL76	VC_A0871	Transcriptional regulator, GntR family	-1,20	0,00284	0,00269
Q9KQ58	VC_2146	Uncharacterized protein	-1,38	0,00181	0,00235
Q9KKP2	ribB	3,4-dihydroxy-2-butanone 4-phosphate synthase	-2,73	0,00036	0,00157
Q9KNL7	greB	Transcription elongation factor GreB	-2,29	0,02154	0,00765
Q9KV61	VC_0296	Biotin carboxyl carrier protein of acetyl-CoA carboxylase	-1,70	0,00429	0,00317
Q9KUN2	VC_0483	Uncharacterized protein	-1,46	0,00180	0,00235
P0C6P9	tpx	Thiol peroxidase	-1,42	0,01847	0,00696
Q9KN91	VC_A0074	GGDEF family protein	-1,35	0,00934	0,00488
Q9KV27	nudC	NADH pyrophosphatase	-1,38	0,00104	0,00224
Q9KTF3	mrdB	Peptidoglycan glycosyltransferase	-1,35	0,00766	0,00476
Q9F854	hisD	Histidinol dehydrogenase	-1,60	0,00994	0,00488
Q9KV12	miaA	tRNA dimethylallyltransferase	-1,44	0,00177	0,00235
Q9KT82	VC_1023	Putative gluconeogenesis factor	-1,72	0,02103	0,00754
Q9KKQ1	VC_A1051	Uncharacterized protein	-1,32	0,00452	0,00324
Q9KKZ9	VC_A0951	UPF0145 protein VC_A0951	-1,30	0,01376	0,00600
Q9KLK6	luxP	Autoinducer 2-binding periplasmic protein LuxP	-1,19	0,00413	0,00310
Q9KTX4	ndk	Nucleoside diphosphate kinase	-1,10	0,01640	0,00653
Q9KMJ8	VC_A0345	Uncharacterized protein	-1,18	0,01699	0,00663
Q9KU82	rimP	Ribosome maturation factor RimP	-1,24	0,01367	0,00600
Q9KSF3	VC_1303	Para-aminobenzoate synthase, component I	-1,14	0,02352	0,00806
Q9KS93	queC	7-cyano-7-deazaguanine synthase	-1,01	0,01568	0,00635
Q9KQM0	VC_1978	5-deoxynucleotidase	-1,18	0,00153	0,00231
Q9KST2	trpE	Anthranilate synthase component 1	-1,86	0,03127	0,00968
Q9KN74	VC_A0091	UPF0251 protein	-1,10	0,01555	0,00634
Q9KL95	VC_A0851	HATPase_c domain-containing protein	-1,55	0,00154	0,00231
Q9KNJ9	VC_2739	AsmA domain-containing protein	-1,16	0,03228	0,00991

1531 **Table S2. Ribosome profiling.**

ID	log2FoldChange	p value adj
Transcripts UP		
VC_RS08405	5,16	2,54E-15
VC_RS08700	4,78	5,99E-03
glpD	4,19	1,40E-25
VC_RS00110	3,89	4,75E-13
VC_RS08400	3,83	3,23E-47
VC_RS07070	3,78	2,77E-05
VC_RS16920	3,64	9,32E-14
iscR	3,56	1,67E-24
VC_RS15320	3,47	4,97E-03
VC_RS16810	3,26	4,95E-04
hscB	3,14	6,58E-29
fadE	3,01	4,79E-14
siaQ	2,98	5,85E-06
VC_RS12540	2,90	2,09E-07
VC_RS15715	2,87	3,51E-03
VC_RS03415	2,76	5,14E-06
pdhR	2,69	4,02E-17
fadB	2,69	3,71E-16
VC_RS05835	2,66	2,21E-11
VC_RS12625	2,63	9,15E-17
VC_RS15780	2,57	3,00E-05
VC_RS06745	2,56	1,00E-03
VC_RS02460	2,53	4,43E-11
VC_RS15675	2,51	1,77E-07
VC_RS03375	2,50	3,27E-13
VC_RS15660	2,50	7,01E-08
VC_RS12840	2,45	1,93E-07
astA	2,43	3,51E-08
VC_RS18335	2,40	4,25E-05
VC_RS18385	2,40	6,53E-07
VC_RS18760	2,38	5,01E-03
VC_RS15265	2,37	1,85E-06
VC_RS15655	2,35	1,32E-08
VC_RS09590	2,34	2,10E-16
VC_RS17980	2,30	2,40E-07
rluC	2,30	3,62E-12
VC_RS08995	2,28	3,72E-05
VC_RS15750	2,25	9,78E-13
VC_RS06650	2,22	2,84E-03
VC_RS06240	2,21	3,77E-07
VC_RS17900	2,20	9,26E-06
dinB	2,19	6,60E-05
VC_RS16075	2,18	1,66E-06

glpK	2,13	5,64E-06
VC_RS03935	2,13	9,02E-06
VC_RS03750	2,13	3,89E-15
VC_RS09530	2,11	1,28E-03
iscA	2,10	7,00E-11
VC_RS18910	2,02	1,35E-03
VC_RS18595	2,00	3,76E-06
VC_RS06645	1,99	5,86E-04
VC_RS17880	1,97	1,27E-06
VC_RS17250	1,96	1,02E-04
VC_RS14235	1,95	7,29E-04
vpsQ	1,94	1,63E-05
VC_RS15795	1,92	3,27E-05
pncB	1,92	2,09E-11
VC_RS14320	1,91	3,76E-03
VC_RS19075	1,89	1,12E-06
VC_RS18065	1,88	2,22E-05
VC_RS05480	1,86	1,03E-03
VC_RS09310	1,86	1,69E-03
VC_RS16025	1,83	1,60E-07
VC_RS05200	1,82	3,76E-03
VC_RS06880	1,81	4,25E-06
VC_RS03615	1,81	9,36E-03
sdhC	1,80	8,98E-06
VC_RS12765	1,80	4,08E-06
vceC	1,77	2,69E-06
VC_RS08690	1,77	1,16E-03
VC_RS18420	1,75	4,95E-06
VC_RS06145	1,75	9,56E-08
VC_RS13705	1,73	3,89E-03
VC_RS09775	1,72	1,29E-05
VC_RS00830	1,72	2,06E-09
VC_RS15990	1,71	4,18E-04
astD	1,69	4,99E-05
rmuC	1,69	3,91E-06
cobA	1,67	6,18E-03
VC_RS06730	1,67	9,56E-03
VC_RS03925	1,67	2,64E-06
rpoE	1,65	3,06E-04
VC_RS13840	1,64	1,26E-06
pspC	1,62	5,50E-04
VC_RS05485	1,61	7,43E-04
VC_RS13775	1,60	2,22E-04
VC_RS13830	1,59	1,63E-05
VC_RS05795	1,59	8,95E-07
VC_RS04070	1,57	1,90E-04

pspA	1,55	6,11E-04
ectB	1,54	6,29E-03
VC_RS18060	1,53	9,22E-06
bioA	1,53	4,28E-03
VC_RS17350	1,50	2,41E-05
VC_RS16055	1,49	3,45E-04
VC_RS03930	1,49	2,68E-05
hppD	1,49	1,68E-03
rmf	1,48	6,04E-03
VC_RS18045	1,48	3,59E-03
pgl	1,47	3,65E-04
VC_RS09410	1,46	1,81E-03
VC_RS15825	1,46	8,01E-04
VC_RS01860	1,46	4,25E-03
VC_RS00045	1,46	2,22E-04
VC_RS08415	1,45	5,19E-05
thiC	1,44	3,32E-05
VC_RS03545	1,43	5,16E-04
VC_RS07590	1,42	2,00E-03
bioF	1,39	3,28E-05
vcrM	1,39	1,90E-03
VC_RS11130	1,38	4,37E-03
VC_RS13575	1,38	3,80E-03
thiD	1,37	1,07E-05
VC_RS17170	1,37	5,86E-04
VC_RS00235	1,37	1,19E-04
VC_RS06940	1,37	1,53E-05
purM	1,37	5,79E-04
emrD	1,35	1,37E-04
rpoS	1,32	9,84E-06
rpsN	1,31	5,86E-04
iscU	1,31	3,91E-04
VC_RS05395	1,30	3,89E-03
purN	1,30	6,54E-05
VC_RS08990	1,29	2,00E-03
truB	1,28	4,26E-04
rnc	1,28	4,81E-03
VC_RS16325	1,28	3,14E-03
miaB	1,25	1,55E-06
VC_RS00525	1,24	1,94E-03
VC_RS00310	1,24	2,05E-03
recN	1,23	1,53E-04
VC_RS00450	1,23	6,52E-03
norR	1,22	7,84E-04
rpmG	1,22	9,32E-03
VC_RS05080	1,20	3,77E-06

VC_RS00360	1,20	7,07E-04
VC_RS17040	1,20	2,06E-03
VC_RS11880	1,20	5,73E-05
zwf	1,19	9,56E-05
rimO	1,18	8,37E-04
xseB	1,18	1,46E-03
fadA	1,17	5,74E-03
pspB	1,17	7,83E-03
nhaA	1,17	2,57E-03
gspI	1,16	3,74E-03
VC_RS00180	1,16	1,52E-03
rluB	1,16	8,17E-05
VC_RS05405	1,15	2,69E-03
queE	1,15	9,97E-03
erpA	1,12	9,42E-03
VC_RS05410	1,11	2,47E-03
dbpA	1,06	7,53E-03
VC_RS15770	1,06	2,50E-03
VC_RS05800	1,06	1,80E-03
VC_RS15765	1,05	4,86E-03
ilvG	1,02	9,03E-04
VC_RS17205	1,02	2,74E-03
cgtA	1,02	2,06E-04
VC_RS08280	1,01	7,16E-04
lepA	0,98	1,30E-03
secD	0,97	1,44E-04
secD	0,97	1,44E-04
thiI	0,95	9,17E-03
yihI	0,94	7,72E-03
nlpD	0,93	6,99E-03
lipB	0,93	3,85E-03
VC_RS03795	0,92	6,44E-03
rpoH	0,91	2,26E-04
VC_RS07895	0,86	9,32E-03
ruvA	0,86	4,66E-03
ruvB	0,83	7,43E-03
mgtE	0,83	2,99E-03
mgtE	0,83	2,99E-03
der	0,82	2,14E-03
lepB	0,77	9,17E-03
Transcripts DOWN		
tgt	-5,96	1,33E-07
treC	-4,79	2,04E-86
VC_RS07220	-4,54	2,03E-02
VC_RS06415	-4,35	1,81E-24
VC_RS08165	-4,34	5,68E-48

VC_RS06535	-4,33	4,12E-20
treB	-4,26	3,95E-77
dcuC	-4,25	5,49E-40
frdD	-4,02	3,04E-05
VC_RS13520	-4,01	8,27E-03
VC_RS12800	-4,01	2,09E-15
VC_RS06405	-3,90	5,49E-40
VC_RS18125	-3,89	1,70E-24
adhE	-3,85	4,00E-38
VC_RS03955	-3,85	1,12E-06
VC_RS03950	-3,76	2,56E-13
frdC	-3,75	2,75E-14
VC_RS03300	-3,73	7,21E-21
VC_RS06410	-3,66	1,68E-19
VC_RS09000	-3,62	6,89E-35
frdA	-3,50	3,01E-12
VC_RS16590	-3,49	2,26E-11
VC_RS18120	-3,45	5,19E-20
VC_RS11425	-3,44	3,82E-18
VC_RS17100	-3,42	5,40E-24
grcA	-3,39	4,67E-14
nrdD	-3,38	6,19E-33
VC_RS14495	-3,36	4,85E-02
pepT	-3,35	8,01E-18
menC	-3,34	2,34E-16
VC_RS03305	-3,30	5,57E-23
VC_RS13030	-3,30	2,56E-03
VC_RS09030	-3,16	1,21E-22
VC_RS10340	-3,13	1,28E-10
VC_RS09395	-3,12	4,11E-18
VC_RS18865	-3,06	6,78E-05
VC_RS09390	-3,06	2,71E-20
menE	-3,05	1,43E-13
yccS	-2,99	1,50E-20
pykF	-2,94	2,21E-27
VC_RS13475	-2,93	4,46E-19
VC_RS04335	-2,90	6,37E-19
nrdG	-2,86	8,31E-09
ompW	-2,82	1,14E-12
VC_RS14490	-2,81	4,01E-02
pfkA	-2,80	1,13E-25
menB	-2,69	5,30E-14
VC_RS16905	-2,69	5,23E-27
VC_RS16240	-2,65	1,77E-14
pflB	-2,55	2,04E-18
VC_RS10735	-2,52	3,50E-09

VC_RS02445	-2,44	3,57E-12
VC_RS10000	-2,42	7,69E-10
vesC	-2,41	4,62E-15
VC_RS14330	-2,41	5,14E-15
VC_RS10325	-2,41	6,01E-11
gap	-2,38	1,72E-13
VC_RS03835	-2,37	3,58E-08
pgi	-2,30	3,04E-18
VC_RS09625	-2,30	4,67E-14
malT	-2,28	1,93E-13
malQ	-2,26	4,59E-15
VC_RS02160	-2,20	1,11E-14
VC_RS05160	-2,19	1,61E-17
VC_RS14510	-2,19	4,33E-04
VC_RS02215	-2,18	1,52E-05
VC_RS17420	-2,18	8,35E-17
glmS	-2,18	3,77E-04
VC_RS14455	-2,16	7,21E-21
bioD	-2,15	2,32E-15
malF	-2,11	7,13E-15
VC_RS06340	-2,07	2,48E-11
VC_RS08370	-2,05	1,61E-03
VC_RS02435	-2,04	7,63E-04
ppc	-2,04	4,69E-17
VC_RS12995	-2,04	5,80E-09
ilvC	-2,01	6,88E-10
gpmM	-2,01	2,13E-13
nhaC	-2,01	5,45E-17
narQ	-2,00	7,24E-04
feoB	-1,95	1,14E-04
VC_RS03315	-1,94	9,33E-10
VC_RS14530	-1,94	1,56E-02
malK	-1,93	4,62E-15
VC_RS03320	-1,92	3,28E-06
raiA	-1,91	6,39E-05
VC_RS08805	-1,90	2,13E-02
malE	-1,90	1,05E-13
VC_RS13960	-1,89	2,50E-04
VC_RS15980	-1,89	2,11E-11
eno	-1,89	3,01E-12
VC_RS14460	-1,89	4,21E-12
edd	-1,88	7,92E-09
VC_RS01665	-1,88	8,78E-06
elbB	-1,88	1,66E-05
malG	-1,88	6,61E-16
tpiA	-1,87	2,63E-10

VC_RS05825	-1,85	4,69E-07
VC_RS05625	-1,84	5,26E-07
VC_RS00575	-1,76	3,28E-04
VC_RS04300	-1,75	9,63E-13
VC_RS08210	-1,73	1,90E-05
VC_RS11965	-1,71	1,10E-07
VC_RS05975	-1,68	4,73E-05
ptsI	-1,68	2,67E-08
VC_RS11420	-1,63	1,01E-05
VC_RS02480	-1,59	4,28E-03
VC_RS18185	-1,58	7,43E-08
folA	-1,58	2,16E-05
VC_RS09155	-1,57	4,41E-05
VC_RS06100	-1,56	7,43E-03
VC_RS13010	-1,55	6,39E-03
tcpP	-1,55	2,45E-06
glgB	-1,55	3,74E-05
VC_RS00620	-1,55	6,37E-09
VC_RS16100	-1,53	1,92E-10
fbaA	-1,52	1,93E-06
VC_RS11495	-1,52	3,89E-04
ushA	-1,51	6,73E-07
hlyA	-1,49	4,31E-08
fdh3B	-1,49	5,16E-06
VC_RS05670	-1,49	1,67E-04
crp	-1,47	5,77E-10
VC_RS07315	-1,46	4,15E-09
VC_RS04785	-1,46	2,40E-07
nagK	-1,44	6,82E-06
lamB	-1,43	7,42E-06
pal	-1,43	2,31E-04
VC_RS02505	-1,42	2,01E-03
VC_RS08795	-1,41	8,87E-03
ccmD	-1,40	4,93E-02
gltB	-1,39	7,58E-08
gltB	-1,39	7,58E-08
VC_RS11435	-1,38	3,62E-05
VC_RS02090	-1,38	1,06E-02
fruA	-1,37	3,76E-10
VC_RS14360	-1,37	6,67E-06
hcp-2	-1,37	1,35E-03
hcp-2	-1,37	1,35E-03
fruB	-1,36	1,89E-07
VC_RS11635	-1,36	1,17E-05
VC_RS16670	-1,35	3,55E-04
VC_RS07305	-1,35	2,69E-06

VC_RS13950	-1,34	1,50E-03
VC_RS08520	-1,34	2,22E-05
menH	-1,33	9,08E-03
VC_RS05665	-1,33	2,65E-03
VC_RS17105	-1,32	1,71E-03
VC_RS02210	-1,32	3,87E-04
ptsG	-1,29	2,17E-06
VC_RS05295	-1,28	1,39E-04
VC_RS01370	-1,27	1,44E-03
pfkB	-1,27	2,74E-05
VC_RS09325	-1,27	4,85E-02
VC_RS02820	-1,25	2,75E-02
galK	-1,24	3,60E-04
VC_RS01625	-1,24	2,75E-03
VC_RS03680	-1,22	2,37E-02
VC_RS18380	-1,21	1,44E-03
katG	-1,21	1,44E-03
pntB	-1,21	1,32E-04
VC_RS07330	-1,21	4,84E-06
VC_RS14215	-1,21	1,92E-02
ccoO	-1,20	4,76E-02
VC_RS01395	-1,20	2,02E-02
tssM	-1,19	6,95E-04
VC_RS01300	-1,19	1,01E-02
asnB	-1,18	3,77E-05
tusB	-1,18	2,69E-03
VC_RS05860	-1,18	4,25E-03
VC_RS14825	-1,18	9,82E-03
VC_RS11350	-1,18	2,09E-03
VC_RS02830	-1,18	3,88E-03
VC_RS14815	-1,17	2,31E-04
VC_RS18835	-1,17	3,09E-02
VC_RS08225	-1,17	2,91E-03
modC	-1,16	3,88E-03
VC_RS16360	-1,16	4,86E-03
VC_RS01390	-1,16	1,96E-04
VC_RS14820	-1,15	3,49E-04
tcpH	-1,15	2,13E-02
VC_RS01790	-1,14	2,16E-05
VC_RS08240	-1,14	1,35E-02
tagO	-1,14	4,81E-02
fliN	-1,14	4,99E-05
VC_RS05660	-1,12	9,93E-03
VC_RS00855	-1,12	2,41E-04
arcA	-1,12	9,12E-03
arcA	-1,12	9,12E-03

VC_RS18700	-1,11	4,29E-03
VC_RS00635	-1,11	3,88E-03
can	-1,11	1,35E-03
VC_RS09920	-1,11	7,19E-05
VC_RS11900	-1,10	1,07E-03
ycfP	-1,09	1,73E-03
galM	-1,08	9,41E-03
VC_RS17495	-1,08	4,37E-05
VC_RS09885	-1,07	7,65E-04
VC_RS12600	-1,07	2,42E-02
VC_RS10600	-1,07	3,60E-04
VC_RS09255	-1,06	2,13E-02
VC_RS11255	-1,06	2,99E-03
oadA	-1,06	1,00E-02
oadA	-1,06	1,00E-02
nudF	-1,05	2,57E-03
VC_RS06640	-1,05	6,18E-04
VC_RS15915	-1,05	6,89E-04
rhtB	-1,04	1,80E-02
rimI	-1,04	3,82E-02
minE	-1,04	1,57E-02
VC_RS17175	-1,04	4,67E-04
VC_RS00770	-1,03	7,83E-03
VC_RS12105	-1,03	1,93E-02
hupA	-1,03	2,50E-03
VC_RS06960	-1,02	3,49E-02
VC_RS10580	-1,02	6,78E-05
VC_RS10825	-1,02	4,93E-02
VC_RS11450	-1,01	1,11E-02
VC_RS03100	-1,01	8,64E-03
chiS	-1,00	7,43E-04

1533 **Table S3. RNA-seq V. cholerae WT/Δtgt, in MH and TOB. Only significant differences higher than 2-**
1534 **fold are shown.**

MH					
locus_tag	old_locus_tag	gene	baseMean	log2FC WT/Δtgt	padj
VC_RS03715	VC0741,VC_0741	tgt	3412	6,91	3,3E-168
VC_RS13030	VC2706,VC_2706	yhhQ	5207	5,12	4,6E-148
VC_RS17680	VC_A0913,VCA0913	hutB	298	3,23	1,1E-06
VC_RS17670	VC_A0911,VCA0911	exbB	234	3,18	5,8E-07
VC_RS17690	VC_A0915,VCA0915	hutD	131	2,91	3,5E-05
VC_RS17675	VC_A0912,VCA0912	exbD	329	2,88	1,6E-09
VC_RS17685	VC_A0914,VCA0914	btuC/fecCD	362	2,80	2,7E-05
VC_RS03875	VC0773,VC_0773	entC	64	2,53	2,4E-04
VC_RS16165	VC_A0576,VCA0576	hutA	4750	2,51	5,1E-06
VC_RS17665	VC_A0910,VCA0910	tonB1	400	2,46	9,5E-07
VC_RS14430	VC_A0229,VCA0229	febD	356	2,44	1,4E-07
VC_RS17655	VC_A0908,VCA0908	hutX	1037	2,37	9,5E-07
VC_RS14435	VC_A0230,VCA0230	fhuC	617	2,34	1,7E-04
VC_RS17660	VC_A0909,VCA0909	hutW	1132	2,23	7,3E-07
VC_RS02435	VC0475,VC_0475	cirA	826	2,02	1,7E-03
VC_RS14425	VC_A0228,VCA0228	fepD	454	2,02	1,9E-07
VC_RS17650	VC_A0907,VCA0907	hutZ	3146	1,87	8,8E-06
VC_RS17955	VC_A0977,VCA0977	yejF	454	1,81	3,9E-08
VC_RS14420	VC_A0227,VCA0227	gcvH	2378	1,78	1,4E-05
VC_RS17950	VC_A0976,VCA0976		103	1,70	2,7E-02
VC_RS08170	VC1688,VC_1688	mglC	137	1,65	1,2E-02
VC_RS07460	VC1542,VC_1542	ligA	54	1,64	1,3E-04
VC_RS03070	VC0606,VC_0606	glnK	174	1,59	7,0E-03
VC_RS07475	VC1545,VC_1545	exbB	306	1,54	1,3E-04
VC_RS07470	VC1544,VC_1544	exbD	354	1,46	4,2E-04
VC_RS16600	VC_A0676,VCA0676	napF	1952	1,45	4,1E-02
VC_RS13690	VC_A0064,VCA0064	thiS	198	1,44	1,8E-03
VC_RS13695	VC_A0065,VCA0065	thiG	180	1,42	6,3E-04
VC_RS01835	VC0365,VC_0365	bfr	2422	1,39	1,1E-06
VC_RS07465	VC1543,VC_1543		1162	1,39	3,2E-04
VC_RS10685	VC2210,VC_2210	viuB	550	1,34	8,9E-04
VC_RS02430	VC0474,VC_0474	irgB	157	1,33	1,8E-02
VC_RS07595	VC1572,VC_1572		27	1,28	2,9E-02
VC_RS00985	VC0201,VC_0201	fhuC	92	1,27	3,2E-02
VC_RS00980	VC0200,VC_0200	fhuA	2454	1,25	3,7E-03
VC_RS07600	VC1573,VC_1573	fumC	197	1,25	9,7E-05
VC_RS10690	VC2211,VC_2211	viuA	527	1,24	4,5E-05
VC_RS07480	VC1546,VC_1546	exbB	303	1,23	2,0E-03
VC_RS03900	VC0778,VC_0778	fepG	53	1,19	4,6E-02
VC_RS03080	VC0608,VC_0608	fbpA	4516	1,18	1,3E-04

VC_RS13685	VC_A0063,VCA0063	ptrB	280	1,16	5,1E-03
VC_RS04975	VC1009,VC_1009		505	1,16	1,1E-05
VC_RS02570	VC0504,VC_0504	susC (tonB-like)	42	1,11	3,2E-02
VC_RS06170	VC1265,VC_1265	cytochrome C	511	1,10	1,3E-02
VC_RS07485	VC1547,VC_1547	exbB	692	1,09	6,0E-04
VC_RS05755	VC1174,VC_1174	trpE	263	1,07	9,7E-05
VC_RS03865	VC0771,VC_0771	vibB	412	1,06	1,1E-03
VC_RS16595	VC_A0675,VCA0675	narQ	770	1,03	4,9E-02
VC_RS16075	VC_A0558,VCA0558	yfjD	516	1,03	2,5E-02
VC_RS01830	VC0364,VC_0364	bfd	321	1,02	8,2E-03
VC_RS14440	VC_A0231,VCA0231	yqhC	272	1,00	2,7E-02
VC_RS02480	VC0486,VC_0486	srlR	748	1	3,2E-03
VC_RS12970	VC2694,VC_2694	sodA	503	0,80	5,1E-03

TOB

locus_tag	old_locus_tag	gene	baseMean	log2FoldChange WT/Δtgt	padj
VC_RS03715	VC0741,VC_0741	tgt	3412	5,991	5,0E-181
VC_RS13030	VC2706,VC_2706	yhhQ	5207	4,392	6,2E-114
VC_RS02575	VC0505,VC_0505		8	3,806	2,8E-02
VC_RS00075	VC0018,VC_0018	ibpA	4235	1,919	1,5E-03
VC_RS04265	VC0855,VC_0855	dnaK	17310	1,863	3,5E-03
VC_RS02570	VC0504,VC_0504	susC (tonB)	42	1,823	2,1E-04
VC_RS04385	VC0885,VC_0885		97	1,812	1,7E-03
VC_RS03575	VC0711,VC_0711	clpB	2525	1,688	1,2E-02
VC_RS04835	VC0977,VC_0977	cnoX	522	1,595	2,3E-03
VC_RS02995	VC0589,VC_0589	yadG	518	1,586	2,3E-02
VC_RS12835	VC2665,VC_2665	groES1	2421	1,555	4,6E-02
VC_RS18020	VC_A0989,VCA0989	dinF	136	1,511	2,5E-02
VC_RS04870	VC0985,VC_0985	htpG	9334	1,507	4,5E-02
VC_RS05980	VC1217,VC_1217	yjgM	88	1,406	7,7E-03
VC_RS04390	VC0886,VC_0886		208	1,381	5,8E-03
VC_RS16915	VC_A0744,VCA0744	glpK	1194	1,317	1,8E-09
VC_RS12880	VC2674,VC_2674	hslU	1673	1,268	1,6E-02
VC_RS12885	VC2675,VC_2675	hslV	365	1,261	5,9E-03
VC_RS00930	VC0188,VC_0188	prlC	2248	1,194	8,4E-03
VC_RS01320	VC0271,VC_0271	corC	728	1,155	1,2E-03
VC_RS02400	VC0468,VC_0468	gshB	1377	1,124	1,8E-04
VC_RS06455	VC1325,VC_1325	mglB	1478	1,089	8,0E-05
VC_RS09260	VC1920,VC_1920	lon	3601	1,066	2,3E-02
VC_RS02395	VC0467,VC_0467	ygqE	541	1,055	6,7E-04
VC_RS17520	VC_A0881,VCA0881		196	1,033	1,4E-02
VC_RS17525	VC_A0882,VCA0882		289	1,021	3,2E-03
VC_RS12360	VC2564,VC_2564	dbpA	618	-1,017	3,0E-02
VC_RS15790	VC_A0494,VCA0494	acetyltransferase	70	-1,028	3,7E-02

VC_RS03960	VC0792,VC_0792	yjfF oad	28	-1,029	2,6E-02
VC_RS14205	VC_A0179,VCA0179	psuT	156	-1,038	3,3E-02
VC_RS18615	VC_1646		27	-1,057	4,6E-02
VC_RS05270	VC1071,VC_1071	arsJ	117	-1,093	4,0E-03
VC_RS07060	VC1458,VC_1458	zot	640	-1,102	1,8E-02
VC_RS09405	VC1953,VC_1953	nupX	95	-1,131	2,3E-02
VC_RS18070	VC_A1000,VCA1000	leuE	62	-1,139	3,8E-02
VC_RS12345	VC2561,VC_2561	cobA	78	-1,143	3,3E-02
VC_RS15320			90	-1,171	1,4E-02
VC_RS06240	VC1279,VC_1279	betT	572	-1,246	9,9E-04
VC_RS15780	VC_A0492,VCA0492	RfbP-related protein	323	-1,262	8,5E-07
VC_RS07075	VC1461,VC_1461	cep ctx	2195	-1,282	1,9E-04
VC_RS12540	VC2600,VC_2600	yejM	397	-1,31	3,0E-03
VC_RS01360	VC0280,VC_0280	cadB	47	-1,346	5,1E-03
VC_RS16860	VC_A0732,VCA0732	ygiW	881	-1,417	1,5E-03
VC_RS18060	VC_A0998,VCA0998	nemA	385	-1,446	3,0E-02
VC_RS08700	VC1801,VC_1801		74	-1,462	2,6E-02
VC_RS01365	VC0281,VC_0281	cadA ldcI	60	-1,489	1,7E-03
VC_RS07640	VC1581,VC_1581	nuoL	56	-1,502	5,4E-03
VC_RS18100	VC_A1006,VCA1006	osmC	77	-1,521	2,0E-03
VC_RS07080	VC1462,VC_1462	rstB2	4846	-1,523	1,2E-04
VC_RS17365	VC_A0847,VCA0847	yjeH	141	-1,535	3,6E-04
VC_RS05275	VC1073,VC_1073		235	-1,617	1,0E-05
VC_RS08705	VC1802,VC_1802		35	-1,77	8,5E-03
VC_RS08695			66	-1,778	1,3E-03
VC_RS08680	VC1798,VC_1798	eha	131	-1,804	2,2E-05
VC_RS08690	VC1800,VC_1800		183	-1,851	8,0E-05
VC_RS07065	VC1459,VC_1459	ace	152	-1,939	4,0E-02
VC_RS08685	VC1799,VC_1799	phage transposase	302	-2,376	1,4E-08
VC_RS07040	VC1454,VC_1454	rstA1	29530	-2,705	1,9E-04
VC_RS07070	VC1460,VC_1460	orfU ctx	1156	-2,774	3,9E-08
VC_RS07085	VC1463,VC_1463	rstA2	29040	-2,893	5,1E-05

1537 **Table S4: Primers, plasmids and strains**

1538

gene expressions from pSEVA

plasmid in strain TOP10	name	primers used for gene amplification
M027	pSEVA238	MCSSEVA238-5 GCAAGAAGCGGATACAGGAG MCSSEVA238-3 GGTTTTCCCAGTCACGACGC
R591	pSEVA-tgt	5tgtEcoRI CGCGGAATTCGTGAAATTAAAATTTGAACTG and 3tgtXbaI CGCGTCTAGATCAGGCTTTGTCTTTTTGTAGTGG
Q298	pSEVA-rsxA	ZIP753 GCCCGAATTCCATTTGCCACTTATTGCG and ZIP754 GCCGCCGAATTCTTACAGTTTCACCAATCCGGTAAAGCC
Q294	pSEVA-soxR	ZIP757 GGGGCCCCCCCCGAATTCGTAAAGCGTTTTTTTAATAAAACGGG and ZIP758 CCGAATTCTTAACGGCTCCACTCTTCTGGATGCGATAAGCG
Q291	pSEVA-katG	ZIP755 GCGCGCCCCGAATTCATTTCCCATTTAGTGAAAAGGG and ZIP756 GAATTCTTACATCGCGGCCAGTTTTGCCACC

tRNA overexpression fragments cloned in pTOPO-blunt-kanamycin R (Ptrc promoter and VCt002 terminator are underlined, anticodon in red)

plasmid in TOP10	name	sequence
L961	Ptrc-eco-tRNA-Tyr wtGUA	GAGCTGTTGACAATTAATCATCCGGCTCGTATAATGTGTGGGGTGGGGTTCCCGAGCG GCCAAAGGGAGCAGACTGTAAATCTGCCGTCACAGACTTCGAAGGTTCGAATCCTTCC CCCACCACCACTTATTCGAGCTTAAGCTCAAAAAACTACA
M660	Ptrc-eco-tRNA-Tyr mutAUA	GAGCTGTTGACAATTAATCATCCGGCTCGTATAATGTGTGGGGTGGGGTTCCCGAGCG GCCAAAGGGAGCAGACTATAAATCTGCCGTCACAGACTTCGAAGGTTCGAATCCTTCC CCCACCACCACTTATTCGAGCTTAAGCTCAAAAAACTACA
L957	Ptrc-eco-tRNA-Asp wt GUC	GAGCTGTTGACAATTAATCATCCGGCTCGTATAATGTGTGGGGAGCGGTAGTTCAGTC GGTTAGAATACCTGCCTGTCACGCAGGGGGTCGCGGGTTCGAGTCCCGTCCGTTCCGC CACTTATTCGAGCTTAAGCTCAAAAAACTACA
L960	Ptrc-vch-tRNA-Tyr wtGUA	GAGCTGTTGACAATTAATCATCCGGCTCGTATAATGTGTGGGGAGGGGTTCCCGAGTG GCCAAAGGGAGCAGACTGTAAATCTGCCGGCTCCGCCTTCGATGGTTCGAATCCGTCC CCCTCCACCACTTATTCGAGCTTAAGCTCAAAAAACTACA
L959	Ptrc-vch-tRNA-Tyr mutAUA	GAGCTGTTGACAATTAATCATCCGGCTCGTATAATGTGTGGGGAGGGGTTCCCGAGTG GCCAAAGGGAGCAGACTATAAATCTGCCGGCTCCGCCTTCGATGGTTCGAATCCGTCC CCCTCCACCACTTATTCGAGCTTAAGCTCAAAAAACTACA
L956	Ptrc-vch-tRNA-Asp wtGUC	GAGCTGTTGACAATTAATCATCCGGCTCGTATAATGTGTGGGGAGCGGTAGTTCAGTC GGTTAGAATACCGGCCTGTCACGCCGGGGGTCGCGGGTTCGAGTCCCGTCCGCTCCG CCACTTATTCGAGCTTAAGCTCAAAAAACTACA
L955	Ptrc-vch-tRNA-mutAspAUC	GAGCTGTTGACAATTAATCATCCGGCTCGTATAATGTGTGGGGAGCGGTAGTTCAGTC GGTTAGAATACCGGCCTATCACGCCGGGGGTCGCGGGTTCGAGTCCCGTCCGCTCCGC CACTTATTCGAGCTTAAGCTCAAAAAACTACA
M651	Ptrc-vch-tRNA-Asn wtGUU	GAGCTGTTGACAATTAATCATCCGGCTCGTATAATGTGTGGTCCTCCTTAGCTCAGTCG GTAGAGCGACGGACTGTTAATCCGCAGGTCGCTGGTTCAAGTCCAGCAGGAGGAGCC ACTTATTCGAGCTTAAGCTCAAAAAACTACA
L962	Ptrc-vch-tRNA-Asn mutAUU	GAGCTGTTGACAATTAATCATCCGGCTCGTATAATGTGTGGTCCTCCTTAGCTCAGTCG GTAGAGCGACGGACTATTAATCCGCAGGTCGCTGGTTCAAGTCCAGCAGGAGGAGCC ACTTATTCGAGCTTAAGCTCAAAAAACTACA
M646	Ptrc-vch-tRNA-HIS wtGUG	GAGCTGTTGACAATTAATCATCCGGCTCGTATAATGTGTGGGTGGCTATAGCTCAGTT GGTAGAGCCCCGGATTGTGATTCCGGTTGTCGTGGGTTCGAGCCCCATTAGCCACCCC ACTTATTCGAGCTTAAGCTCAAAAAACTACA
L997	Ptrc-vch-tRNA-HIS mutAUG	GAGCTGTTGACAATTAATCATCCGGCTCGTATAATGTGTGGGTGGCTATAGCTCAGTT GGTAGAGCCCCGGATTATGATTCCGGTTGTCGTGGGTTCGAGCCCCATTAGCCACCCC ACTTATTCGAGCTTAAGCTCAAAAAACTACA
M653	Ptrc-vch-tRNA-Phe wtGAA	GAGCTGTTGACAATTAATCATCCGGCTCGTATAATGTGTGGGCCCGGATAGCTCAGTC GGTAGAGCAGAGGATTGAAAATCCTCGTGTCGGTGGTTCGATTCCGCCTCCGGGCACC ACTTATTCGAGCTTAAGCTCAAAAAACTACA

translational fusions ordered in pUC_IDT (carbenicillin R)

plasmid in strain DH5α	name	sequence

R973	Ptrc-rsxATAC-gfp	TTGACAATTAATCATCCGGCTCGTATAATGTGTGGAATTGTGAGCGGATAACAATTTCACACAGGA AACAGCGCCGCATGACCGAATACCTTTTGTTGTTAATCGGCACCGTGCTGGTCAATAACTTTGTAC TGGTGAAGTTTTTGGGCTTATGTCCTTTTATGGGCGTATCAAAAAAACTAGAGACCGCCATTGGCA TGGGGTTGGCGACGACATTCGTCCTCACCTTAGCTTCGGTGTGCGCTTACCTGGTGGAAAGTTAC GTGTTACGTCCGCTCGGCATTGAGTACCTGCGCACCATGAGCTTTATTTTGGTGATCGCTGTCGTA GTACAGTTCACCGAAATGGTGGTGCACAAAACCAGTCCGACACTCTACCGCCTGCTGGGCATTTTC CTGCCACTCATCACCACCAACTGTGCGGTATTAGGGGTTGCGCTGCTCAACATCAACGAAAATCAC AACTTTATTCAATCGATCATTTACGGTTTTGGCGCTGCTGTTGGCTTCTCGCTGGTGCTCATCTTGT TCGCTTCAATGCGTGAGCGAATCCATGTAGCCGATGTCCCCGCTCCCTTTAAGGGCGCATCCATTG CGATGATCACCGCAGGTTTAATGTCTTTGGCCTTTATGGGCTTTACCGGATTGGTGAAACTGGCTA GCAAAGGAGAAGAACTTTTCACTGGAGTTGTCCCAATTCTTGTTGAATTAGATGGTGATGTTAATG GGCACAAATTTTCTGTCAGTGGAGAGGGTGAAGGTGATGCTACATACGGAAAGCTTACCCTTAAA TTTATTTGCACTACTGGAAAACTACCTGTTCCATGGCCAACACTTGTCACTACTTTGACCTATGGTG TTCAATGCTTTTCCCGTTATCCGGATCATATGAAACGGCATGACTTTTTCAAGAGTGCCATGCCCGA AGGTTATGTACAGGAACGCACTATATCTTTCAAAGATGACGGGAACTACAAGACGCGTGCTGAAG TCAAGTTTGAAGGTGATACCCTTGTTAATCGTATCGAGTTAAAAGGTATTGATTTTAAAGAAGATG GAAACATTCTCGGACACAAACTCGAGTACAACTATAACTCACACAATGTATACATCACGGCAGACA AACAAAAGAATGGAATCAAAGCTAACTTCAAAATTCGCCACAACATTGAAGATGGAGGCGTTCAA CTAGCAGACCATTATCAACAAAATACTCCAATTGGCGATGGCCCTGTCCTTTTACCAGACAACCATT ACCTGTCGACACAATCTGCCCTTTCGAAAGATCCCAACGAAAAGCGTGACCACATGGTCCTTCTTG AGTTTGTAACTGCTGCTGGGATTACACATGGCATGGATGAGCTCTACAAATAA
R972	Ptrc-rsxATATWT-gfp	TTGACAATTAATCATCCGGCTCGTATAATGTGTGGAATTGTGAGCGGATAACAATTTCACACAGGA AACAGCGCCGCATGACCGAATATCTTTTGTTGTTAATCGGCACCGTGCTGGTCAATAACTTTGTAC TGGTGAAGTTTTTGGGCTTATGTCCTTTTATGGGCGTATCAAAAAAACTAGAGACCGCCATTGGCA TGGGGTTGGCGACGACATTCGTCCTCACCTTAGCTTCGGTGTGCGCTTATCTGGTGGAAAGTTACG TGTTACGTCCGCTCGGCATTGAGTATCTGCGCACCATGAGCTTTATTTTGGTGATCGCTGTCGTAG TACAGTTCACCGAAATGGTGGTGCACAAAACCAGTCCGACACTCTATCGCCTGCTGGGCATTTTCC TGCCACTCATCACCACCAACTGTGCGGTATTAGGGGTTGCGCTGCTCAACATCAACGAAAATCACA ACTTTATTCAATCGATCATTTATGGTTTTGGCGCTGCTGTTGGCTTCTCGCTGGTGCTCATCTTGTTC GCTTCAATGCGTGAGCGAATCCATGTAGCCGATGTCCCCGCTCCCTTTAAGGGCGCATCCATTGCG ATGATCACCGCAGGTTTAATGTCTTTGGCCTTTATGGGCTTTACCGGATTGGTGAAACTGGCTAGC AAAGGAGAAGAACTTTTCACTGGAGTTGTCCCAATTCTTGTTGAATTAGATGGTGATGTTAATGG GCACAAATTTTCTGTCAGTGGAGAGGGTGAAGGTGATGCTACATACGGAAAGCTTACCCTTAAAT TTATTTGCACTACTGGAAAACTACCTGTTCCATGGCCAACACTTGTCACTACTTTGACCTATGGTGT TCAATGCTTTTCCCGTTATCCGGATCATATGAAACGGCATGACTTTTTCAAGAGTGCCATGCCCGA AGGTTATGTACAGGAACGCACTATATCTTTCAAAGATGACGGGAACTACAAGACGCGTGCTGAAG TCAAGTTTGAAGGTGATACCCTTGTTAATCGTATCGAGTTAAAAGGTATTGATTTTAAAGAAGATG GAAACATTCTCGGACACAAACTCGAGTACAACTATAACTCACACAATGTATACATCACGGCAGACA AACAAAAGAATGGAATCAAAGCTAACTTCAAAATTCGCCACAACATTGAAGATGGAGGCGTTCAA CTAGCAGACCATTATCAACAAAATACTCCAATTGGCGATGGCCCTGTCCTTTTACCAGACAACCATT ACCTGTCGACACAATCTGCCCTTTCGAAAGATCCCAACGAAAAGCGTGACCACATGGTCCTTCTTG AGTTTGTAACTGCTGCTGGGATTACACATGGCATGGATGAGCTCTACAAATAA
R975	Ptrc-gfpTAC	GAGCTGTTGACAATTAATCATCCGGCTCGTATAATGTGTGGAATTGTGAGCGGATAACAATTTCAC ACAGGAAACACATATGCGTAAAGGAGAAGAACTTTTCACTGGAGTTGTCCCAATTCTTGTTGAATT AGATGGTGATGTTAATGGGCACAAATTTTCTGTCAGTGGAGAGGGTGAAGGTGATGCAACATAC GGAAAACTTACCCTTAAATTTATTTGCACTACTGGAAAACTACCTGTTCCATGGCCAACACTTGTCA CTACTTTCGGTTACGGTGTTCAATGCTTTGCGAGATACCCAGATCATATGAAACAGCATGACTTTTT CAAGAGTGCCATGCCCGAAGGTTACGTACAGGAAAGAACTATATTTTTCAAAGATGACGGGAACT ACAAGACACGTGCTGAAGTCAAGTTTGAAGGTGATACCCTTGTTAATAGAATCGAGTTAAAAGGT ATTGATTTTAAAGAAGATGGAAACATTCTTGGACACAAATTGGAATACAACTACAACTCACACAAT GTATACATCATGGCAGACAAACAAAAGAATGGAATCAAAGTTAACTTCAAAATTAGACACAACAT TGAAGATGGAAGCGTTCAACTAGCAGACCATTACCAACAAAATACTCCAATTGGCGATGGCCCTG TCCTTTTACCAGACAACCATTACCTGTCCACACAATCTGCCCTTTCGAAAGATCCCAACGAAAAGA GAGACCACATGGTCCTTCTTGAGTTTGTAACAGCTGCTGGGATTACACATGGCATGGATGAACTAT ACAAATAA
R974	Ptrc-gfpTAT	GAGCTGTTGACAATTAATCATCCGGCTCGTATAATGTGTGGAATTGTGAGCGGATAACAATTTCAC ACAGGAAACACATATGCGTAAAGGAGAAGAACTTTTCACTGGAGTTGTCCCAATTCTTGTTGAATT AGATGGTGATGTTAATGGGCACAAATTTTCTGTCAGTGGAGAGGGTGAAGGTGATGCAACATAT GGAAAACTTACCCTTAAATTTATTTGCACTACTGGAAAACTACCTGTTCCATGGCCAACACTTGTCA CTACTTTCGGTTATGGTGTTCAATGCTTTGCGAGATATCCAGATCATATGAAACAGCATGACTTTTT CAAGAGTGCCATGCCCGAAGGTTATGTACAGGAAAGAACTATATTTTTCAAAGATGACGGGAACT ATAAGACACGTGCTGAAGTCAAGTTTGAAGGTGATACCCTTGTTAATAGAATCGAGTTAAAAGGT ATTGATTTTAAAGAAGATGGAAACATTCTTGGACACAAATTGGAATATAACTATAACTCACACAAT GTATATATCATGGCAGACAAACAAAAGAATGGAATCAAAGTTAACTTCAAAATTAGACACAACAT TGAAGATGGAAGCGTTCAACTAGCAGACCATTATCAACAAAATACTCCAATTGGCGATGGCCCTG TCCTTTTACCAGACAACCATTATCTGTCCACACAATCTGCCCTTTCGAAAGATCCCAACGAAAAGAG AGACCACATGGTCCTTCTTGAGTTTGTAACAGCTGCTGGGATTACACATGGCATGGATGAACTATA TAAATAA

plasmid in strain (WT/*Δtgt*)	codon replacement	introduction of point mutation in circular pTOPO-TA (kanamycin R) by PCR using primers :
N509/N511	bla wt	Tyr103TAC Asp129GAT
N512/N514	bla Tyr103TAC > Tyr TAT synonymous	ZIP555 GACTTGGTTGAGTATTCACCAGTCACAGAAAAGC ZIP556 TCTGTGACTGGTGAATACTCAACCAAGTCATTCTGAGAATAG
plasmid in strain TOP10	primers for transcriptional fusion PrsxA-gfp	
Q282	ZIP796 ZIP812 ZIP813 ZIP200	GGATACAAAAAAGTAAACCC CTCCTTTACGCATAGTTATATAAATGTTTGCTTCCGATCCCGGCATTATCCTG CAGGATAATGCCGGGATCGGAAGCAAACATTTATATAACTATGCGTAAAGGAG TATCAAGCTTATTTGTATAGTTCATCCATGCC
target for amplification	primers for q-RT-PCR tRNAs	
tRNATyr	ZIP719 ZIP720	GGAGGGGTTCCCGAGTGG GGTGGAGGGGGACGGATT
tRNAAsp	ZIP721 ZIP722	GGAGCGGTAGTTCAGTCG TGGCGGAGCGGACGGGAC
tRNAHis	ZIP723 ZIP724	GTGGCTATAGCTCAGTTG TGGGGTGGCTAATGG
tRNAAsn	ZIP725 ZIP726	TCCTCCTTAGCTCAGTCGG TGGCTCCTCCTGCTGG
gyrA	gyrA_F gyrA_R	AAT GTG CTG GGC AAC GAC TG GAG CCA AAG TTA CCT TGG CC
target for amplification	primers for digital-RT-PCR fluorescent probes	
tgt		fwd CAA CAC CAC TGG ATC CTC ATT rev GGT AGT AAC GCA GGT TAT GG 5' - [FAM] A CCT GCA TCA TCT GGA TCG CTG TAA - 3' [BHQ2]
rsxA		fwd TCA CGC ATT GAA GCG AAC rev CAC CAA CTG TGC GGT ATT AG 5' - [FAM] A GCG CCA AAA CCA TAA ATG ATC GAT - 3' [BHQ2]
gyrA		fwd AAT GTG CTG GGC AAC GAC TG rev GAG CCA AAG TTA CCT TGG CC 5' - [CY5] - CAC CCT CAT GGT GAC AGT GCG GTT T - 3' [BHQ2]
Strains		
V. cholerae	strain #	reference
N16961 hapR+	F606	laboratory collection
N16961 hapR+ ΔlacZ	K329	Babosan et al, 2022
Δtgt::spec	J420	Babosan et al, 2022
ΔtolA::kan	J983	Negro et al, 2019
Δcrp::kan	Q081	Deletion of *crp* in F606 as described in Lang et al, 2021
ΔrluF::kan	M567	Babosan et al, 2022
ΔrluF::kan Δtgt::spec	M569	Deletion of *rluF* in J420, as described for deletion of *rluF* in WT in Babosan et al, 2022
E. coli	strain #	construction
MG1655	C349	laboratory collection
Δtgt::kan	J233	P1 transduction of tgt::kan from Keio collection into MG1655
Δtgt	R181	Kanamycin resistance cassette was removed using the FLP/FRT system (Zhu et al, 1995)
ΔrsxA::kan	R207	P1 transduction of tgt::kan from Keio collection into MG1655
Δtgt ΔrsxA::kan	R223	P1 transduction of rsxA::kan from Keio collection into R181 *Δtgt*

1539

1540

1541

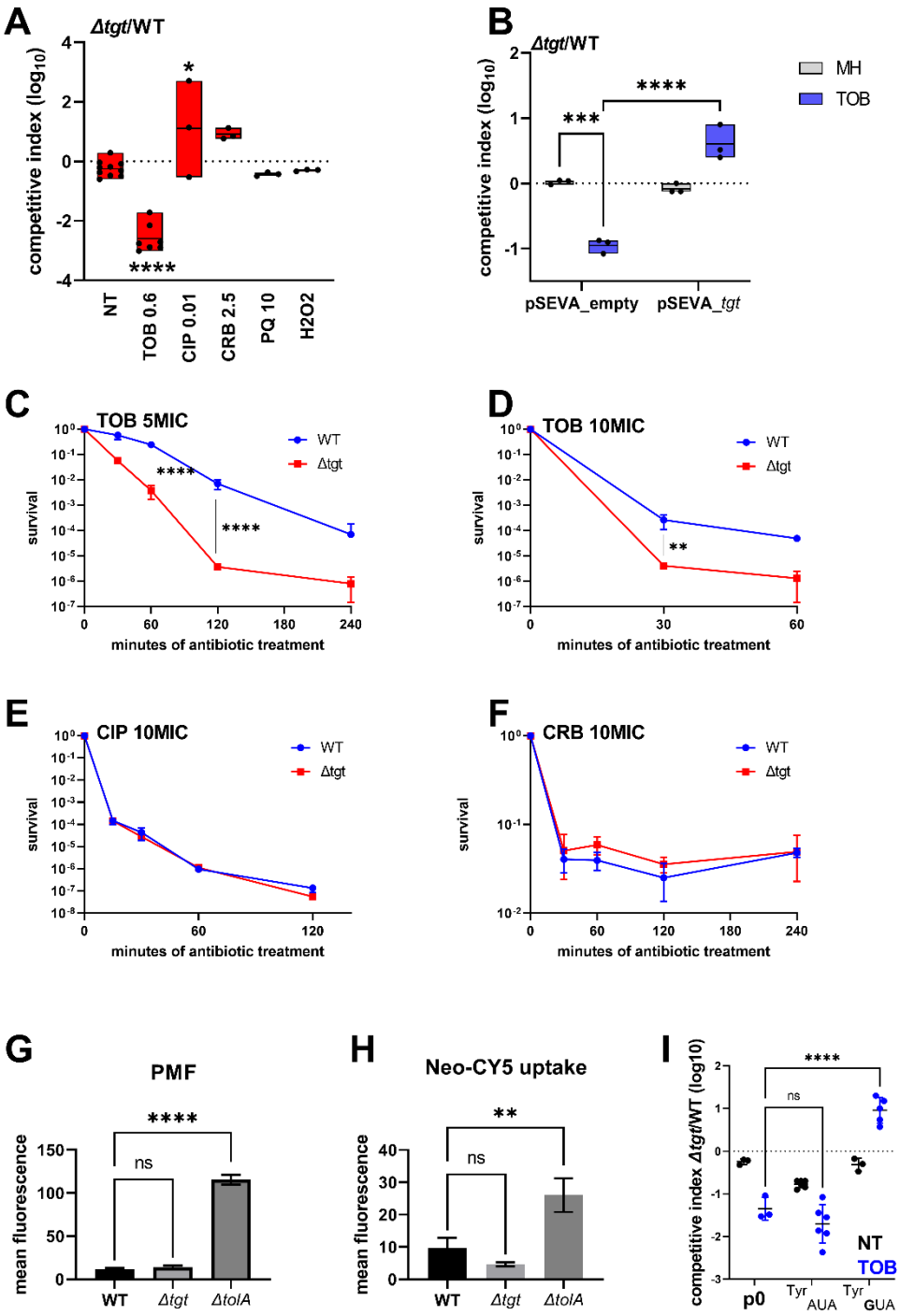

Figure 1. *V. cholerae Δtgt* shows decreased aminoglycoside tolerance. A. Competition experiments between WT and *Δtgt* with the indicated antibiotic or oxidant at sub-MIC concentration. *NT: non-treated.* TOB: tobramycin 0.6 µg/ml; CIP: ciprofloxacin 0.01 µg/ml; CRB: carbenicillin 2.5 µg/ml; PQ: paraquat 10 µM; H_2O_2: 2mM. **B.** Competition experiments between WT and *Δtgt* carrying the indicated plasmids. pSEVA-*tgt*: plasmid expressing *tgt* using the XylS regulated Pm promoter, which is activated using sodium benzoate. MH: *non-treated*. **CDEF**. Survival of exponential phase cultures after various times of incubation (indicated in minutes on the X-axis) with the indicated antibiotic at lethal concentration: 5MIC: 5 times the MIC; 10MIC: 10 times the MIC. **G.** PMF measurement of exponential phase cultures using fluorescent Mitotracker dye, measured using flow cytometry. **H**. Neomycin uptake measurement by flow cytometry using fluorescent Cy5 coupled neomycin. **I.** Competition experiments between WT and *Δtgt* carrying either empty plasmid (p0), or a plasmid overexpressing $tRNA^{Tyr}$ with the native GUA anti-codon, or with the synthetic AUA anticodon. The anticodon sequence is indicated (e.g. $tRNA^{Tyr}_{AUA}$ decodes the UAU codon). *NT: non-treated.* TOB: tobramycin 0.6 µg/ml. For multiple comparisons, we used one-way ANOVA. **** means p<0.0001, *** means p<0.001, ** means p<0.01, * means p<0.05. ns: non-significant. Number of replicates for each experiment: 3<n<8.

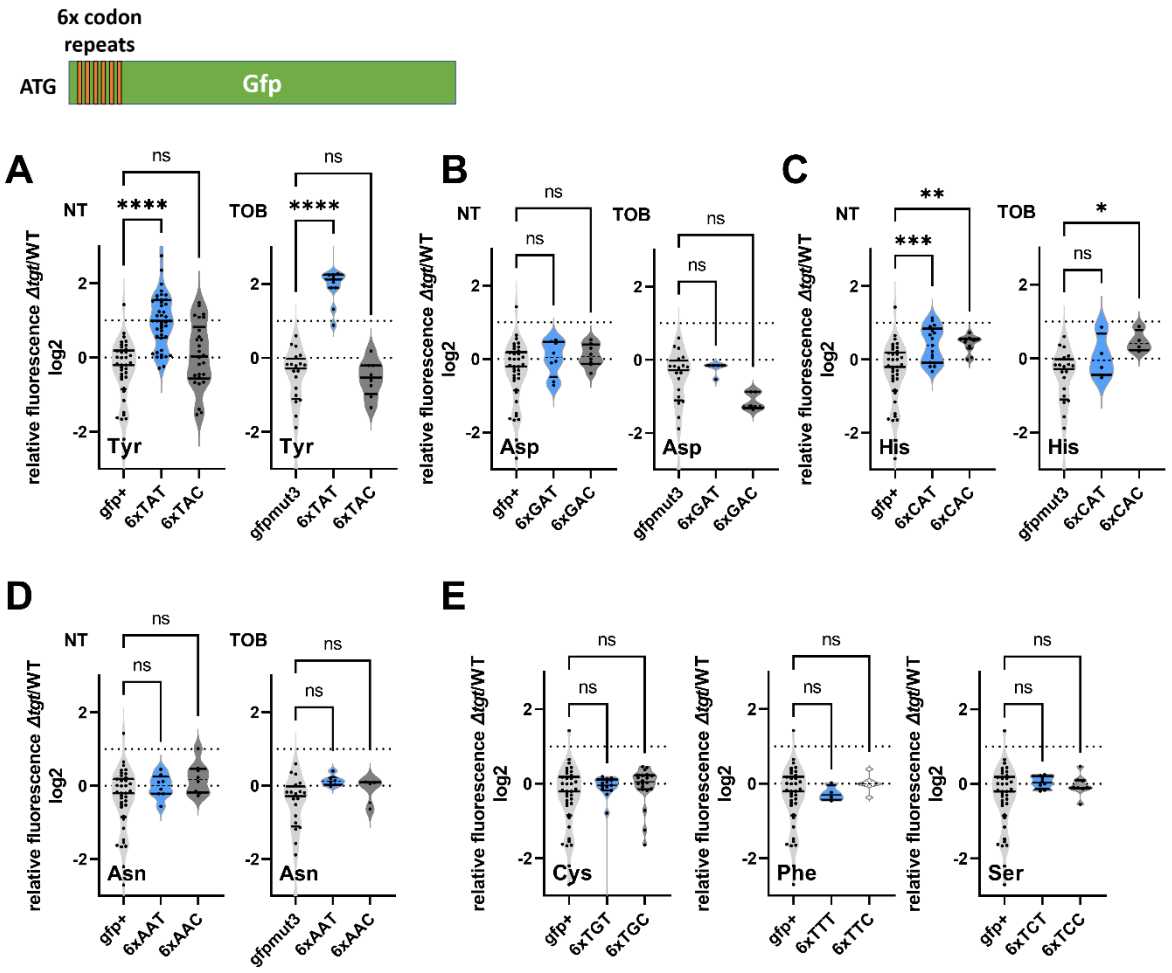

Figure 2. Codon decoding differences for *V. cholerae* WT and *Δtgt*. A. to E. Codon specific translation efficiency in WT and *Δtgt* using 6xcodon stretches inserted in GFP. Y axis represents the relative fluorescence of a given GFP in Δtgt over the same construct in WT. NT: non-treated; TOB: tobramycin at 0.4 µg/ml. Each specified codon is repeated 6x within the coding sequence of the GFP (e.g. TACTACTACTACTACTAC). For multiple comparisons, we used one-way ANOVA. **** means p<0.0001, *** means p<0.001, ** means p<0.01, * means p<0.05. ns: non-significant. Number of replicates for each experiment: 3<n, each dot represents one replicate.

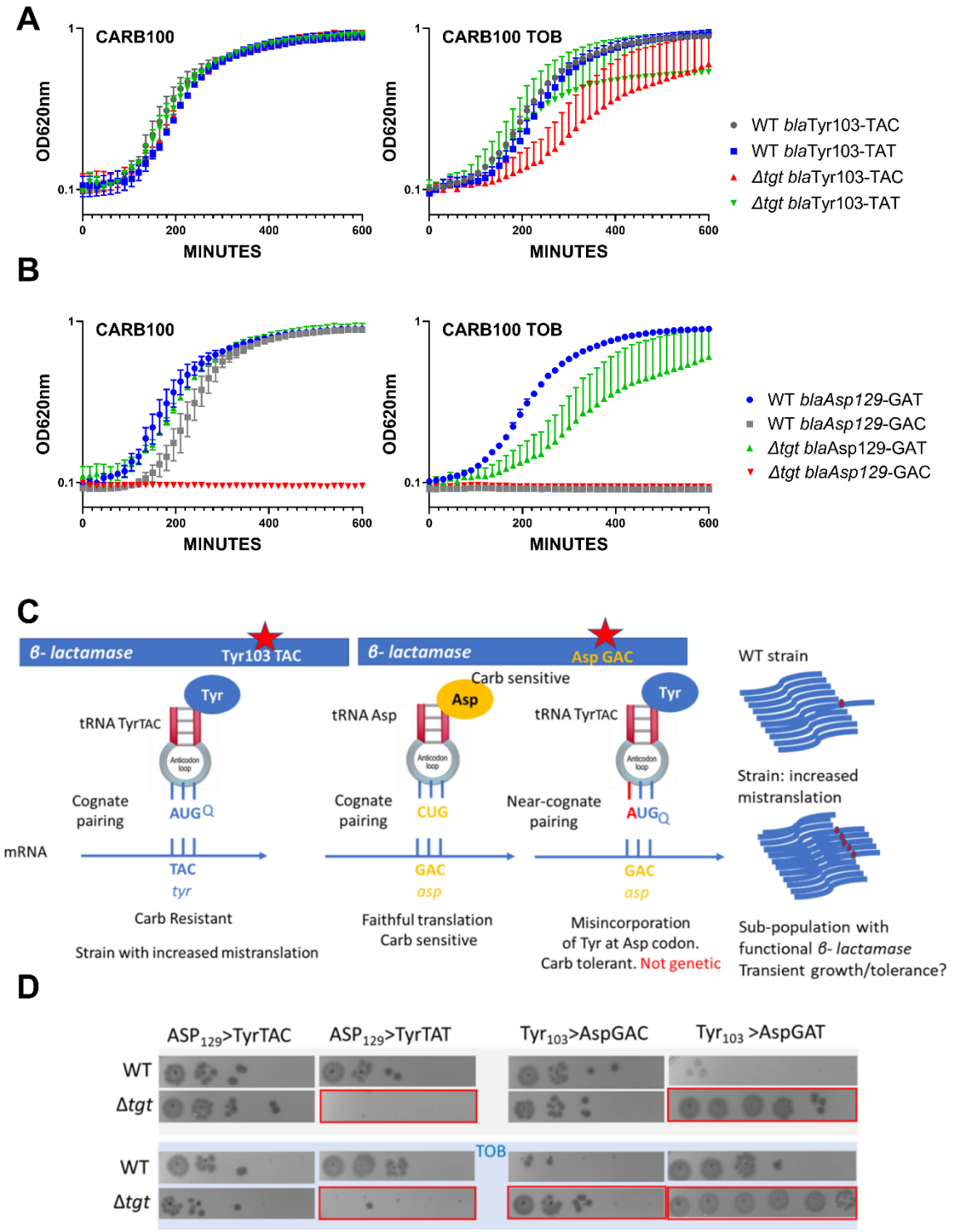

Figure 3. Differential translation at tyrosine and aspartate codons evaluated by growth on carbenicillin of mutated β-lactamase reporters. **A.** The catalytic tyrosine at position 103 was tested in its native sequence (TAC), or with the synonymous TAT mutation. **B**. The catalytic aspartate at position 129 was tested in its native sequence (GAT), or with the synonymous GAC mutation. **A and B.** Growth on microtiter plates. Growth was followed by measuring the OD 620 nm every 15 minutes during 600 minutes. CARB was used at 100 µg/ml. When present, TOB was used 0.2 µg/ml (20% of MIC). Curves represent mean and standard errors from biological duplicates. **C:** rationale. **D.** Cells were grown to early exponential phase without carbenicillin, and with (down) or without (top) tobramycin 20% of MIC, and treated with carbenicillin at 10xMIC for 20h. Dilutions were spotted on plate without carbenicillin. Surviving cells shown here are sensitive to carbenicillin (no growth on carbenicillin containing plates), suggesting that increased or decreased survival was due to increased (erroneous translation) or decreased (faithful translation) β-lactamase activity at the time of treatment. Number of replicates for each experiment: 3. One representative experiment is shown.

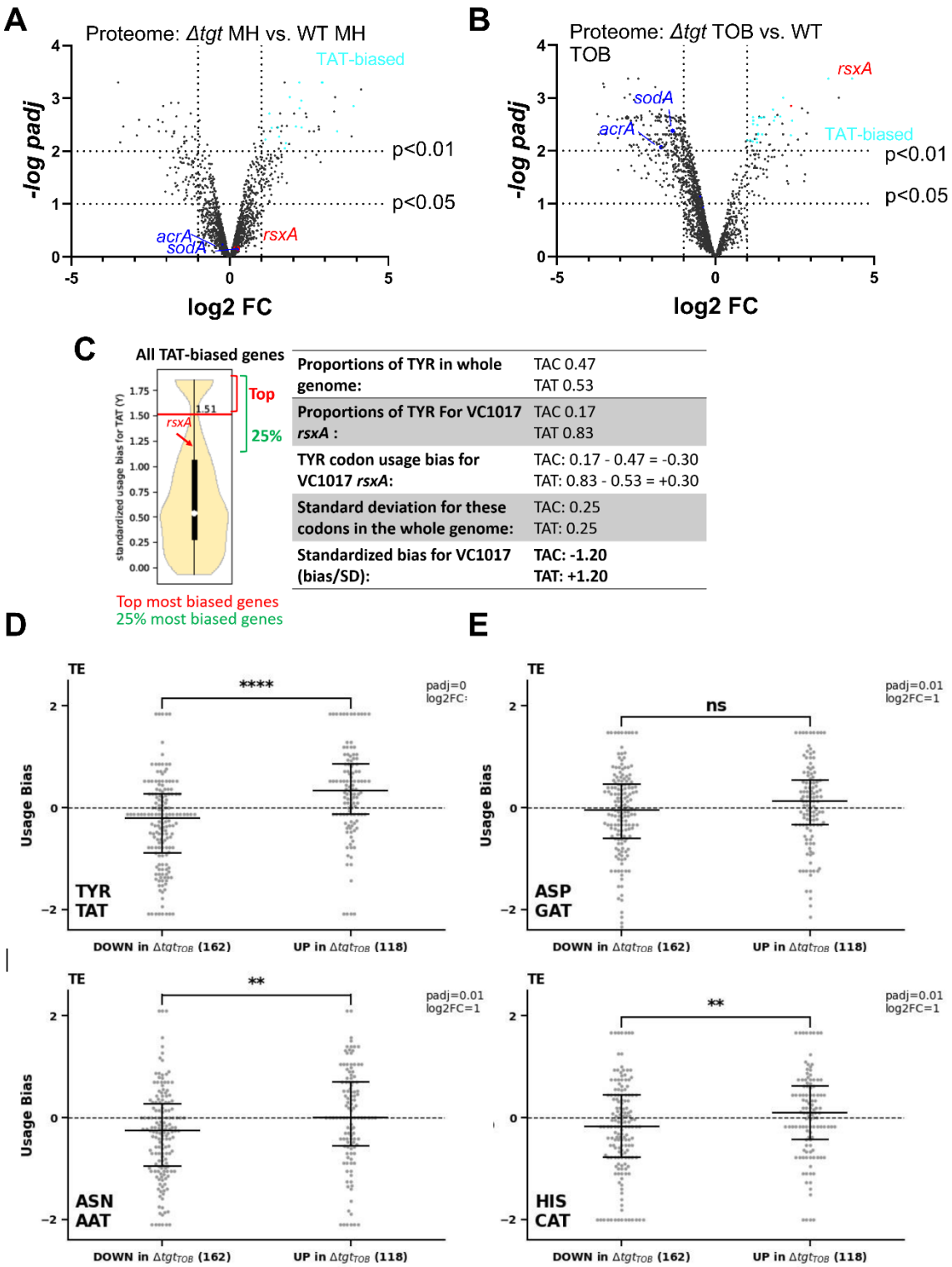

Figure 4. Post-transcriptional regulation in *Δtgt* and Tyr codon usage bias. A. and B. Volcano plots showing less and more abundant proteins in proteomics analysis (performed in triplicates) in *Δtgt* compared to WT during growth without antibiotics (A. where MH is the growth medium), or in sub-MIC TOB at 0.4 µg/ml (B.). **C.** Codon usage bias calculation example with VC1017 *rsxA* tyrosine TAC and TAT codons. **D. to G.** Plots showing codon usage bias for genes lists that are up or down in ribosome profiling analysis (performed in triplicates), normalized to RNA-seq values for each gene, for codons decoded by tRNAs with Q modification. Each dot represents one gene of the lists. TE: translation efficiency (Riboseq value normalized to RNA-seq value).

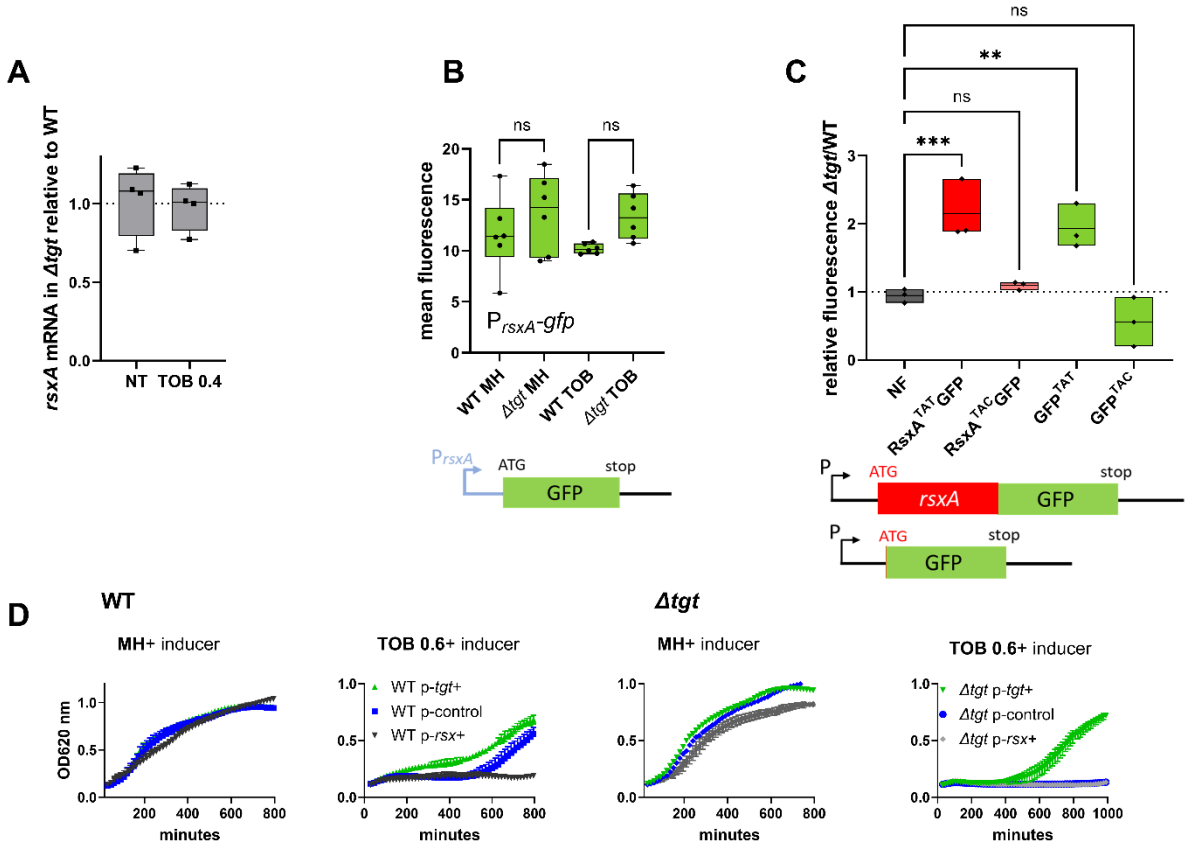

Figure 5. Post-transcriptional upregulation of RsxA in *Δtgt* due to a Tyr codon bias towards TAT and toxicity in sub-MIC TOB. A. *rsxA* mRNA levels measured by digital RT-PCR. 4 biological replicates. **B.** Transcriptional expression levels from the *rsxA* promoter measured by flow cytometry. 6 biological replicates **C.** Translational fusion of *rsxA* to *gfp* and *gfp* alone, with differences in codon usage. 3 biological replicates. One-way ANOVA was used to determine the statistical differences (p-value) between groups. *** means p<0.001, ** means p<0.01, ns: non-significant. **D.** Growth curves in microtiter plate reader, in *V. cholerae* in indicated conditions. P-*tgt*+: pSEVA expressing *tgt*. P-*rsx*+: pSEVA expressing rsxA. P-control: empty pSEVA. Inducer: DAPG (see methods). 2 biological replicates and standard errors are shown for each curve.

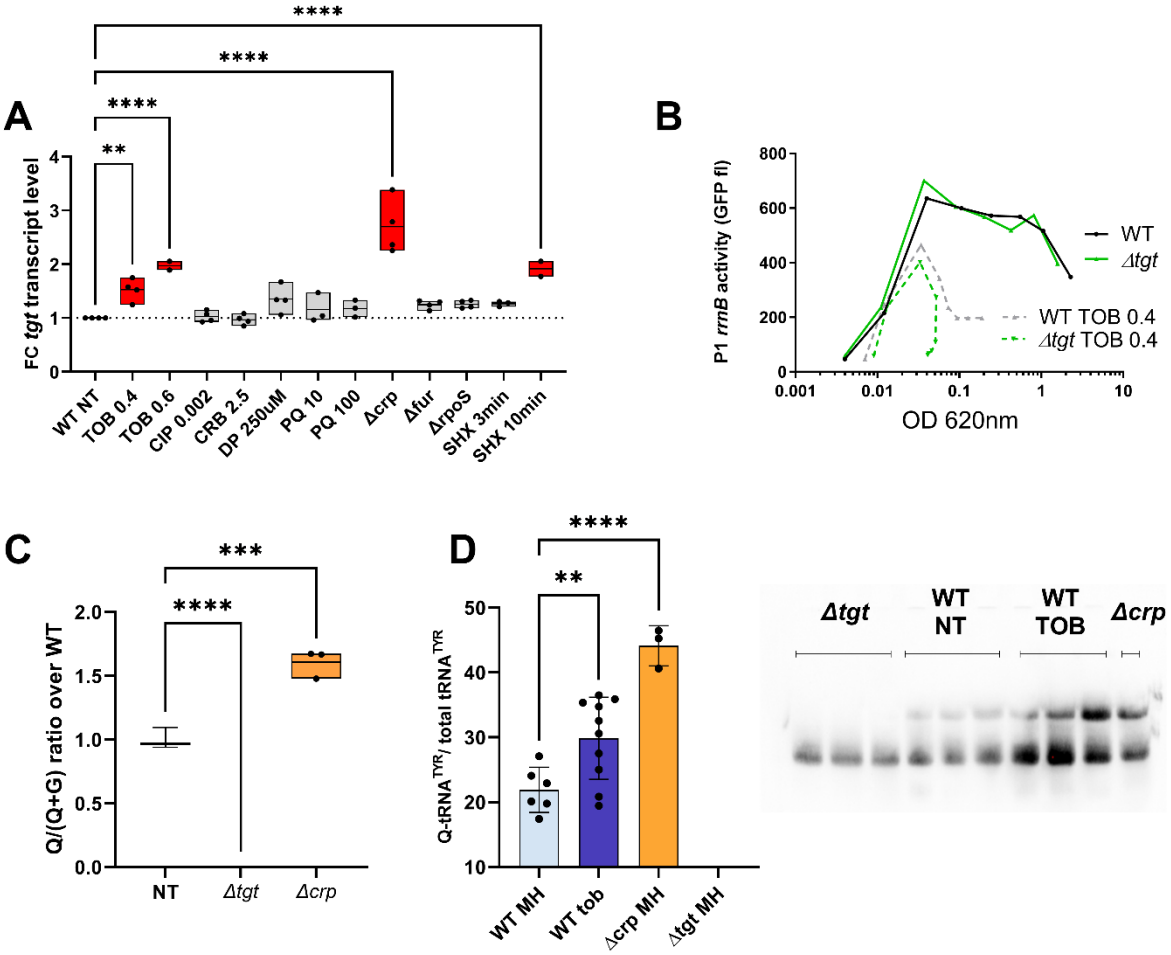

Figure 6. Regulation of *tgt* expression and tRNA Q levels. A: *tgt* transcript levels measured by digital-RT-PCR. Y-axis represents relative abundance compared to the non-treated (NT) condition in WT. **B.** Stringent response induction measured with *P1rrn-gfp* reporter shown as fluorescence (Y-axis) as a function of growth (X-axis: OD 600 nm). **C.** Q levels in tRNA enriched RNA extracts, measured by mass spectrometry**. D.** Northern blot and quantification of Q levels in $tRNA^{Tyr}$. The lower band in the gel corresponds to unmodified $tRNA^{Tyr}$. The upper band corresponds to Q-modified tRNA-Tyr. *Δtgt* is the negative control without modification of $tRNA^{Tyr}$. A representative gel is shown. Histograms show the quantification of Q-modified $tRNA^{Tyr}$ over total $tRNA^{Tyr}$**,** as follows: Q-modified $tRNA^{Tyr}$/(Q-modified $tRNA^{Tyr}$ + $tRNA^{Tyr}$ without Q)= upper band/(upper band + lower band). 2.5 µg of in tRNA enriched RNA extracts were deposited in lanes WT NT, WT TOB and *Δcrp*. 0.9 µg was deposited in lanes *Δtgt.* Number of replicates for each experiment: 3. For multiple comparisons, we used one-way ANOVA (for A. C. E.). **** means $p<0.0001$, *** means $p<0.001$, ** means $p<0.01$. Only significant differences are shown.

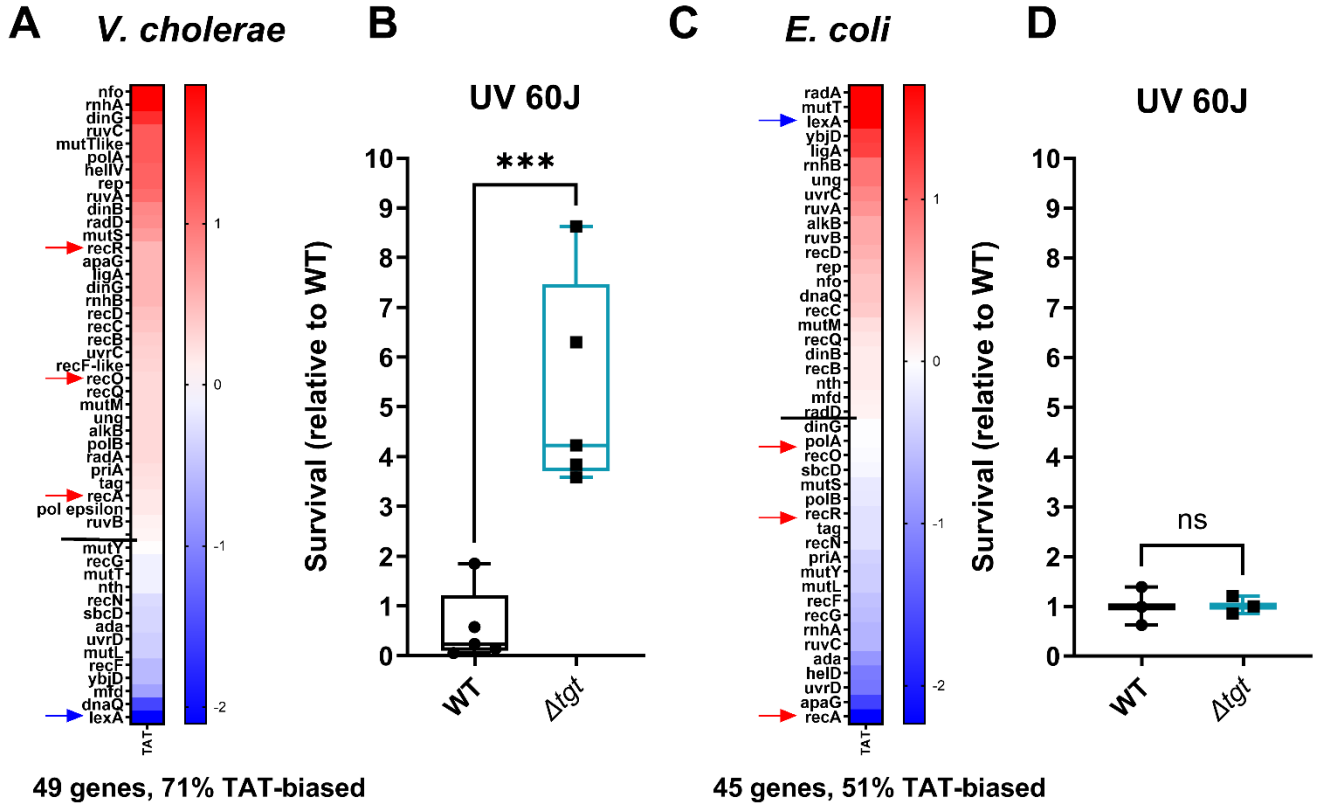

Figure 7. DNA repair after UV irradiation is more efficient in *V. cholerae Δtgt*. A and C. Tyrosine codon usage of DNA repair genes A: in *V. cholerae. C: in E. coli.* Red indicates positive codon usage bias, i.e. TAT bias. Blue indicates negative codon usage bias for TAT, i.e. TAC bias. **B and D.** Survival of *Δtgt* relative to WT after UV irradiation (linear scale) B: in *V. cholerae. D: in E. coli.* For multiple comparisons, we used one-way ANOVA. **** means p<0.0001, ns: non-significant.

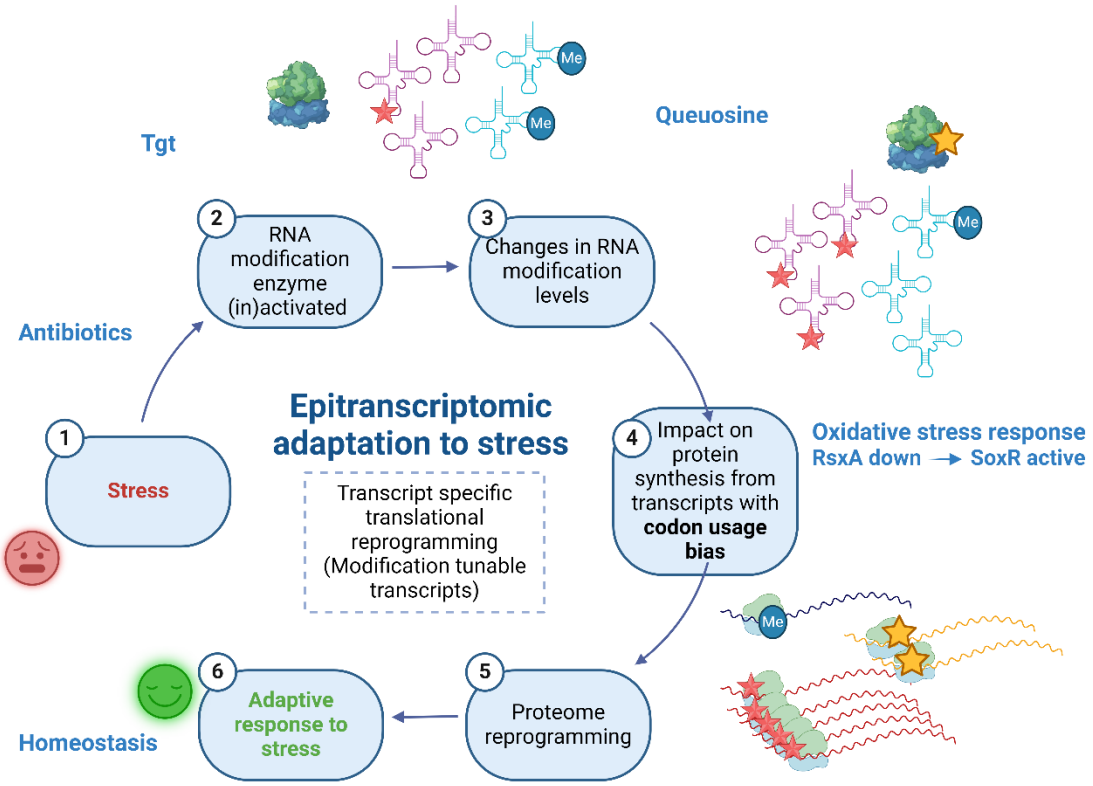

Figure 8. Model. Upon exposure to sub-MIC aminoglycosides, the expression of *tgt* is up-regulated in *V. cholerae* and influences the decoding of tyrosine TAC vs TAT codons. This leads to differential translation from transcripts bearing a codon usage bias for tyrosine codons. The *rsxA* transcript bears a tyrosine codon bias and its translation can be tuned by tRNA Q modification. RsxA is an anti-SoxR factor. SoxR controls a regulon involved in oxidative stress response. When RsxA levels are high, SoxR is increasingly inactivated and oxidative stress response efficiency decreases. It has been previously shown that sub-MIC aminoglycosides trigger oxidative stress in *V. cholerae*{Baharoglu, 2013 #720}. Increasing RsxA levels thus reduces fitness in TOB by hampering efficient oxidative stress response. As a corollary, decreased RsxA would lead to increased expression of the SoxR regulon, which would allow for more efficient response to oxidative stress, and increased fitness in the presence of sub-MIC TOB. We propose that when Tgt/Q levels in tRNA increase, RsxA synthesis is low and active SoxR levels are high, facilitating the bacterial response to aminoglycoside dependent oxidative stress. Created with BioRender.com

Supplementary Figures

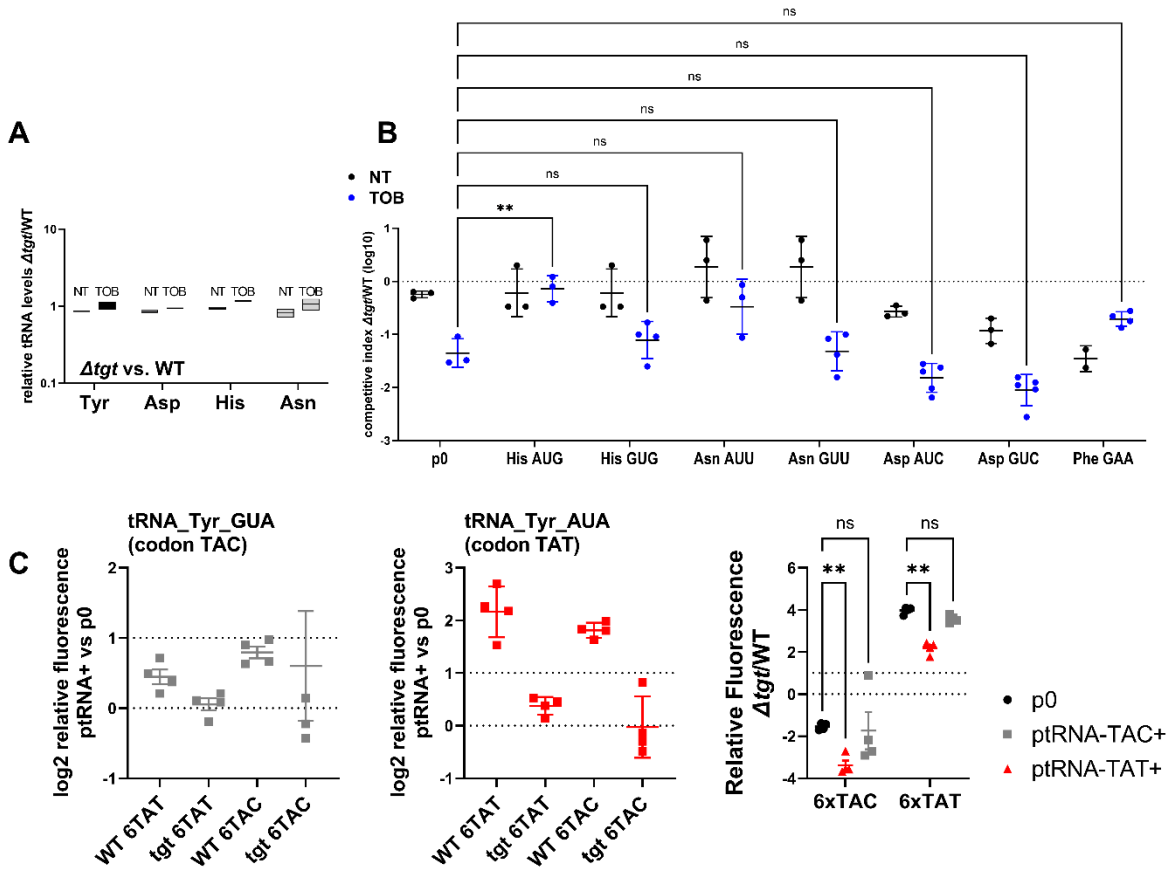

Figure S1. Impact of tRNA overexpression on fitness during growth in sub-MIC TOB. A. Absence of *tgt* does not visibly affect endogenous tRNA-GUN levels. qRTPCR. A: relative tRNA abundance in *Δtgt* compared to WT strain in the absence of treatment (NT) and in the presence of sub-MIC tobramycin (TOB). **B.** In vitro competition experiments between *V. cholerae* WT and *Δtgt* strains, carrying a plasmid overexpressing the indicated tRNA; in the absence (NT) or presence of sub-MIC tobramycin (50% of the MIC, TOB 0.6 µg/ml). NT: no antibiotic treatment. The Y-axis represents $\log_{10}$ of competitive index calculated as described in the methods. A competitive index of 1 indicates equal growth of both strains. The X-axis indicates which tRNA is overexpressed, from the high copy pTOPO plasmid. The anticodon sequence is indicated (e.g. $tRNA^{Tyr}_{AUA}$ decodes the TAT codon). The following tRNAs-GUN are the canonical tRNAs which are present in the genome, and modified by Tgt: Tyr_{GUA}, His_{GUG}, Asn_{GUU}, Asp_{GUC}. The following tRNAs-AUN are synthetic tRNAs which are not present in the genome: Tyr_{AUA}, His_{AUG}, Asn_{AUU}, Asp_{AUC}. $tRNA^{Phe}_{GAA}$ is used as non Tgt-modified control. p0 is the empty plasmid. **C. Codon specific translation efficiency in WT and *Δtgt* using 6xcodon stretches inserted in GFP**. Left: Y axis represents the relative fluorescence of the indicated gfp variant in WT and *Δtgt* strains carrying indicated tRNA overexpression plasmid normalized to fluorescence with empty plasmid (no tRNA overexpression). Right: ratio of *Δtgt* over WT. Y axis represents the relative fluorescence of a given GFP in *Δtgt* over the same construct in WT. Each specified codon is repeated 6x within the coding sequence of the GFP (e.g. TACTACTACTACTAC). P0: both WT *Δtgt* carry empty plasmid. $ptRNA^{Tyr}_{GUA}$: overexpressing $tRNA^{Tyr}$ with GUA anticodon. $ptRNA^{Tyr}_{AUA}$: overexpressing tRNA-Tyr with AUA anticodon. For multiple comparisons, we used one-way ANOVA on GraphPad Prism. **** means $p<0.0001$, ** means $p<0.01$, * means $p<0.05$. Number of replicates for each experiment: $3<n<8$. In A, only significant differences are indicated. ns means non-significant.

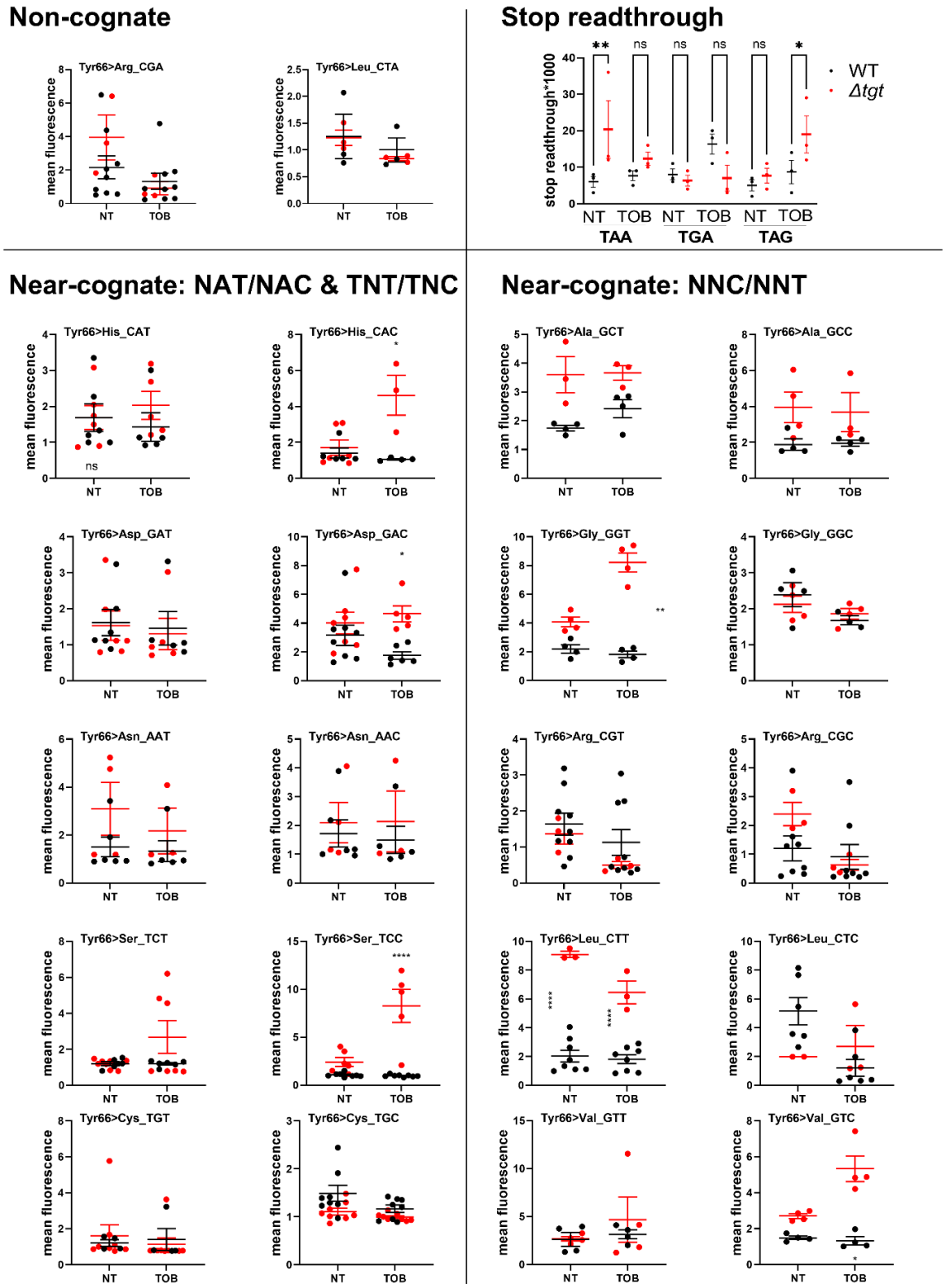

Figure S2. Q modification impacts decoding fidelity in *V. cholerae*. Stop codon readthrough levels show increased mistranslation at TAA and TAG for *Δtgt*. Blue: WT. Red: *Δtgt.* NT: no treatment. *TOB:* growth in the presence of tobramycin at 20% of the MIC. Reporters described in {Fabret, 2021 #1572}. Y axis represents stop codon readthrough*1000. The other graphs show mean fluorescence of gfp reporters where the tyrosine codon at position 66 was replaces with indicated non-cognate or near-cognate codons. Fluorescence was measured on overnight cultures grown either in MH medium without treatment (NT: non-treated), or with sub-MIC TOB (0.2 µg/ml). In black: fluorescence in the WT strain. Red: fluorescence in the *Δtgt* strain. Number of biological replicates: between 3 and 8. For comparisons between 2 groups (WT vs *Δtgt)*, first an F-test was performed in order to determine whether variances are equal or different between comparisons. For comparisons with equal variance, Student's t-test was used. For comparisons with significantly different variances, we used Welch's t-test. (*: p<0.05, **: p<0.01, ****: p<0.0001).

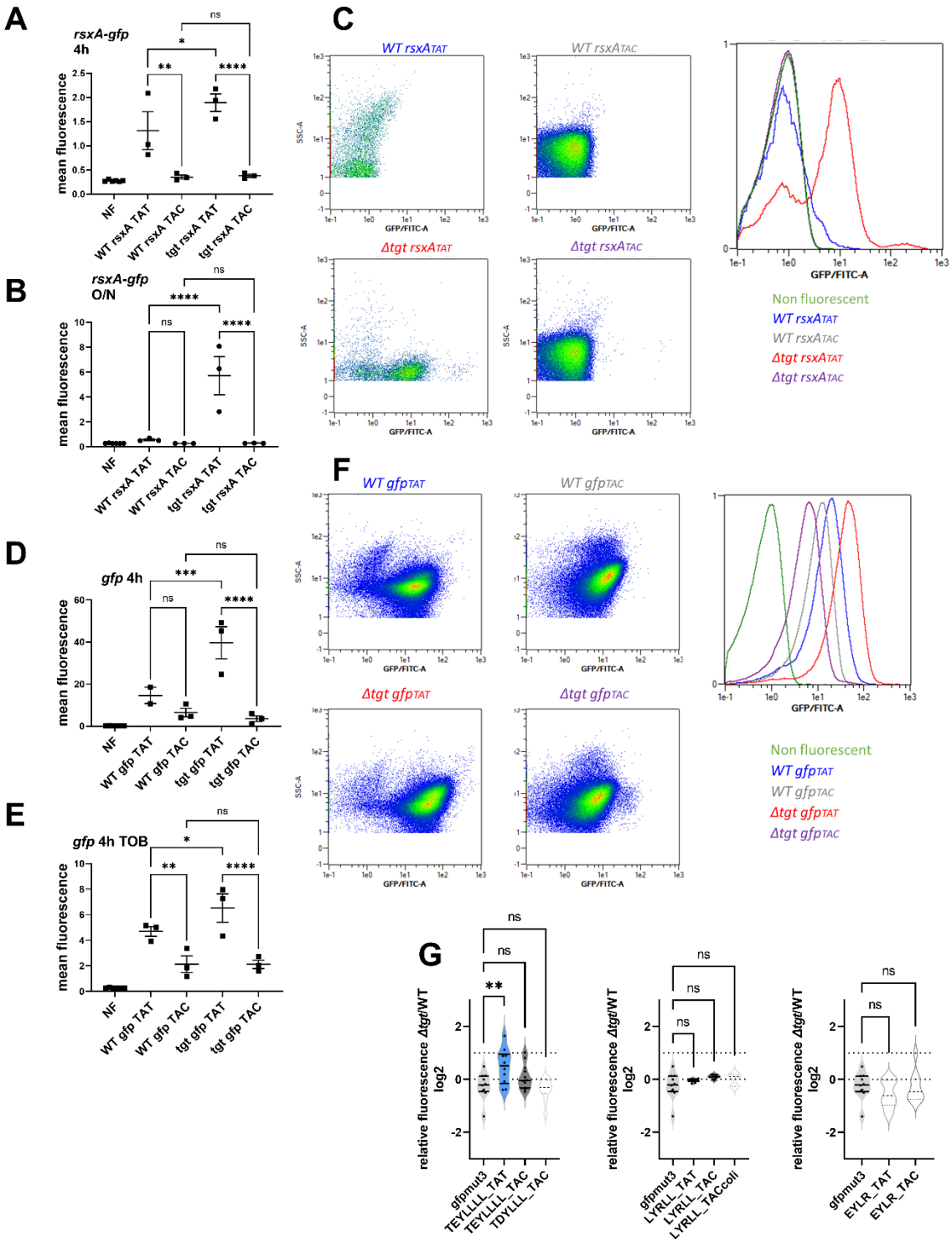

Figure S3. Post-transcriptional upregulation of RsxA in *Δtgt* due to a Tyr codon bias towards TAT and toxicity in sub-MIC TOB. ABC. Translational fusion of TAC and TAT versions of *rsxA* to *gfp* (A. 4 hours exponential phase cultures, B. overnight stationary phase cultures). **DEF**. TAC and TAT versions of *gfp* alone (C. 4 hours exponential phase cultures without antibiotics, D. in the presence of sub-MIC TOB), measured by flow cytometry. Y-axis represents mean fluorescence. **C and F** show representative examples of fluorescence observed with indicated reporters. **G**. Relative fluorescence of *Δtgt* compared to WT, various sequences displayed by *rsxA* inserted in *gfp* after its ATG codon, measured by flow cytometry. We used either the native TAT or the TAC replacement while keeping the remaining sequence unchanged. For multiple comparisons, we used one-way ANOVA. **** means p<0.0001, *** means p<0.001, ** means p<0.01, * means p<0.05. ns: non-significant. Number of replicates for each experiment: 3<n, each dot represents one replicate.

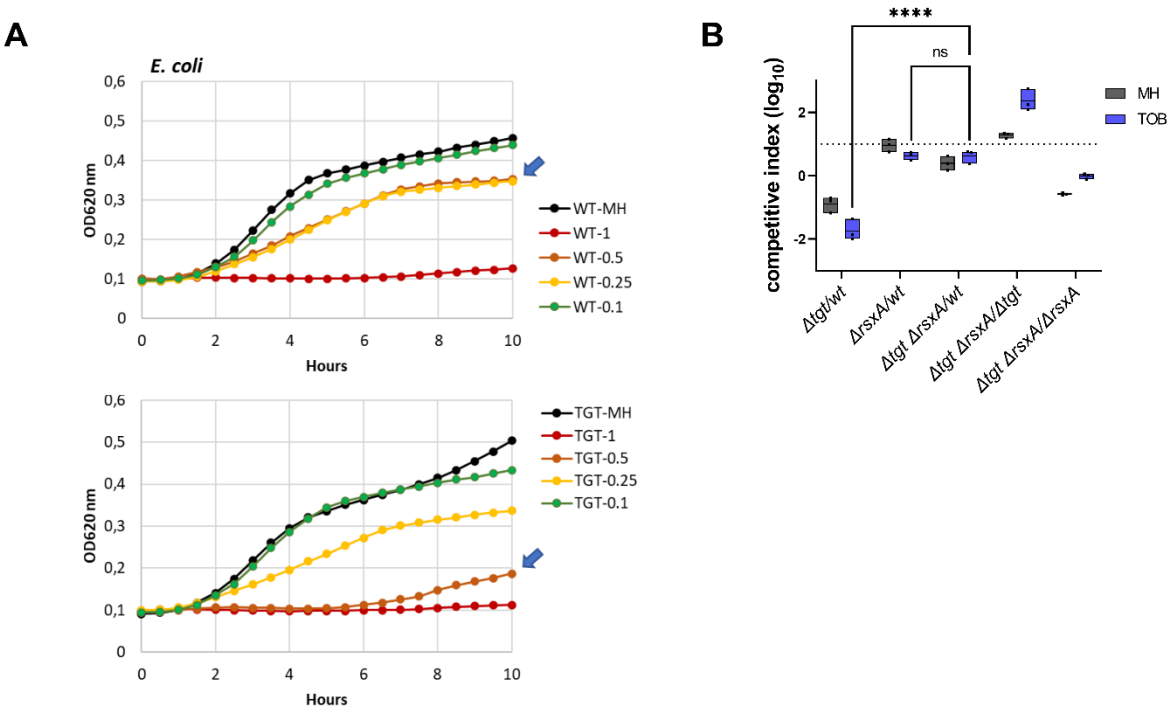

Figure S4. *rsxA* levels impact growth in the presence of sub-MIC TOB in *E. coli*. A. Growth curves in microtiter plate reader, in *E. coli* WT and *Δtgt* in MH or in the presence of tobramycin at the indicated concentrations (in µg/mL). **B.** Competition experiments in *E. coli*, with indicated strains, in MH or TOB (0.4 µg/ml). For multiple comparisons, we used one-way ANOVA. **** means p<0.0001, *** means p<0.001, ** means p<0.01, * means p<0.05. ns: non-significant. Number of replicates for each experiment: 3<n, each dot represents one replicate.

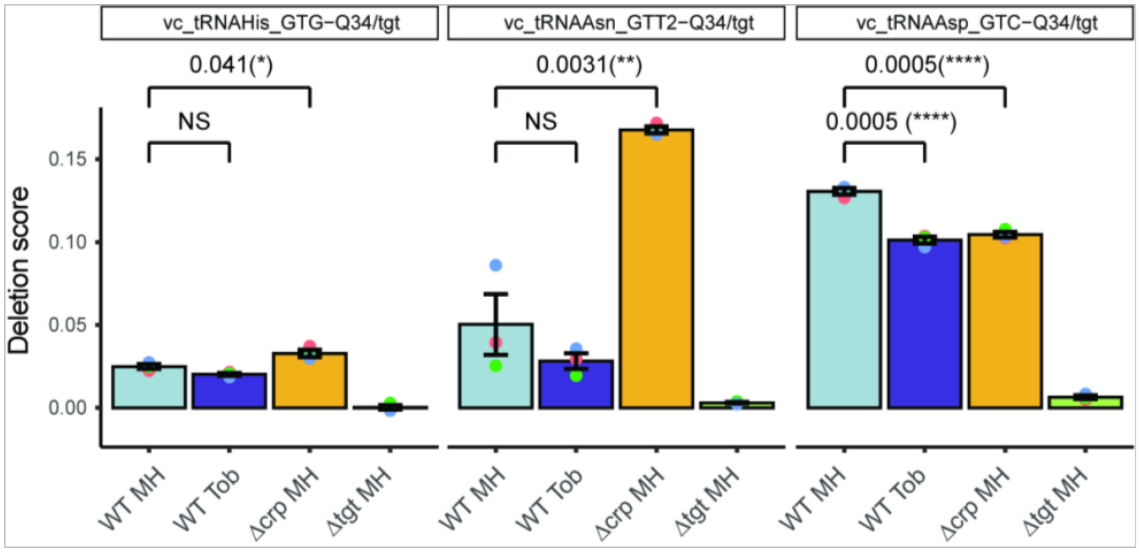

Figure S5. **Q detection and quantification by $IO4^-$ oxidation coupled to deep sequencing**. The Y-axis represents deletion score, which correlates with the Q34 level in tRNA. Results for tRNAs His, AsnGUU2 and Asp are shown. Analysis was performed for three biological replicates (shown as colored dots) and at least two technical replicates for each strain (only mean of technical replicates is shown). p-values are calculated by two-tailed T-test, error bars correspond to standard error of the mean.

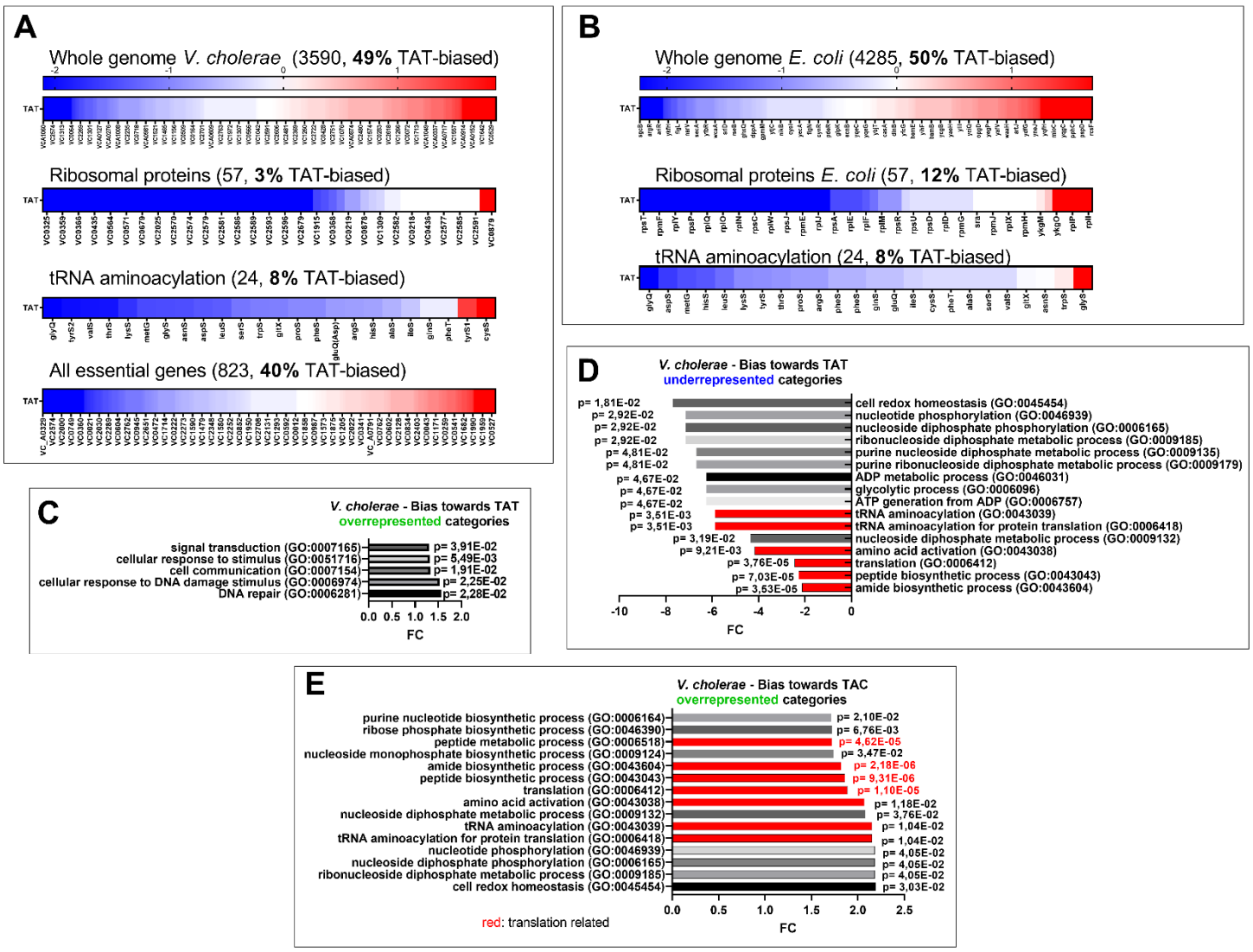

Figure S6. Codon usage. A and B: Tyrosine codon usage in A: *V. cholerae* and B: *E. coli* in the whole genome and selected groups of genes. Red indicates positive codon usage bias, i.e. TAT bias. Blue indicates negative codon usage bias for TAT, i.e. TAC bias. **CDE.** Gene ontology enrichment analysis in *V. cholerae* of **C:** overrepresented gene categories with TAT usage bias**. D:** underrepresented gene categories with TAT usage bias**. E:** overrepresented gene categories with TAC usage bias.